U.S. DEPARTMENT OF THE INTERIOR
U.S. GEOLOGICAL SURVEY

MAGNETOTELLURIC DATA IN THE PAHUTE MESA AND OASIS VALLEY AREAS, NYE COUNTY, NEVADA

By

Clifford J. Schenkel

Open-File Report 98-504

Prepared in cooperation with the Nevada Field Office
U.S. Department of Energy
(Interagency Agreement DE-AI08-96NV11967)

Table of Contents

Illustrations

Tables

Appendices

Magnetotelluric Data in the Pahute Mesa and
Oasis Valley Areas, Nye County, Nevada

by

Clifford J. Schenkel

Introduction

In October 1997 and March 1998 the U.S. Geological Survey (USGS) collected magnetotelluric (MT) to determine major subsurface structures from their resistivity structure. The objective of these measurements was to aid in evaluating the regional hydrological flow patterns of the western part of the southwestern Nevada volcanic field. Figure 1 is a regional map showing the areas of the October 1997 and March 1998 surveys. The October surveys focused on the northern part of Thirsty Canyon on Pahute Mesa of the Nevada Test Site (NTS) and Nellis Air Force Range (NAFR). The March field session was in Oasis Valley (OV) basin, north of Beatty, Nevada. The purpose of this report is to present the MT data.

The MT Method

The MT method is discussed in Vozoff (1971, 1986, and 1991) and Furgerson (1982). This method is an electromagnetic (EM) method that uses measurements of the natural electric (E) and magnetic (H) time-varying fields on the earth's surface to infer the subsurface electrical resistivity structure.

Natural sources of MT fields above frequencies of about 1 Hz are thunderstorms worldwide; discharges from lightning radiate fields that propagate around the world in the earth-ionosphere cavity. At frequencies below 1 Hz, the bulk of the signal is due to current systems in the magnetosphere set up by solar activity.

These sources create a spectrum of EM fields in the frequency band 10^{-4} to 10^{4} Hz, which provide information to delineate structures at depth from a few tens of meters to the upper mantle at a few tens of kilometers. MT data at various frequencies provide a means to distinguish spatial variations in resistivity vertically and laterally. The EM field penetration, which decays exponentially, is related to the frequency and resistivity of the medium. A common term to measure penetration depth is the skin depth (δ) which is the depth where the field has decayed to 1/e of its surface value.

$$\delta = \sqrt{\frac{\rho}{\mu \pi f}} \approx 500\sqrt{\frac{\rho}{f}} \qquad (1)$$

where δ is in meters, μ is the magnetic permeability and is approximately with the free space value ($4\pi \cdot 10^{-7}$ H/m), ρ is the resistivity (Ω-m) and f is the frequency (Hz). Higher frequencies map near surface resistivity distribution. Lower frequencies provide information on deeper structures.

Lightning discharges and magnetospheric current systems produce time-varying H-fields, which behave almost like plane waves at the surface of the earth. Most of the energy is reflected but a small amount is propagated vertically downward into the earth. Through Faraday's Law the H-fields produce an electromotive force (*emf*) in the conducting earth that causes electric currents to flow within the earth. These E-fields are measured on the surface by an average of the voltage drop across two electrodes. The E-fields are more locally sensitive to the conductivity distribution than the H-fields. From the amplitude, phase, and directional relationship between E- and H-fields on the surface, one can infer the distribution of subsurface electrical resistivity.

For a layered half-space only horizontal E-fields are induced. If the ground is inhomogeneous, there will be horizontal gradients in the E-fields producing secondary H-fields including a vertical (*Hz*) component, which is not present in a layered earth. In the frequency domain, the measured orthogonal components of the H-field (*Hx* and *Hy*) are related to *Ex*, *Ey*, and *Hz* through the tensor relation. However, if *Hz* is not measured (as in this report), the tensor relation simply relate the H-fields to E-fields by:

$$\begin{vmatrix} Ex \\ Ey \end{vmatrix} = \begin{vmatrix} Zxx & Zxy \\ Zyx & Zyy \end{vmatrix} \cdot \begin{vmatrix} Hx \\ Hy \end{vmatrix} \quad (2)$$

where *Zxx, Zxy, Zyx, Zyy* are components of the impedance tensor (***Z***). If the impedance tensor is rotated so that the diagonal elements are minimized (close to zero), the off-diagonal elements, *Zxy* and *Zyx,* are called the principle impedances and the angle of rotation is the impedance strike direction. The impedance strike direction and its orthogonal complement make up the principle axes; the impedance strike has an inherent 90° shift ambiguity that is usually resolved from the tipper data (see Vozoff, 1991), or from the frequency relationships of the various impedance elements.

Typically, for MT soundings, the impedance tensor is rotated to the principle axis (minimizing the diagonal elements) and is presented for the off-diagonal elements, *Zxy* and *Zyx*. The apparent resistivity (ρ) is calculated from these impedance tensor elements and is plotted as a function of frequency. However, for continuous profiling the survey is configured to maximize the response of targets perpendicular to the survey line direction. Furthermore, continuous profiling can be used to average out small and shallow inhomogeneities that can adversely affect the interpretation of single or few soundings. If the data collected at a site whose axis differ from the profile direction, these impedances can be rotated to the corresponding profile direction.

Data Acquisition

Data were collected using the MT-1 system developed by Electromagnetic Instruments, Inc. (EMI). The H-field was measured using an induction coil; the voltage drop across two ($Cu - CuSO_4$) porous pot electrodes separated by a fixed length approximated the E-field.

Figure 2 illustrates the two MT configurations used for this experiment: dual soundings and continuous profiling. To reduce the effects of noise on the signal, remote referencing was employed (Gamble and others, 1979 and Furgerson, 1982). This requires a separate set of E-fields and H-fields measurements at a site removed from the survey. Dual soundings measure simultaneous orthogonal E-fields and H-fields at each location where one set of measurements can be used as a remote reference for the other (local) and vise-versa. Continuous profiling combines several contiguous *Ex*-fields for each setup of *Ey, Hx,* and *Hy* along a profile (Torres-Verdin, 1991 and Torres-Verdin and Bostick, 1992). The advantage of continuous profiling over a line of separate soundings is to reduce the problems associated with small and near-surface structures caused by inadequate spatial sampling of the EM-fields. However, this type of survey requires more time and effort to setup.

E-fields and H-fields were digitally recorded and stored as time series. The processing was done in the frequency domain using the software package, MTR95 from EMI. Time series are decimated to obtain lower frequencies. All time series are Fourier transformed; the Fourier coefficients are used to estimate cross spectra from which the impedances are computed. From these impedances, the apparent resistivity, phase, coherency, skew, impedance rotation angle, and tipper (if *Hz* is measured) are calculated for different frequencies.

Data

MT sites were collected over magnetic and gravity features that were discussed by in Grauch and others (1997). Continuous profiling and soundings were conducted in October 1997: in the March 1998 survey only dual sounding method was used. Figures 2 and 3 show the locations of the MT sites. Tables A1 and A2 in Appendix A list the site coordinates.

For the data in this experiment, two frequency bands were collected: 175-4.5Hz (high) and 11-0.32Hz (mid). Table 1 shows the acquisition settings. The mid-band was decimated to produce a low-band of 1.4-0.01Hz. Filters settings for the high band were set automatically by the acquisition software.

Band	Sampling		Segments	Blocks	Filter	
	Frequency (Hz)	Length			High Pass (Hz)	Low Pass (Hz)
high	500	512	4	3	1.00	94.00
mid	32	512	32	8	0.0008	16.00

Table 1: Setting of acquisition parameters

A continuous profiling survey planned for the northern end of the Thirsty Canyon gravity lineament (TCL) from well PM2 to well UE20F was divided due to ruggedness of the terrain and the noise problem caused by the recently installed power lines (Figure 3). The two shortened lines traversed across the two structures of interest, the fault located just east of well PM2 (Line p1) and the TCL (Line p2). Continuous profiling using 100m electrode spacing spanned 700m. Each setup had seven *Ex* for a single *Ey, Hx,* and *Hy* as shown in Figure 2. Profile azimuths for Lines p1 and p2 were 150° and 125°, respectively. Two dual sounding profiles were collected (Figure 4): Line b obliquely crossed the TCL near well PM3 approximately 5km southwest of Line p2 and Line m crossed the Buckboard Mesa magnetic lineament (BML), east of Thirsty Canyon. The dual sounding profiles used the configuration in Figure 2 with soundings 500m apart and electrode separation of 100m.

Sounding profiles for the March 1998 session (Figure 4) were collected in the northern end (Line n) of the OV basin and in the southern end (Line s). The northwest segment of Line n (n01-n08) was across the extreme southern end of the TCL. The north-south segment of Line n (n06, n09-n14) crossed several gravity and magnetic features as defined by Tom Hildenbrand (USGS, Menlo Park, unpublished data, 1998). In the southern end of OV basin, two profiles crossed a basin edge inferred by gravity (heavy light gray line in Figure 4: Hildenbrand, USGS, Menlo Park, unpublished data). The dual sounding configuration (Figure 2) was employed with 500m station separation and 50m electrode spacing.

Data are plotted by profile lines in Appendix B. The apparent resistivity, phase, impedance strike, and skew are plotted versus the frequency for each MT site. For continuous profiling data, the x-axis is defined as the azimuth direction of the survey. For Line p1 and p2 the azimuths are 150° (true) and 125° (true), respectively. For all the dual sounding stations (Lines b, m, n, and s), data are plotted with the x-axis true north and the y-axis true east.

Acknowledgements

I wish to thank Gary Dixon, Jerry Magner, and Doug Trudeau of the USGS for arranging the logistics on the Nevada Test Site and for facilitating the work here. I wish to thank Glenn Coffer for access to his properties. Lastly, I am very grateful to Don Schaefer, Jay Sampson, Jackie Williams, Bob Bisdorf, Roy Kipfinger, Jeff Davidson, and Ted Asch (from EMI) who assisted in the collection of the field data on Pahute Mesa and in Oasis Valley. This work is part of an interagency effort between the USGS and the U.S. Department of Energy and was funded through the Interagency Agreement DE-AI08-96NV11967.

References

Furgerson, R.B., 1982, Remote-reference magnetotelluric survey, Nevada Test Site and vicinity, Nevada and California, with an introduction by D.B. Hoover: U.S.G.S. Open-File report 82-465, 156 p.

Gamble, T.D., Goubau, W.M., and Clarke, J., 1979, Magnetotellurics with remote reference: Geophysics, 44, 53-68.

Grauch V.J.S., Sawyer D.A., Fridrich C.J., and Hudson M.R., 1997, Geophysical interpretations west of and within the northwestern part of the Nevada test site: U.S.G.S. Open-File report 97-476, 45p.

Torres-Verdin, C., 1991, Continuous profiling of magnetotelluric fields: Ph.D. thesis, University of California, Berkeley.

Torres-Verdin, C. and Bostick, F.X., Jr., 1992, Principles of spatial surface electric field filtering in magnetotellurics; Electromagnetic array profiling (EMAP): Geophysics, 57, 603-622.

Vozoff, K., 1972, The magnetotelluric method in the exploration of sedimentary basins: Geophysics, 37, p. 98-141.

Vozoff, K. (*editor*), 1986, Magnetotelluric Methods: Geophysics reprint series no. 5, Society of Exploration Geophysicists, Tulsa, OK, 763p.

Vozoff, K., 1991, The magnetotelluric method: *in* Nabighian, M.N., Ed., Electromagnetic Methods in Applied Geophysics, v. 2, Application, Part B, Society of Exploration Geophysicists, Tulsa, p. 641-711.

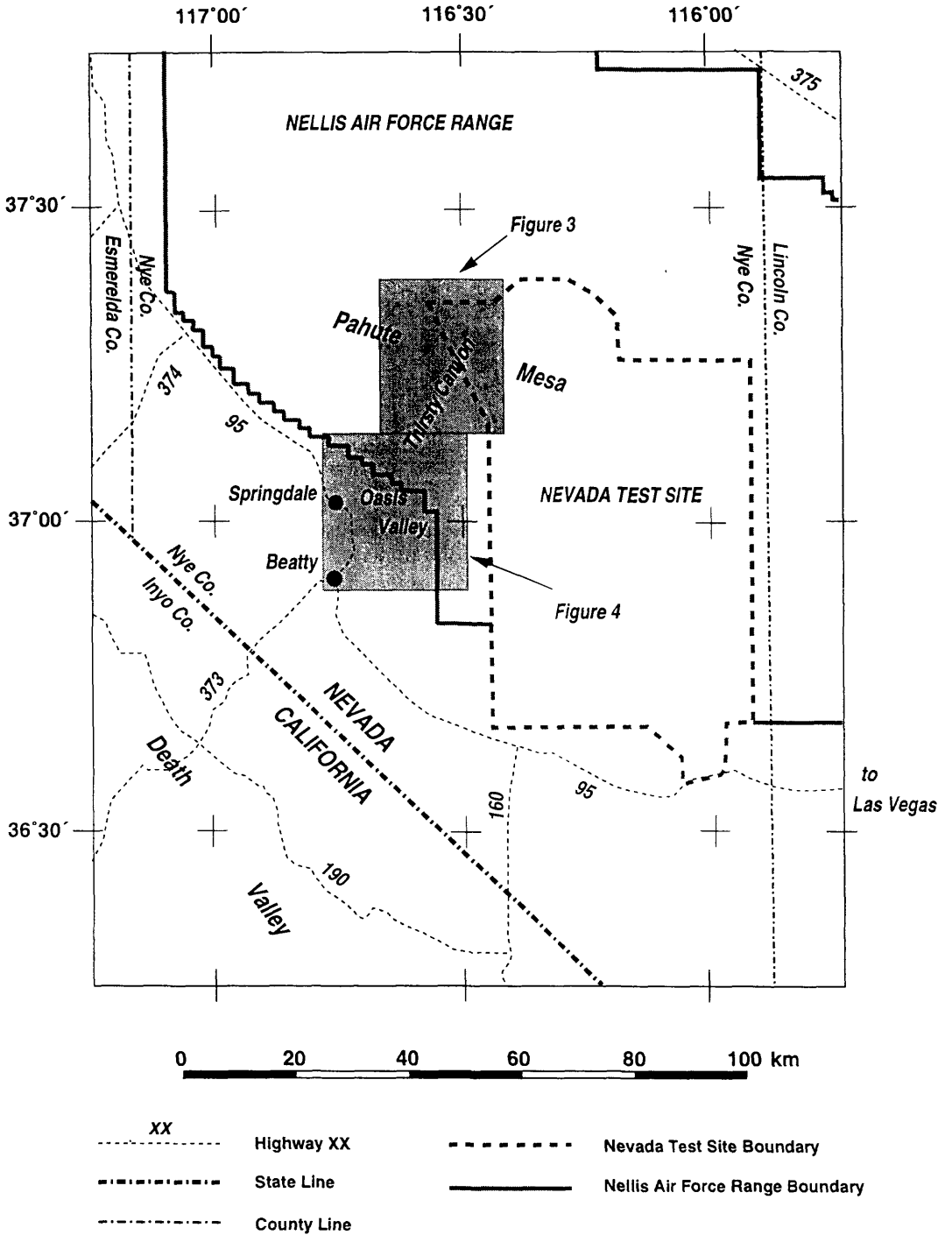

Figure 1: Regional Map of Study Area

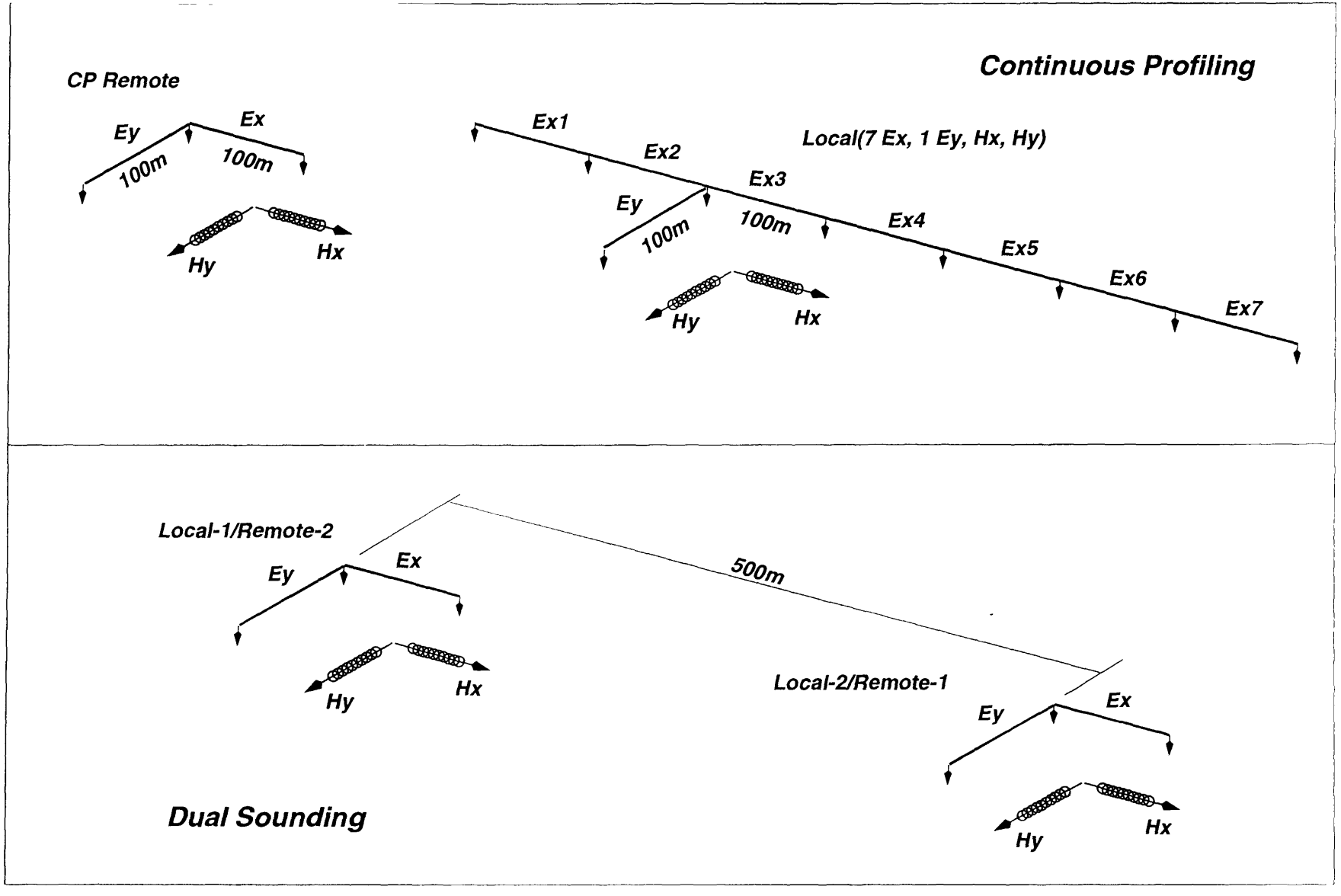

Figure 2: MT System Configurations

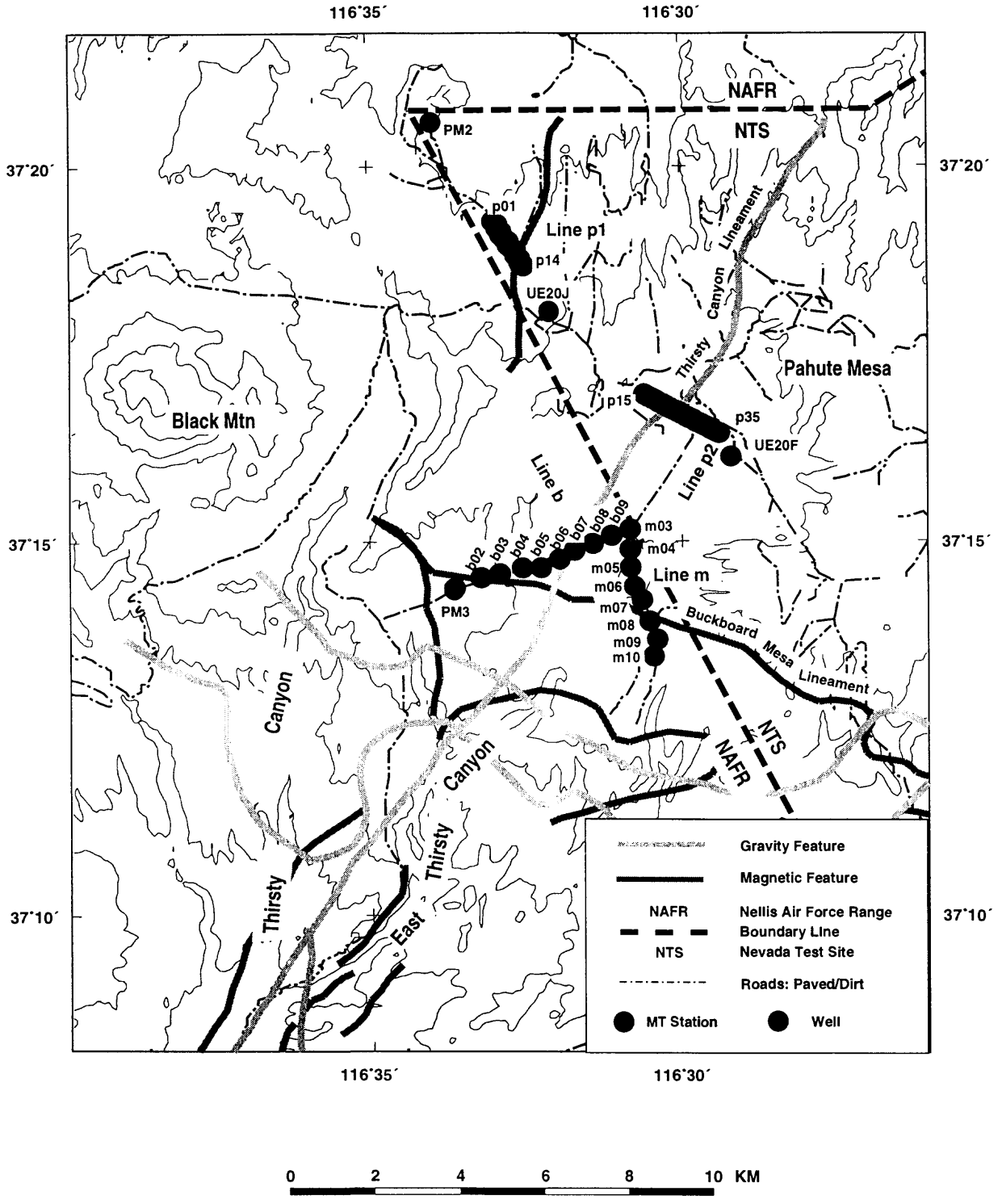

Figure 3: Map of the MT sites: Pahute Mesa, October 1997.

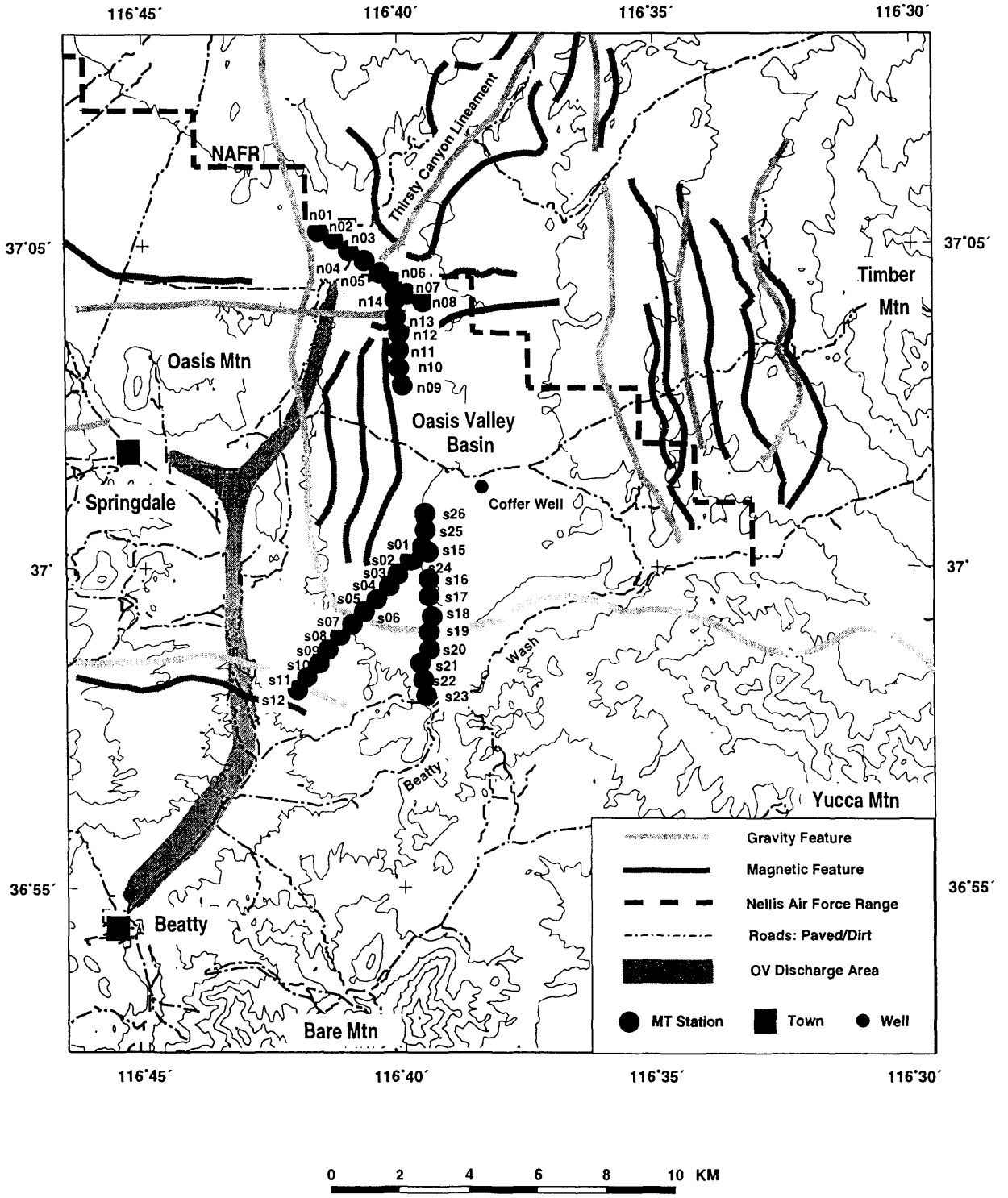

Figure 4: Map of the MT sites: Oasis Valley, March 1998.

Appendix A: MT Site Coordinates

Table A1: MT site coordinates: Pahute Mesa, October 1997. This table has the site identification, x coordinate, y coordinate, and elevation. Horizontal x and y coordinates are in meters UTM zone 11 using North American horizontal datum of 1927. The elevations are in meters using North American vertical datum of 1929. For the continuous profiling lines, the base station for each spread (7 sites) is listed. The base station (third site in the spread) is the location where *Ex, Ey, Hx,* and *Hy* are measurement and is used to calculate the impedance of each station.

Table A2: MT site coordinates: Oasis Valley, March 1998. Location parameters are the same as explained in Table A1 caption.

Continuous Profile - Line p1				
Site Number	Base Station	x km	y km	elevation m
p01	c03	540005	4130330	1714.50
p02	c03	540058	4130245	1717.55
p03	c03	540112	4130161	1720.60
p04	c03	540166	4130077	1722.12
p05	c03	540220	4129993	1725.17
p06	c03	540274	4129908	1734.31
p07	c03	540328	4129824	1746.50
p08	c10	540382	4129740	1752.60
p09	c10	540436	4129656	1760.22
p10	c10	540490	4129571	1764.79
p11	c10	540544	4129487	1766.93
p12	c10	540598	4129403	1767.84
p13	c10	540652	4129319	1767.84
p14	c10	540706	4129234	1769.36

Continuous Profile - Line p2				
Site Number	Base Station	x km	y km	elevation m
p15	c17	543550	4126105	1853.18
p16	c17	543637	4126057	1862.33
p17	c17	543725	4126009	1862.33
p18	c17	543812	4125961	1879.09
p19	c17	543900	4125914	1859.28
p20	c17	543988	4125866	1834.90
p21	c17	544075	4125818	1840.99
p22	c24	544163	4125770	1842.52
p23	c24	544251	4125723	1844.04
p24	c24	544338	4125675	1845.56
p25	c24	544426	4125627	1847.09
p26	c24	544513	4125579	1848.61
p27	c24	544601	4125532	1850.14
p28	c24	544689	4125484	1847.09
p29	c31	544776	4125436	1847.09
p30	c31	544864	4125388	1851.66
p31	c31	544952	4125341	1854.71
p32	c31	545039	4125293	1851.66
p33	c31	545127	4125245	1853.79
p34	c31	545214	4125197	1855.32
p35	c31	545302	4125150	1856.54

Sounding Profile - Line m			
Site Number	x km	y km	elevation m
m03	543160	4122740	1890.67
m04	543190	4122250	1902.87
m05	543150	4121800	1903.48
m06	543275	4121330	1900.43
m07	543450	4120995	1895.25
m08	543595	4120460	1888.85
m09	543795	4120010	1876.65
m10	543700	4119595	1884.58

Sounding Profile - Line b			
Site Number	x km	y km	elevation m
b01	539673	4122548	1785.51
b02	540125	4122681	1794.33
b04	540601	4122791	1801.04
b05	541055	4122791	1801.95
b06	541475	4122001	1810.81
b07	541853	4122221	1819.03
b08	542303	4122391	1840.99
b09	542763	4122591	1874.51

Table A1: MT site coordinates: Pahute Mesa, October 1997.

Sounding Profile - Line s (South OV)			
Site Number	x meters	y meters	elevation meters
s01	530284	4095297	1315.21
s02	529946	4094918	1280.77
s03	529632	4094522	1246.33
s04	529301	4094179	1246.63
s05	528974	4093796	1211.28
s06	528625	4093449	1203.66
s07	528245	4093068	1194.21
s08	527893	4092741	1172.87
s09	527593	4092330	1172.87
s10	527306	4091936	1203.96
s11	526983	4091535	1128.98
s12	526671	4091157	1111.00
s15	530492	4095157	1299.36
s16	530462	4094373	1295.4
s17	530475	4093890	1278.94
s18	530560	4093294	1279.25
s19	530478	4092832	1263.09
s20	530480	4092330	1221.03
s21	530210	4091931	1203.96
s22	530278	4091452	1207.31
s23	530429	4090981	1187.81
s24	530011	4094944	1280.46
s25	530348	4095778	1309.73
s26	530424	4096252	1313.08

Sounding Profile - Line n (North OV)			
Site Number	x meters	y meters	elevation meters
n01	527356	4104342	1251.81
n02	527787	4104128	1237.18
n03	528300	4103791	1210.97
n04	528680	4103507	1220.72
n05	529127	4103158	1223.47
n06	529526	4102893	1232.61
n07	529978	4102543	1245.41
n08	530424	4102336	1254.86
n09	529780	4099936	1264.62
n10	529709	4100440	1281.99
n11	529722	4100946	1267.36
n12	529721	4101422	1259.13
n13	529620	4101888	1263.09
n14	529559	4102385	1251.51

Table A2: MT site coordinates for March 1998.

Appendix B: MT Data Plots

Plots of the apparent resistivity, impedance phase, impedance strike, and skew are plotted versus frequency (log-scale). For the apparent resistivity (log-scale) and impedance phase plots, solid squares are the *xy*-mode (*Ex/Hy*) and the solid diamond are the *yx*-mode (*Ey/Hx*). The apparent resistivity (ρ_{ij}) and impedance phase (θ_{ij}) are calculated from

$$\rho_{ij} = 1/(5f)\left|Z_{ij}\right|^2 \text{ and } \theta_{ij} = \tan^{-1}\left[\mathrm{Im}(Z_{ij})/\mathrm{Re}(Z_{ij})\right],$$

respectively where *i* and *j* are *x* or *y*. The impedance strike is described in the section: "The MT Method." The impedance skew is the ratio: |*Zxx*+*Zyy*|/|*Zyx*-*Zxy*| and is a measure of dimensionality. For a two-dimensional (or less) situation the skew is theoretically zero but data noise can strongly influence this parameter.

The data are plotted by profile lines. Data from Pahute Mesa area were acquired using continuous profiling ("p1" and "p2") as well as dual-sounding lines ("b" and "m"). Data from Oasis Valley area were acquired using duel sounding lines ("s" and "n"). Each plot is labeled with the station identification.

For continuous profiling lines the x-axis is defined as the line azimuth: Line p1 was 150° (true) and Line p2 was 125° (true). For all duel-soundings (Lines b, m, n, and s) the data are plotted with the x-axis true north and the y-axis true east.

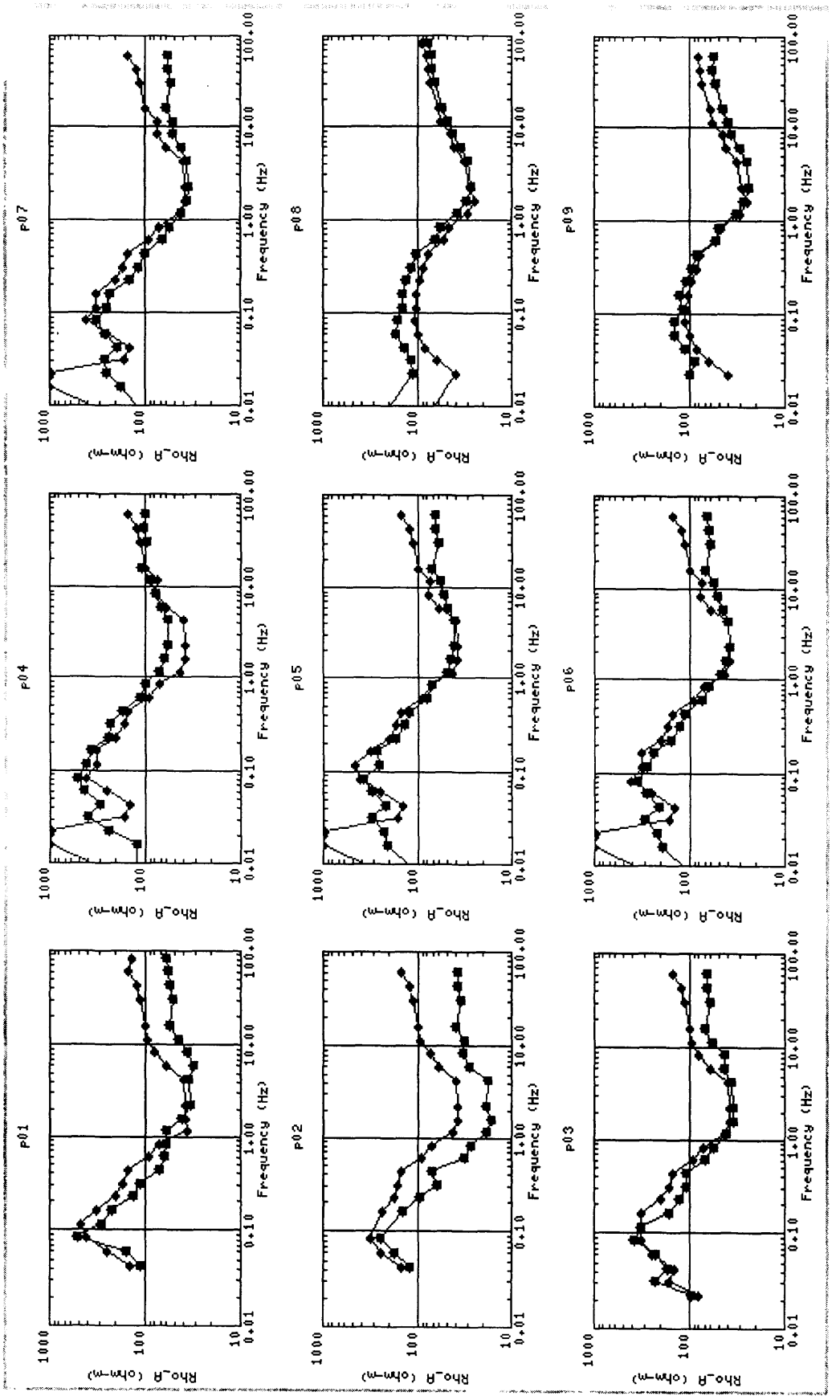

Figure B1.1: Line p1 - Apparent Resistivity, site p01-p14

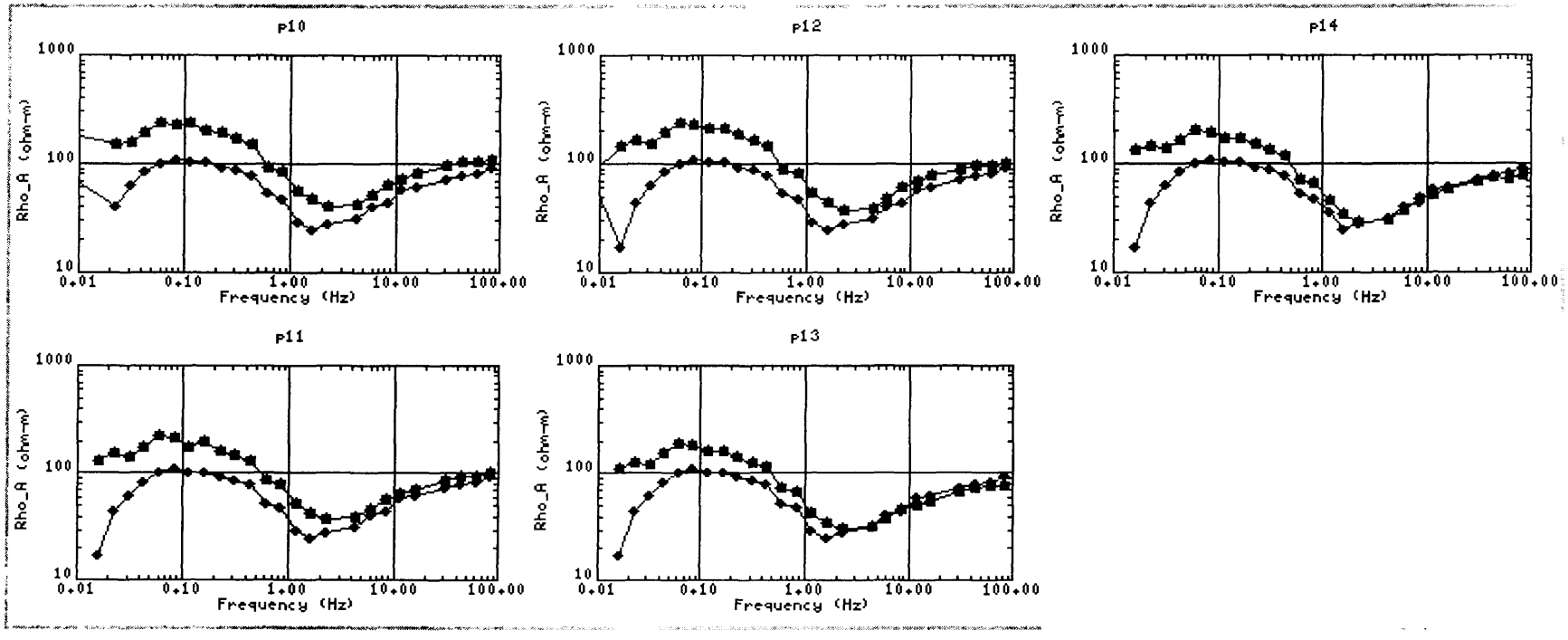

Figure B1.1: Line p1 - Apparent Resistivity, site p01-p14

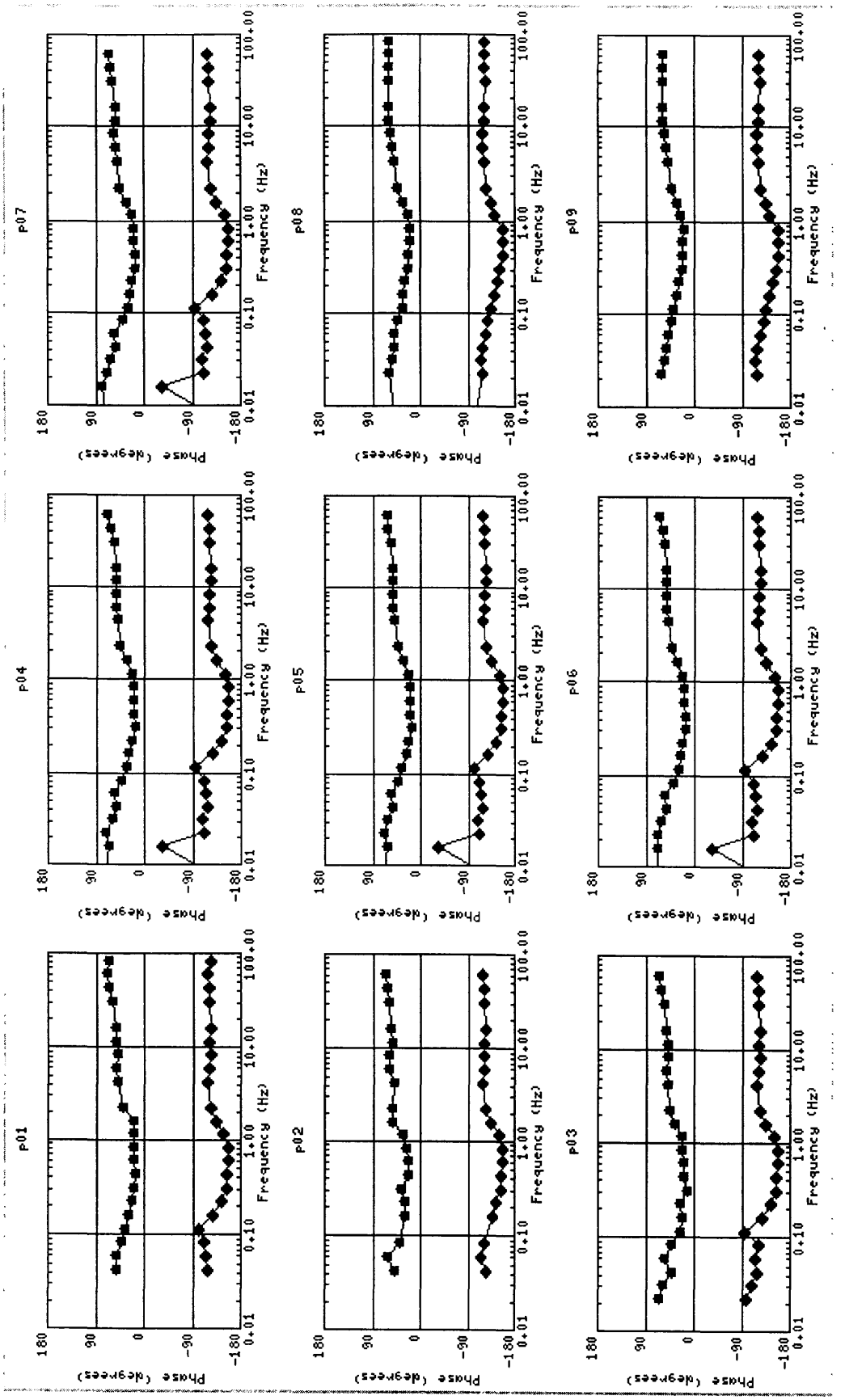

Figure B1.2: Line p1 - Impedance Phase, site p01-p14

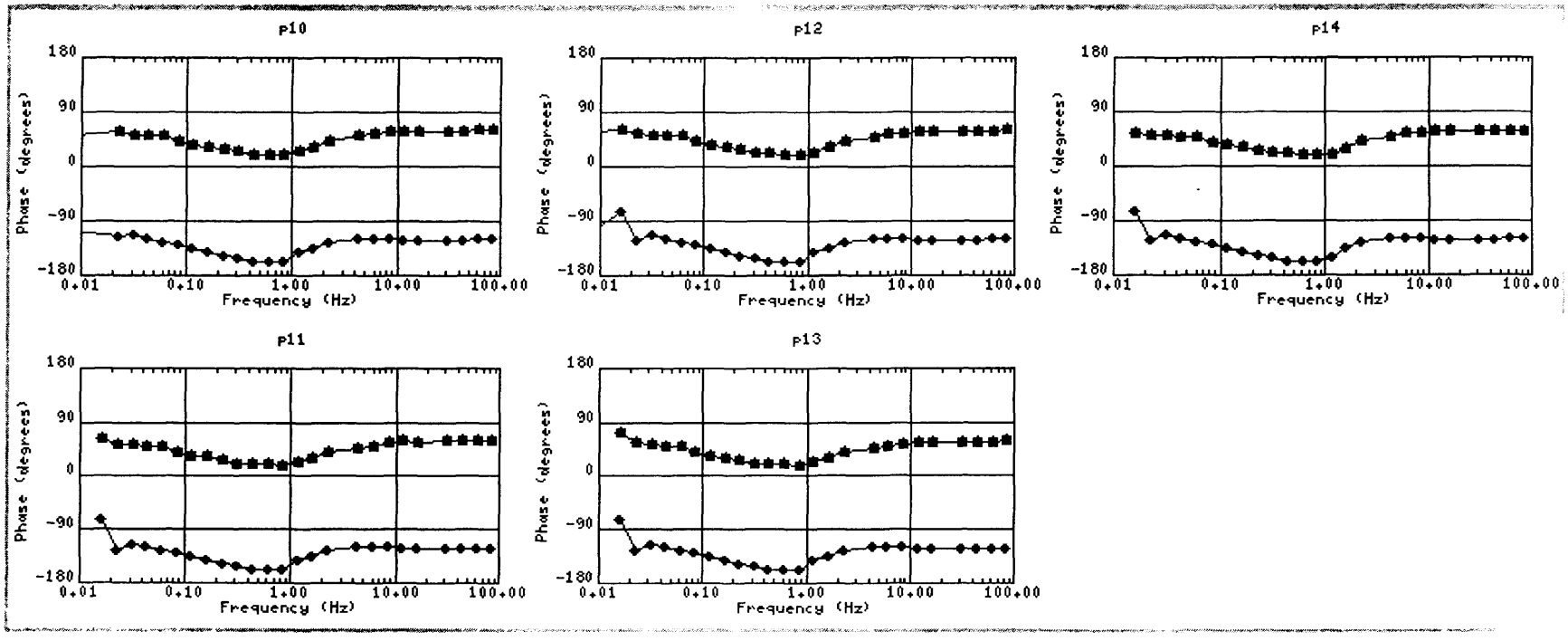

Figure B1.2: Line p1 - Impedance Phase, site p01-p14

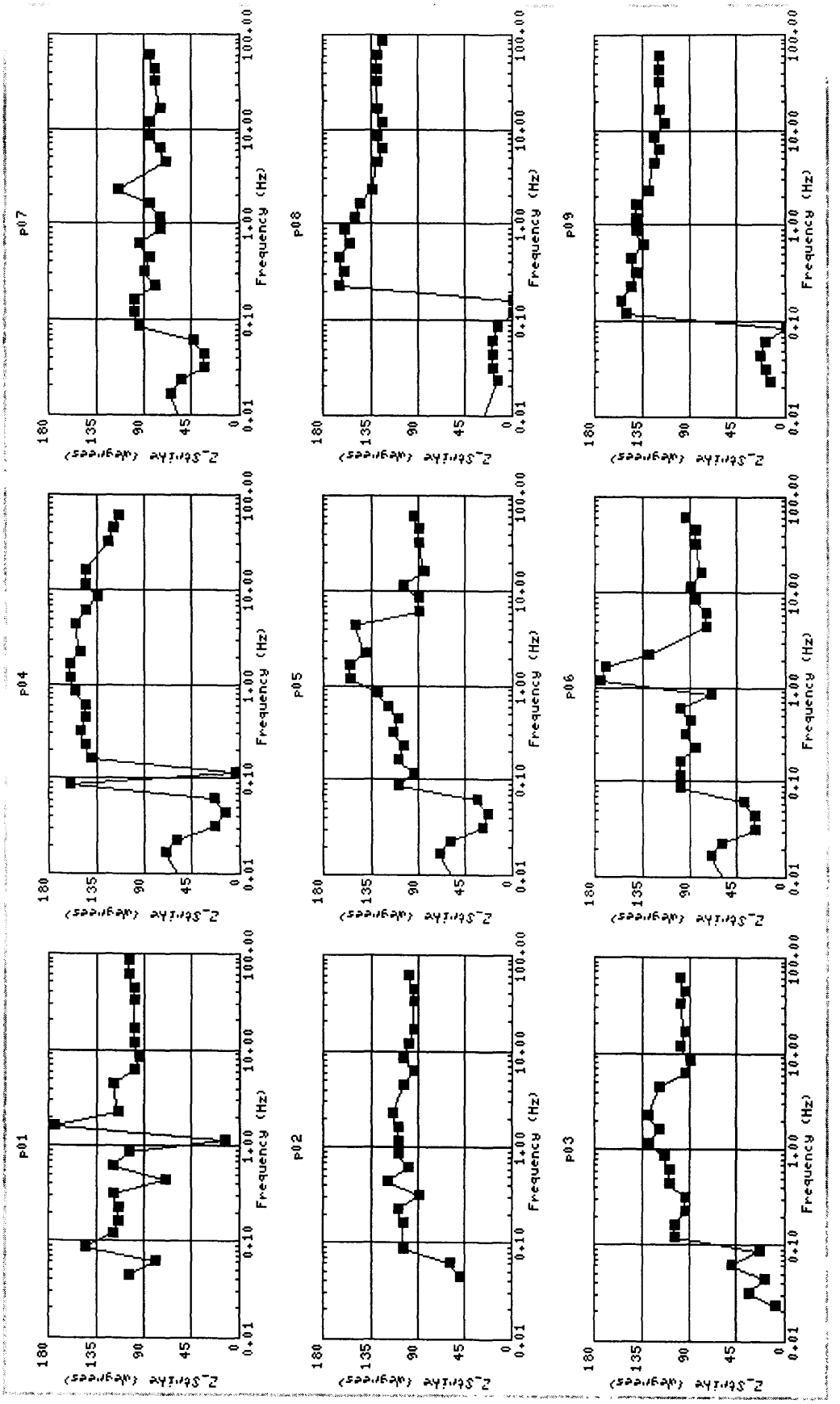

Figure B1.3: Line p1 - Impedance Strike, site p01-p14

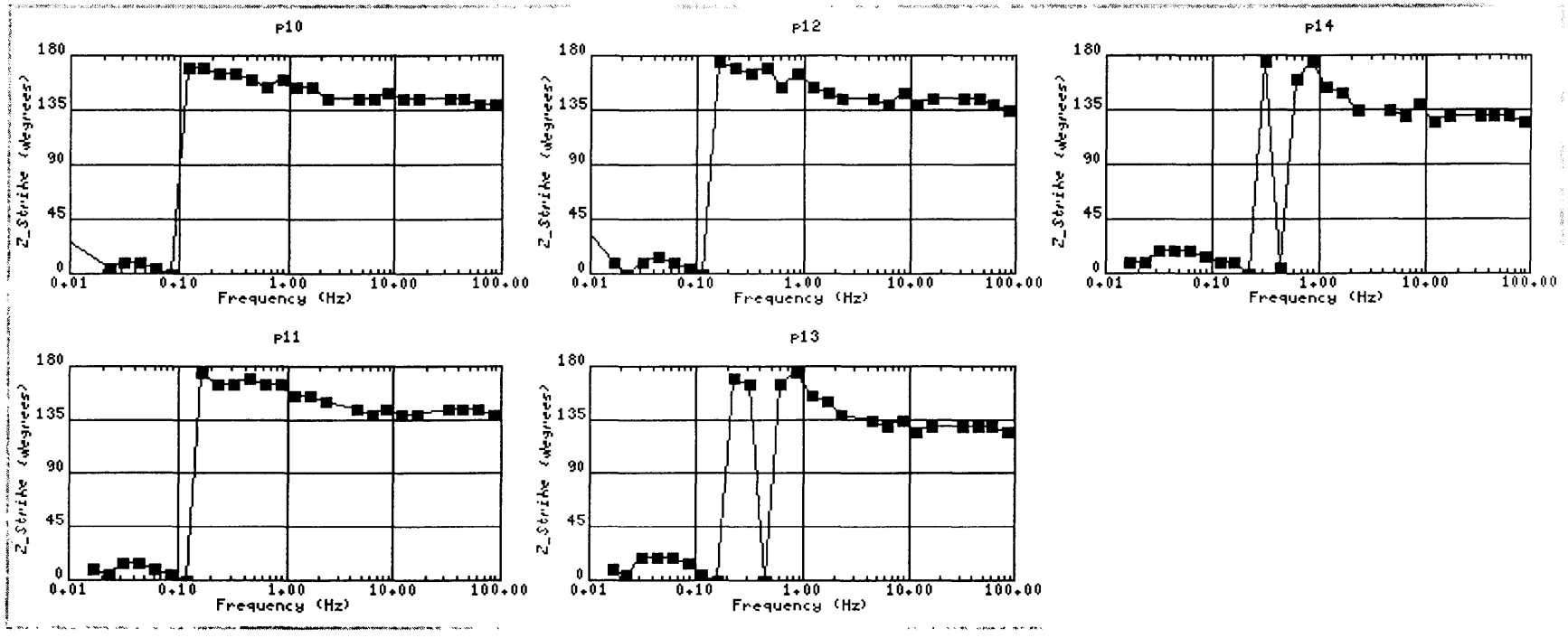

Figure B1.3: Line p1 - Impedance Strike, site p01-p14

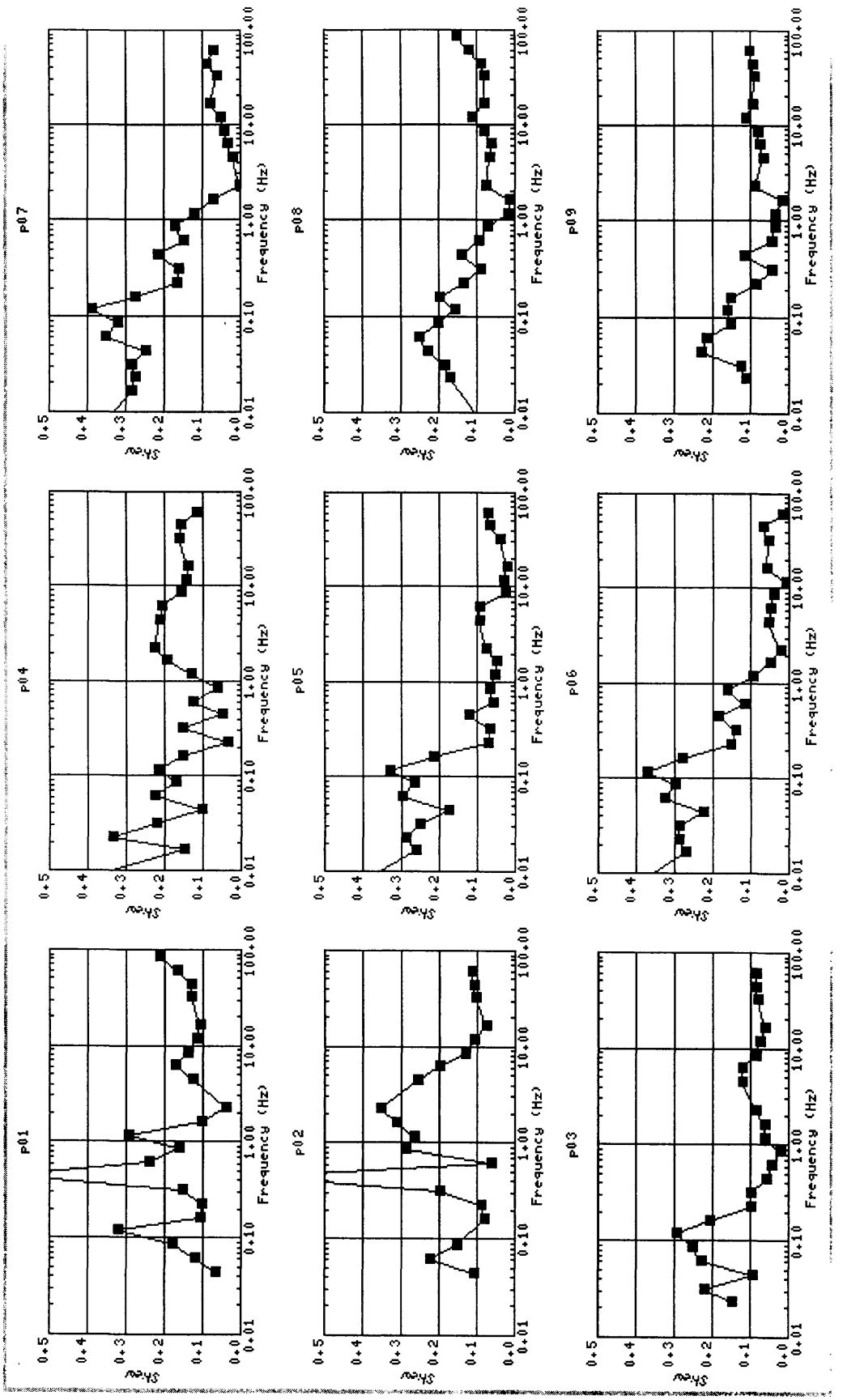

Figure B1.4: Line p1 - Impedance Skew, site p01-p14

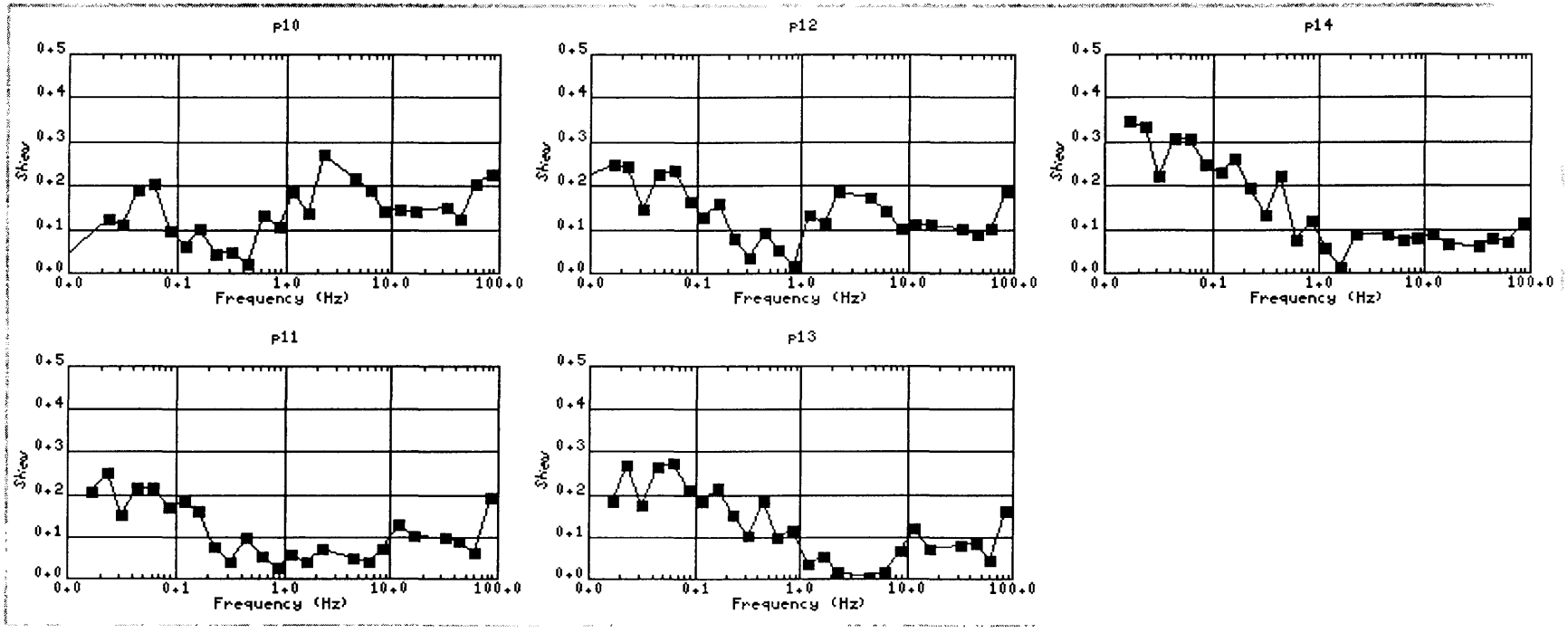

Figure B1.4: Line p1 - Impedance Skew, site p01-p14

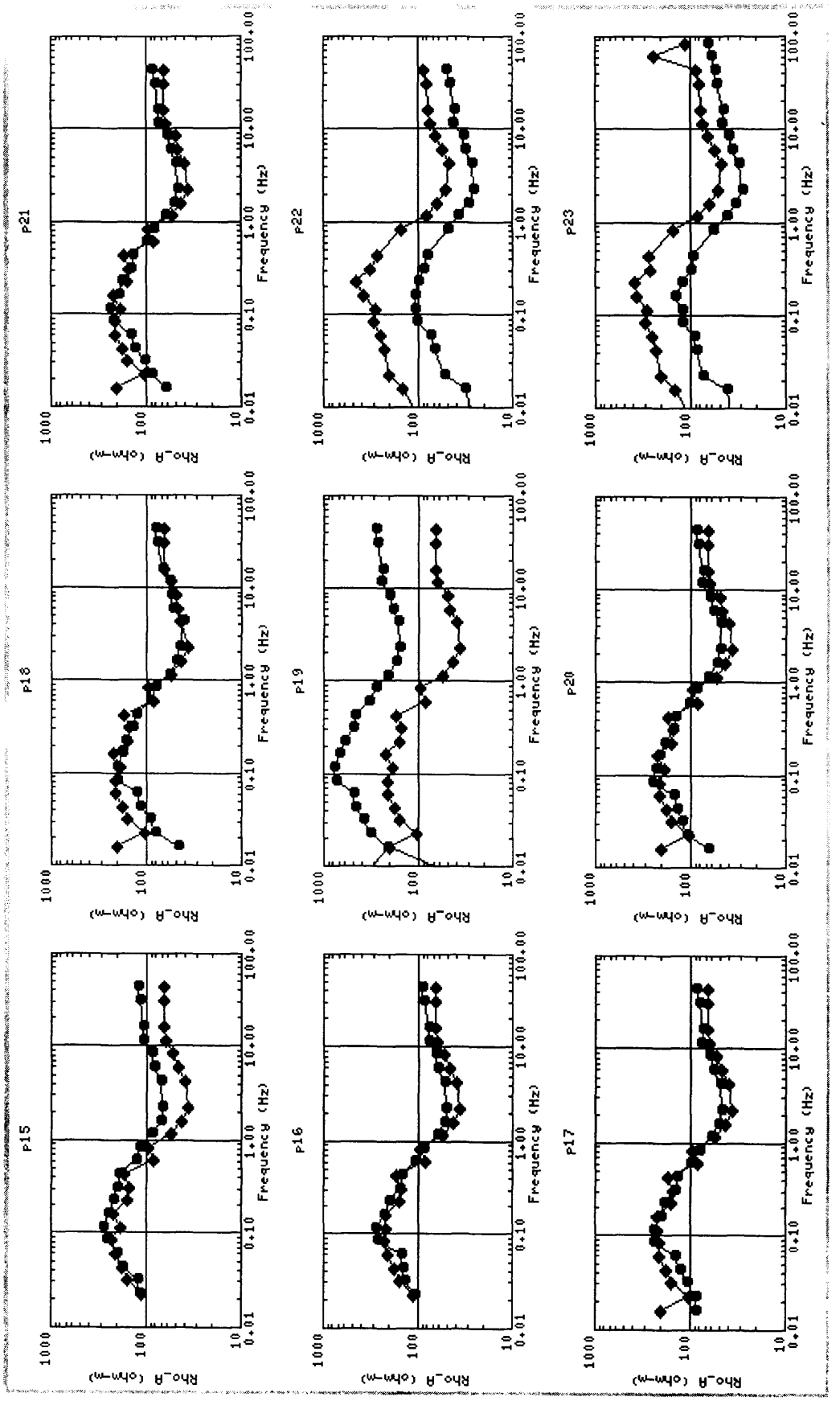

Figure B2.1: Line p2 - Apparent Resistivity, site p15-p35

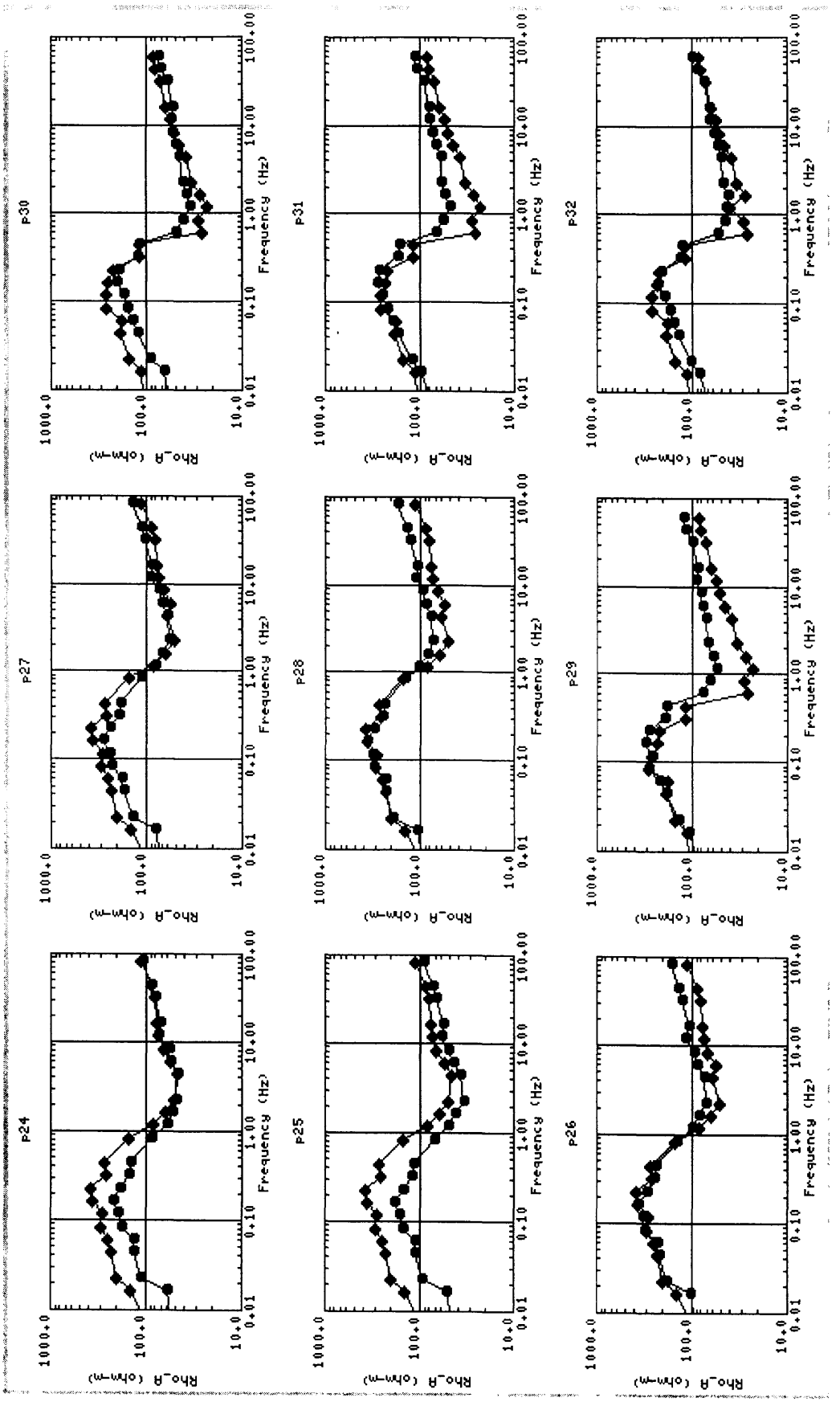

Figure B2.1: Line p2 - Apparent Resistivity, site p15-p35

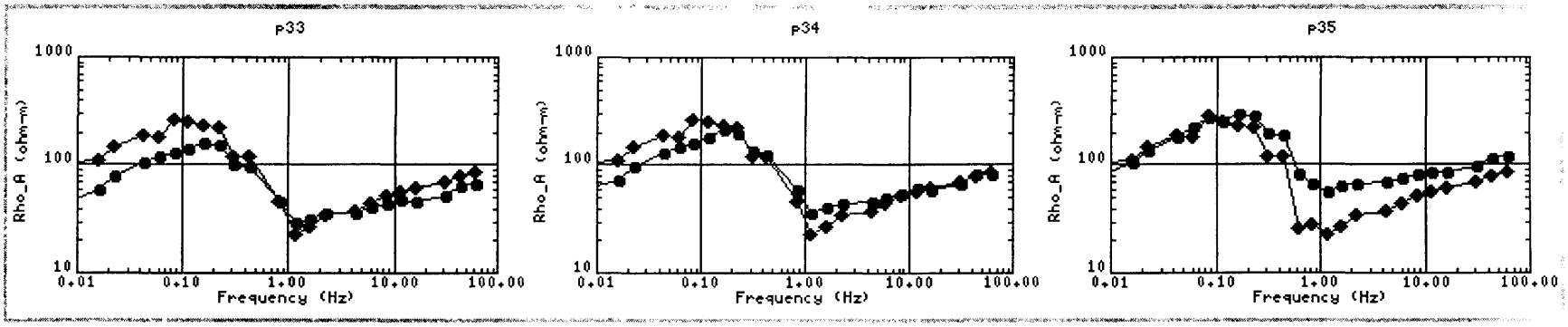

Figure B2.1: Line p2 - Apparent Resistivity, site p15-p35

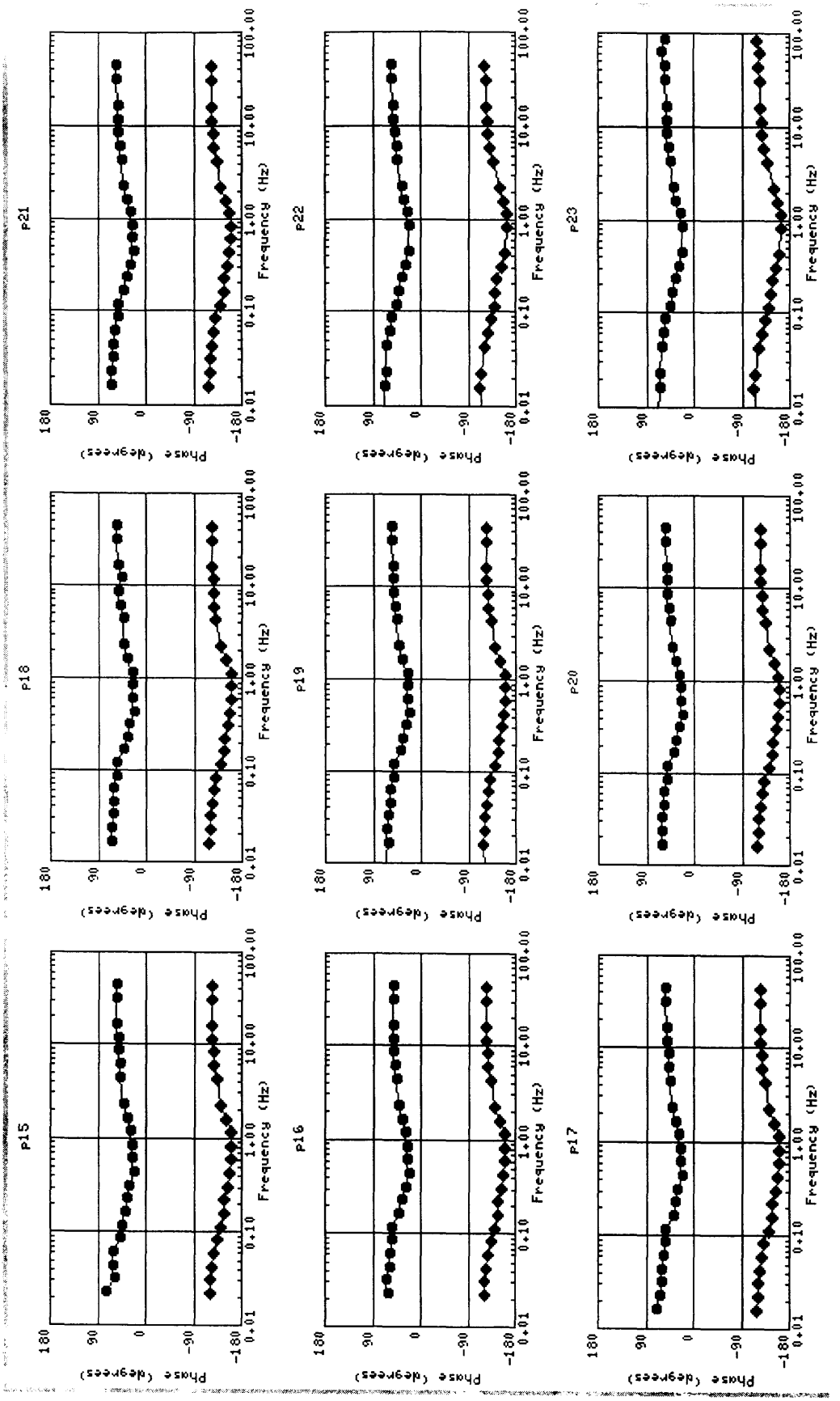

Figure B2.2: Line p2 - Impedance Phase, site p15-p35

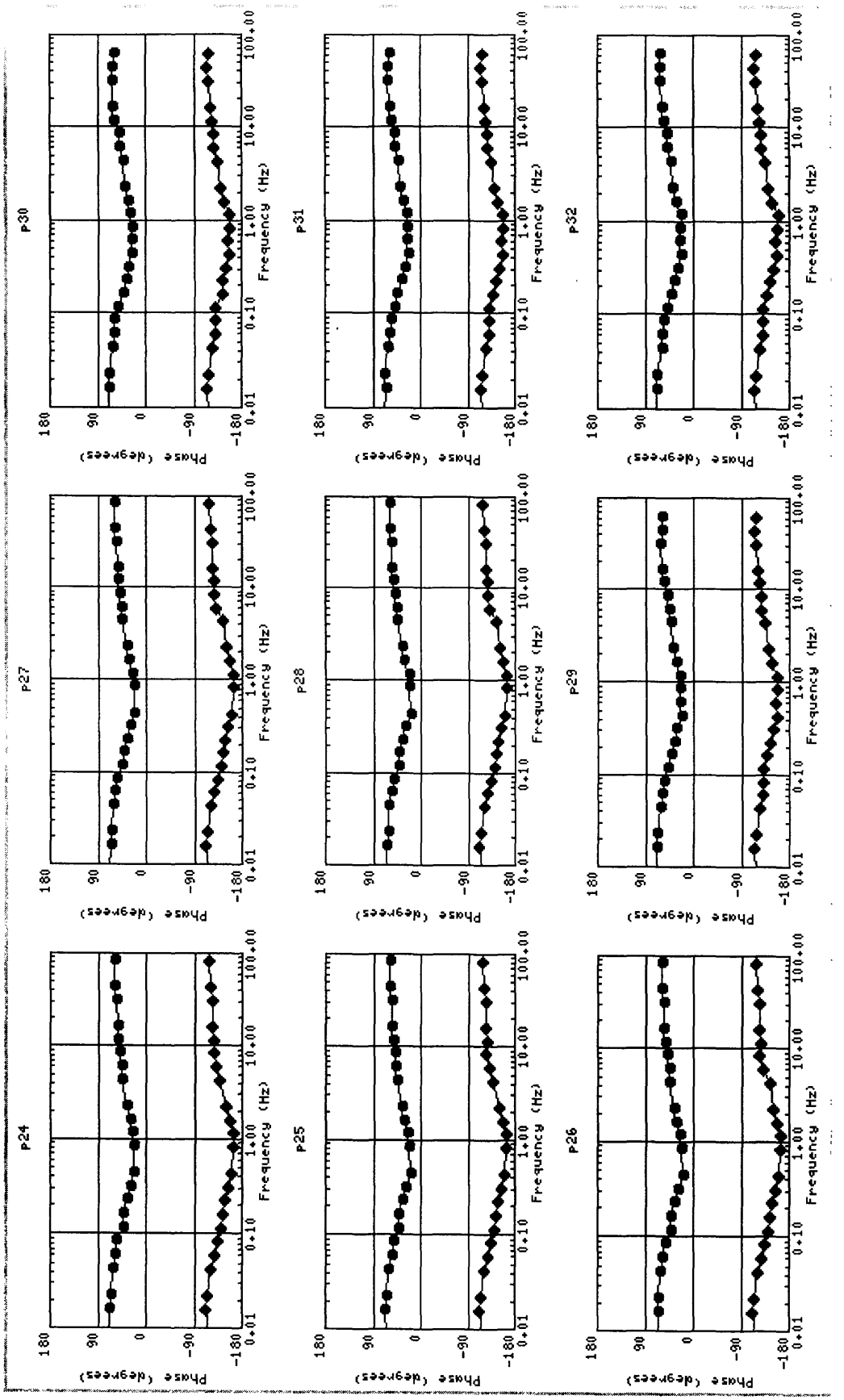

Figure B2.2: *Line p2 - Impedance Phase, site p15-p35*

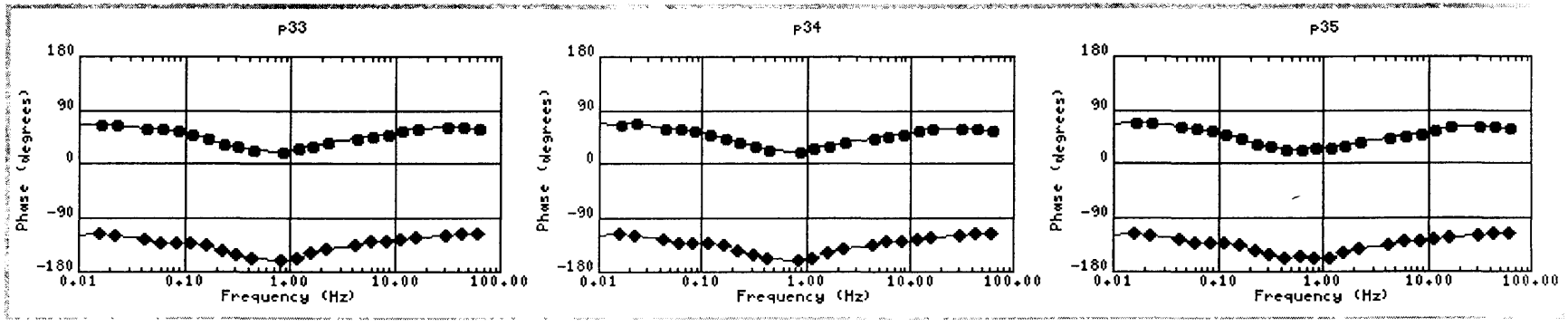

Figure B2.2: Line p2 - Impedance Phase, site p15-p35

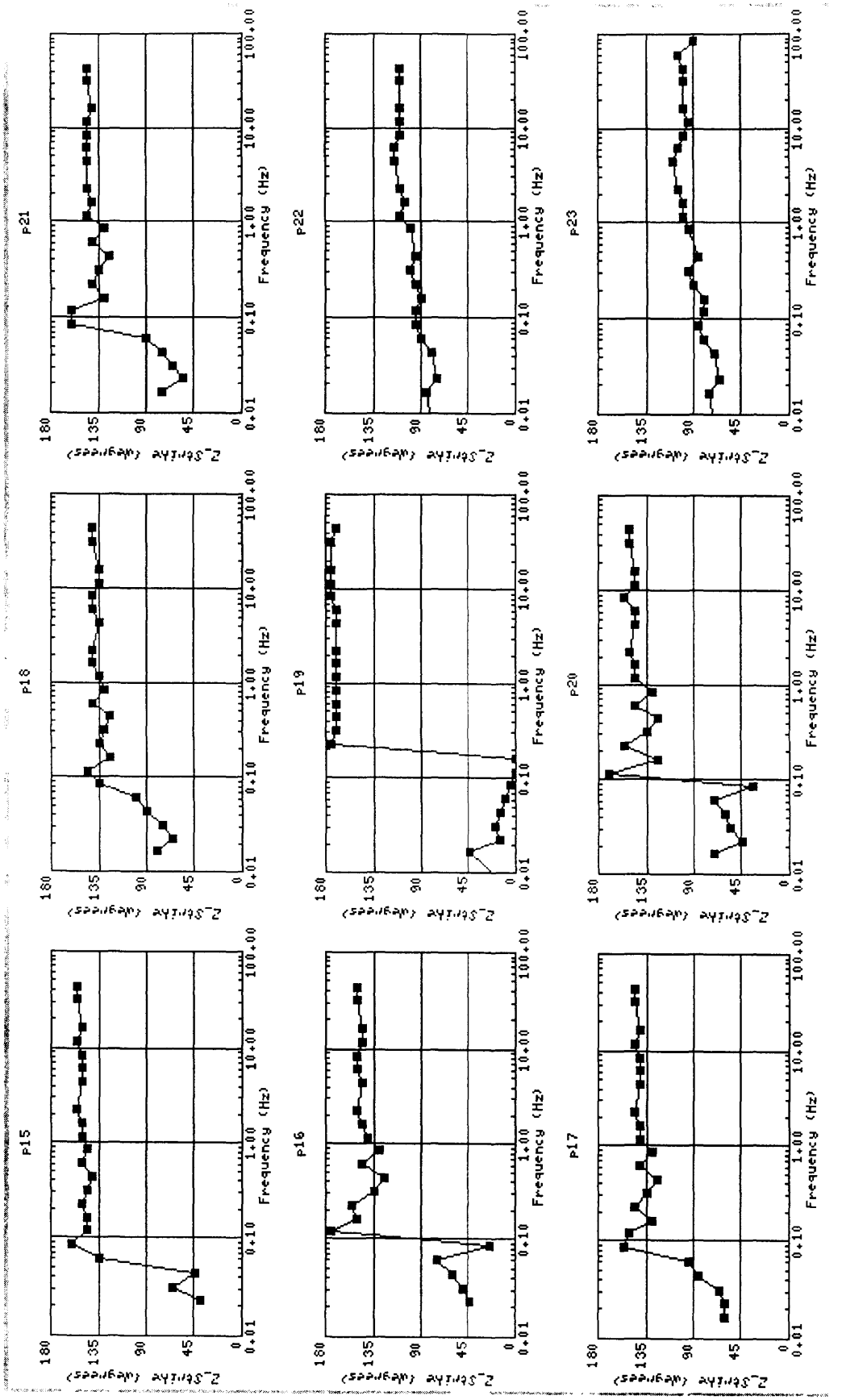

Figure B2.3: Line p2 - Impedance Strike, site p15-p35

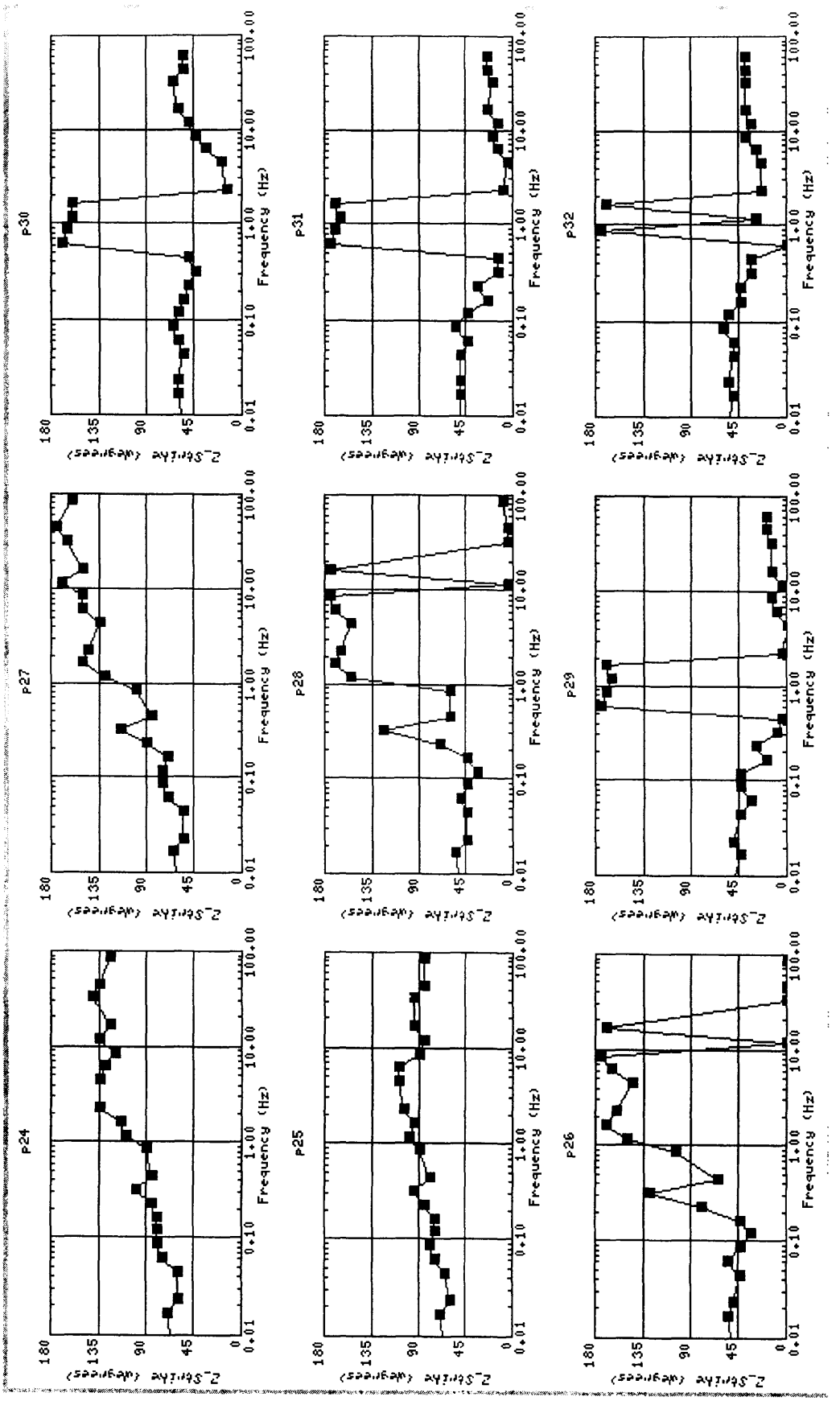

Figure B2.3: Line p2 - Impedance Strike, site p15-p35

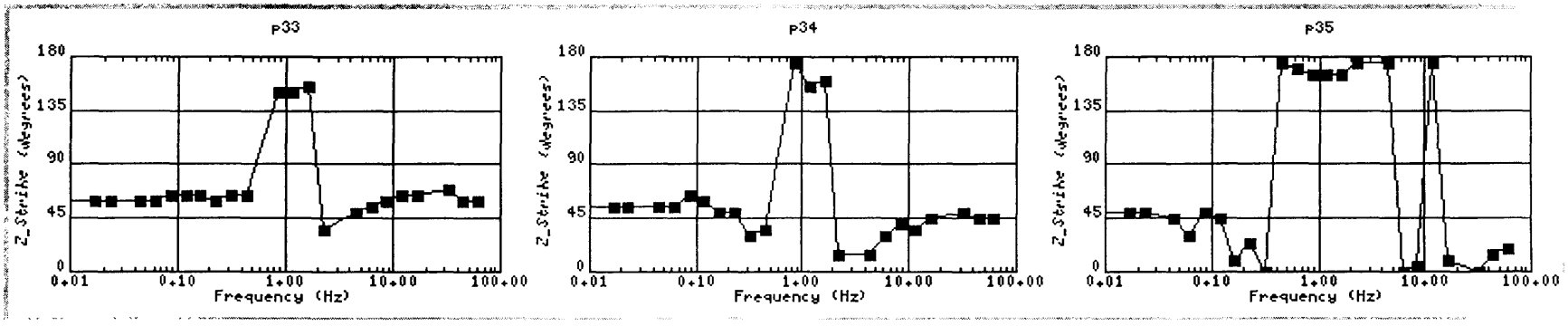

Figure B2.3: Line p2 - Impedance Strike, site p15-p35

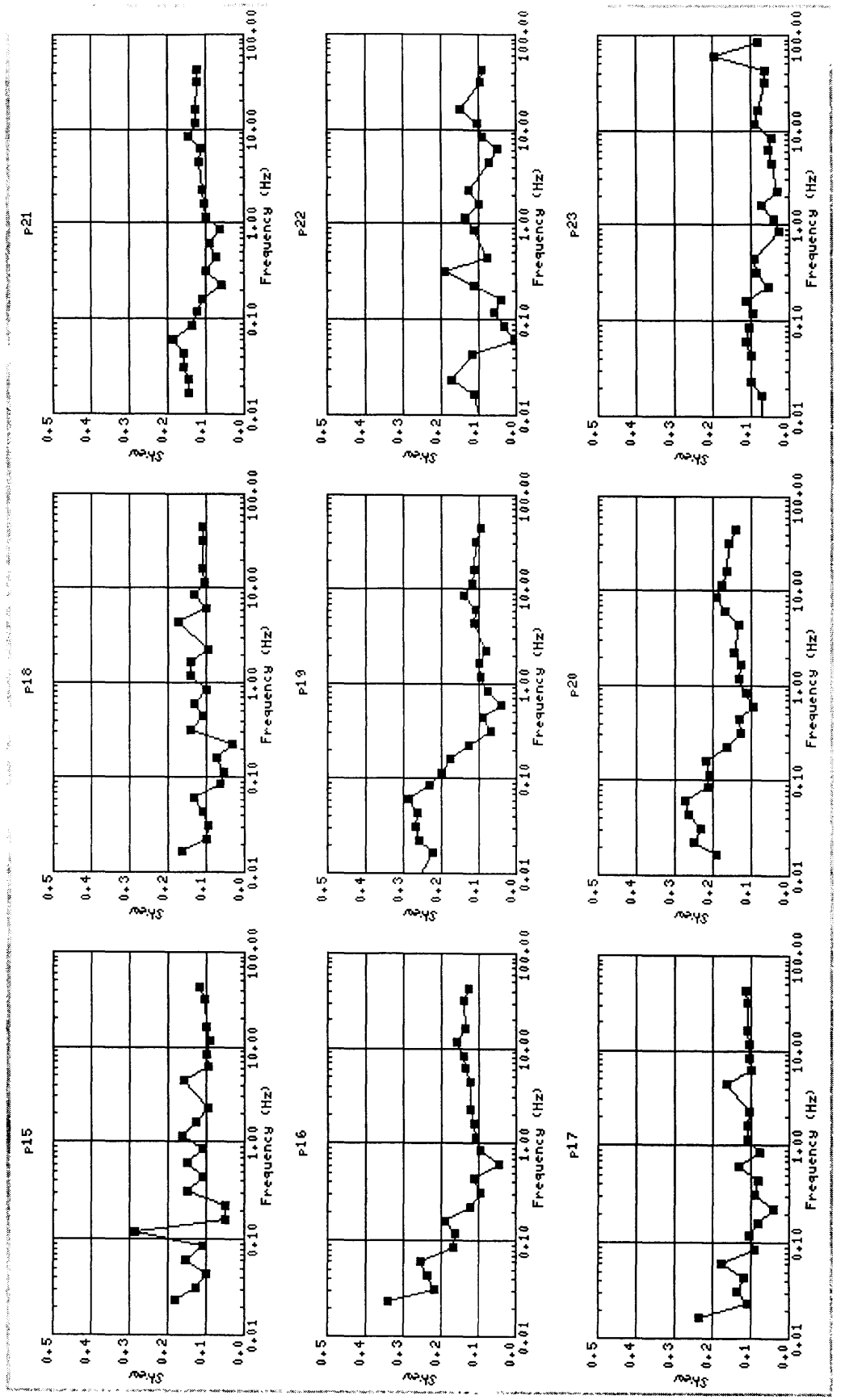

Figure B2.4: Line p2 - impedance Skew, site p15-p35

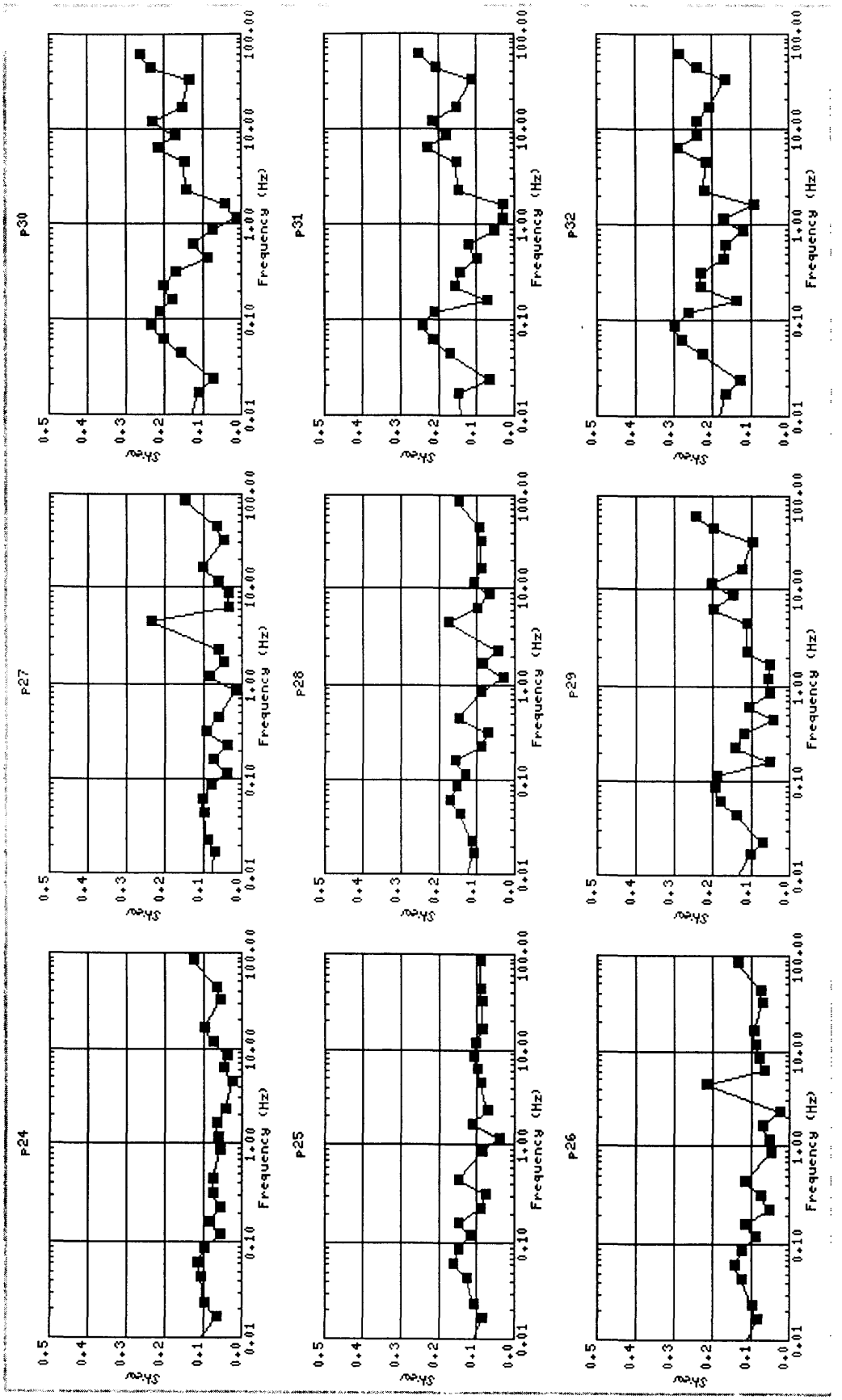

Figure B2.4: Line p2 - impedance Skew, site p15-p35

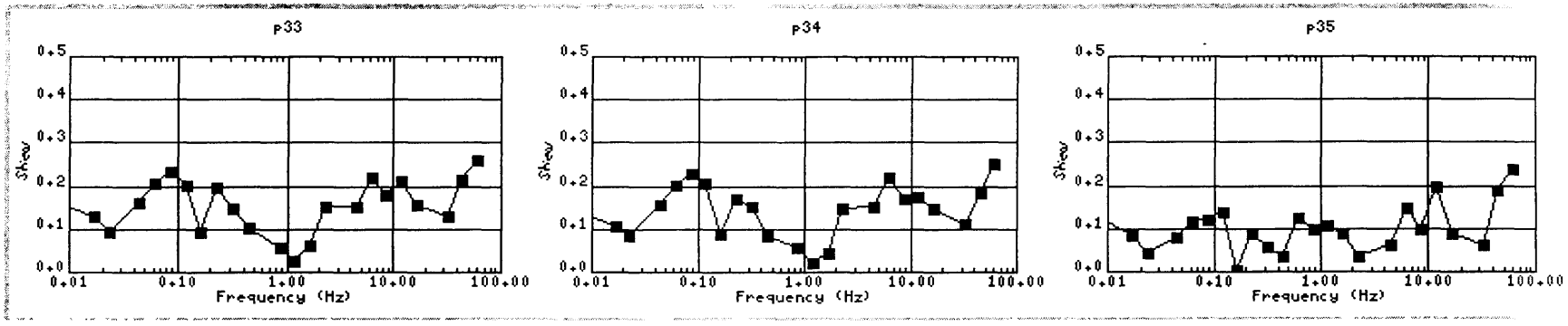

Figure B2.4: Line p2 - impedance Skew, site p15-p35

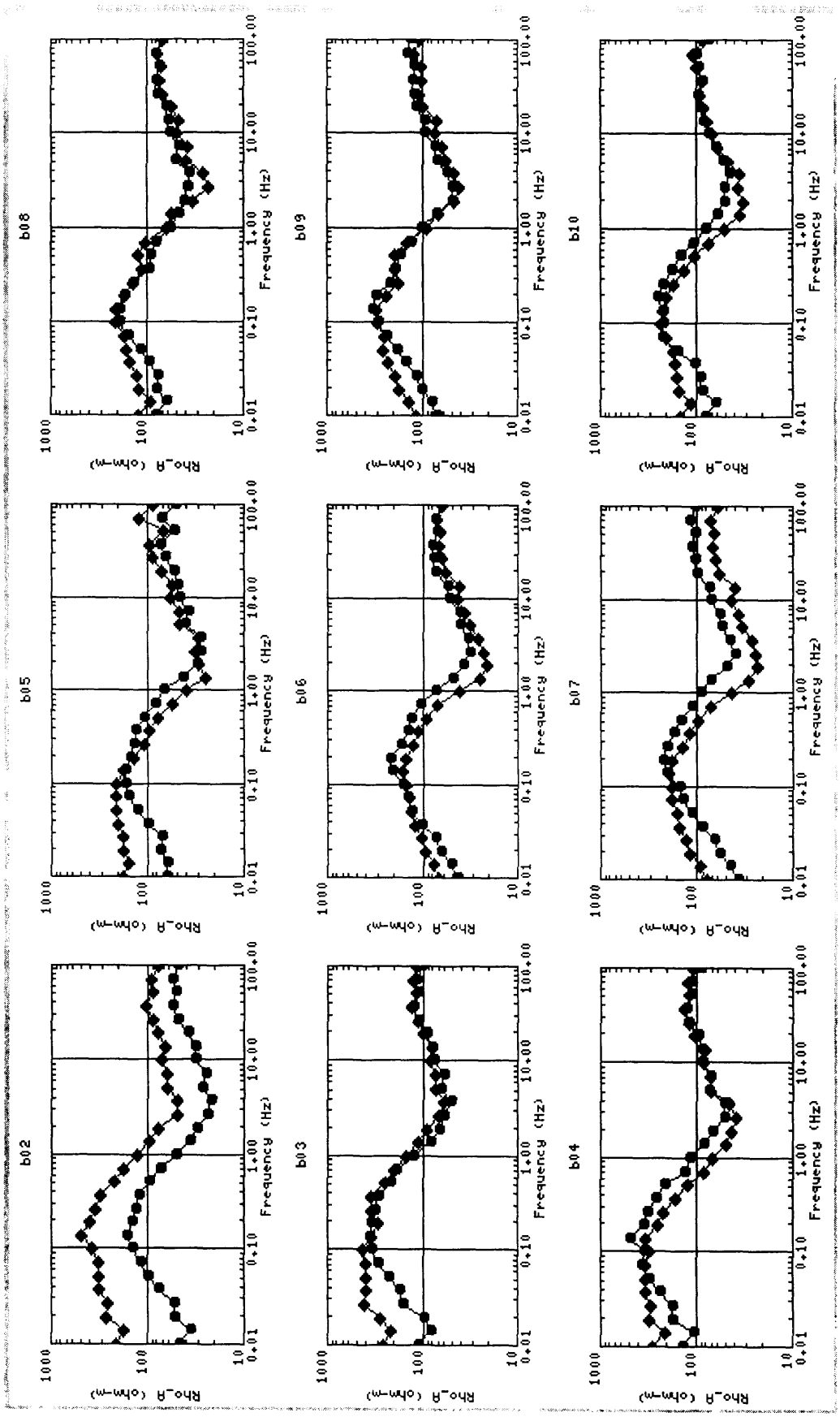

Figure B3.1: Line b - Apparent Resistivity, site b02-b09

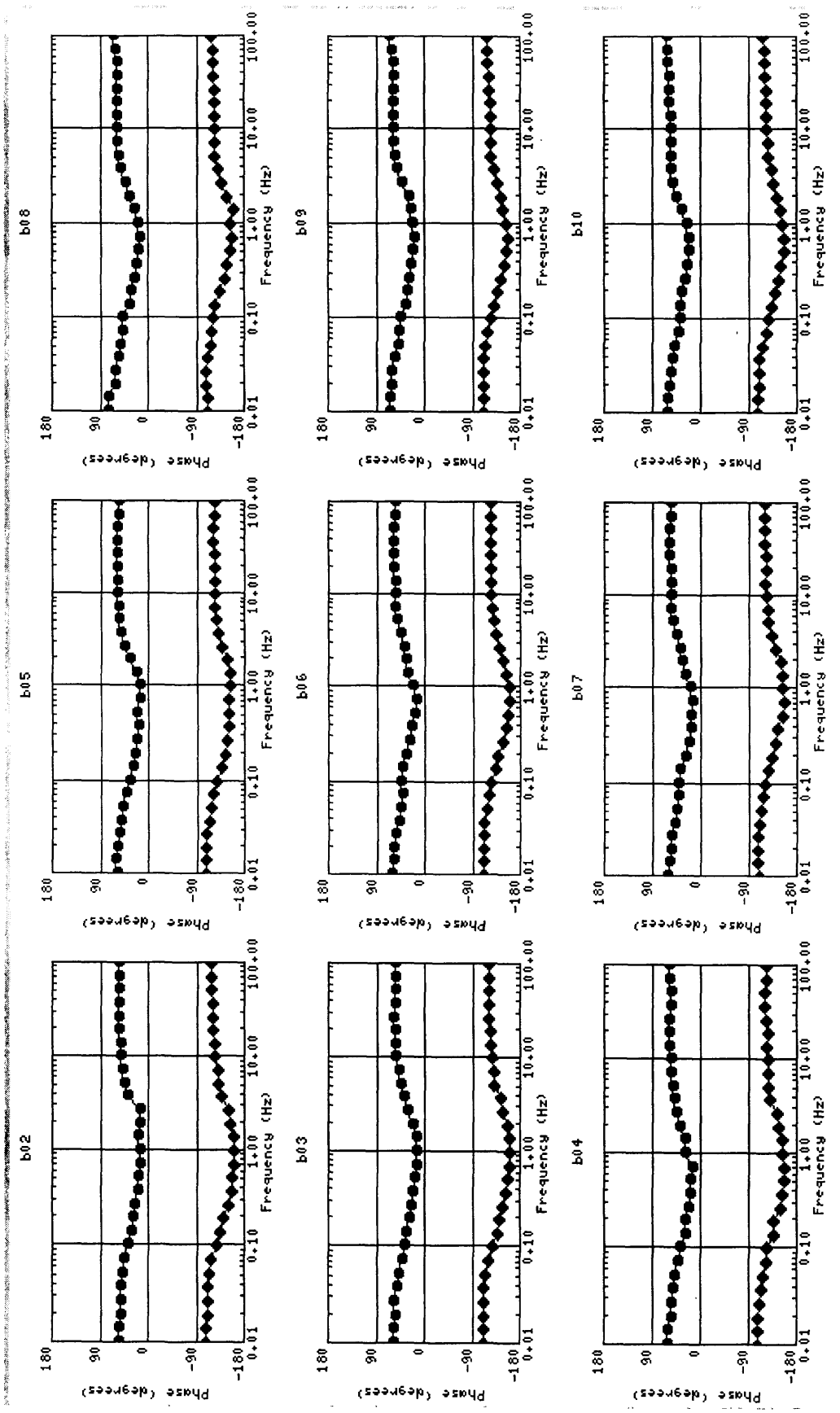

Figure B3.2: Line b - Impedance Phase, site b02-b09

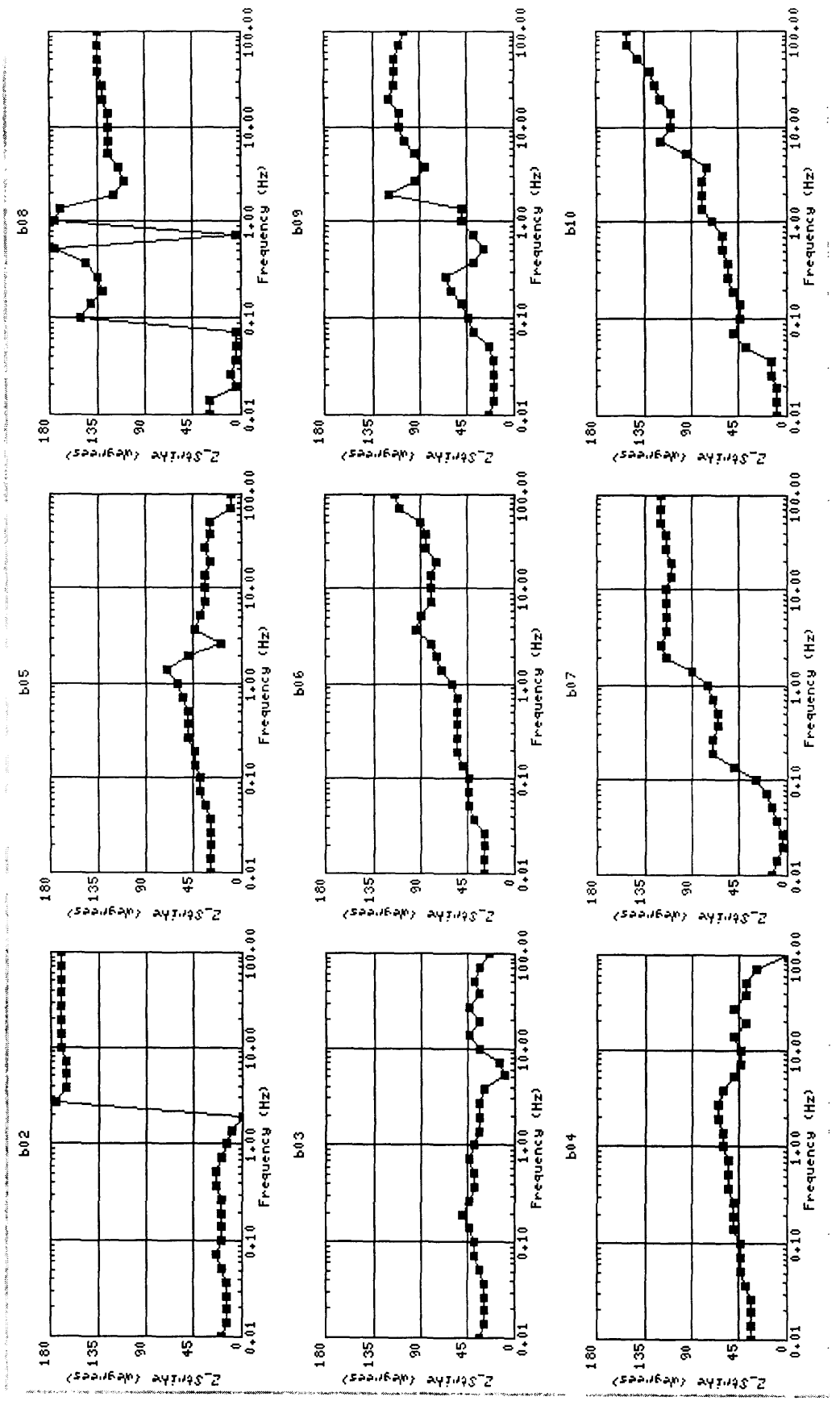

Figure B3.3: Line b - Impendance Strike, site b02-b09

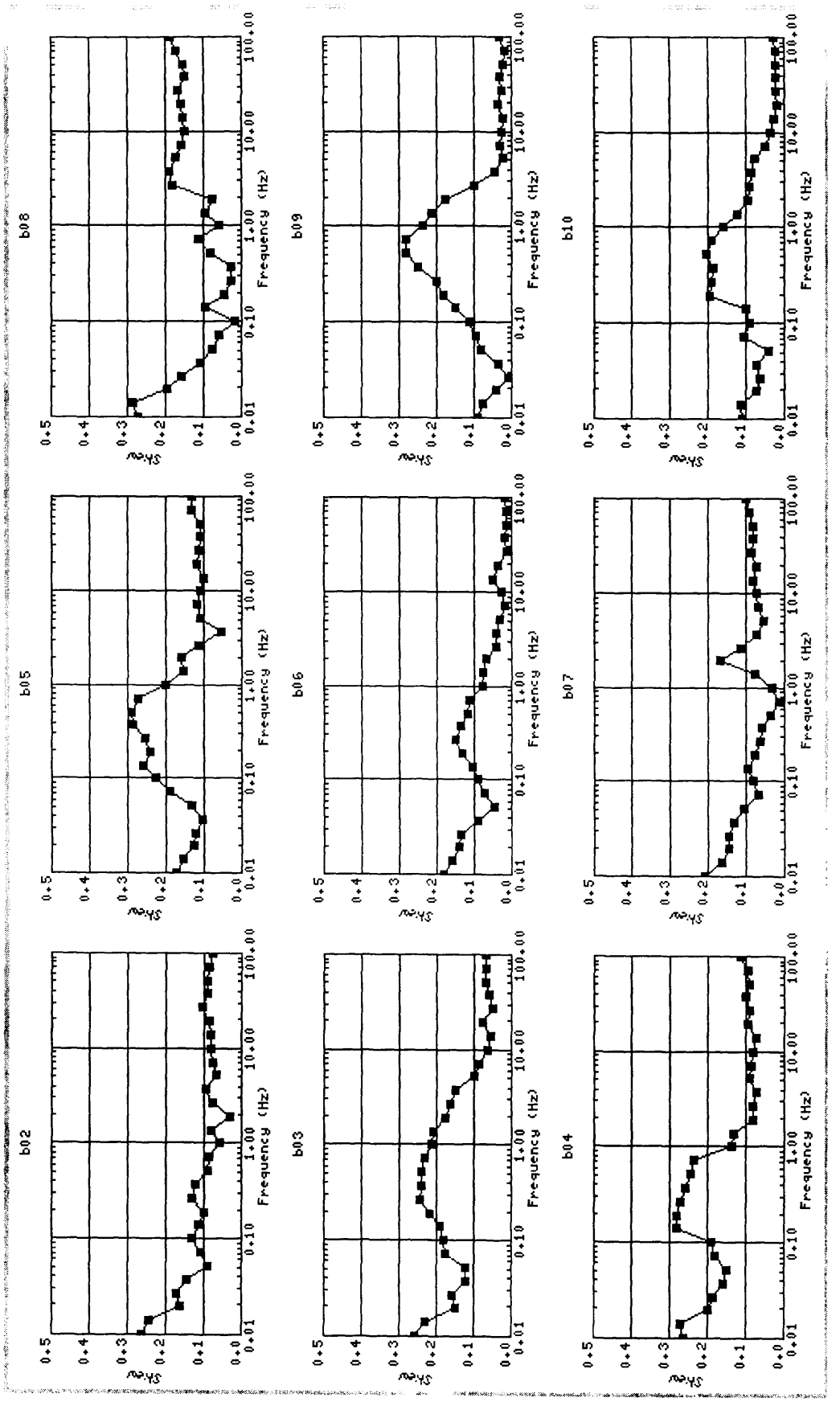

Figure B3.4: Line b - Impendance Skew, site b02-b09

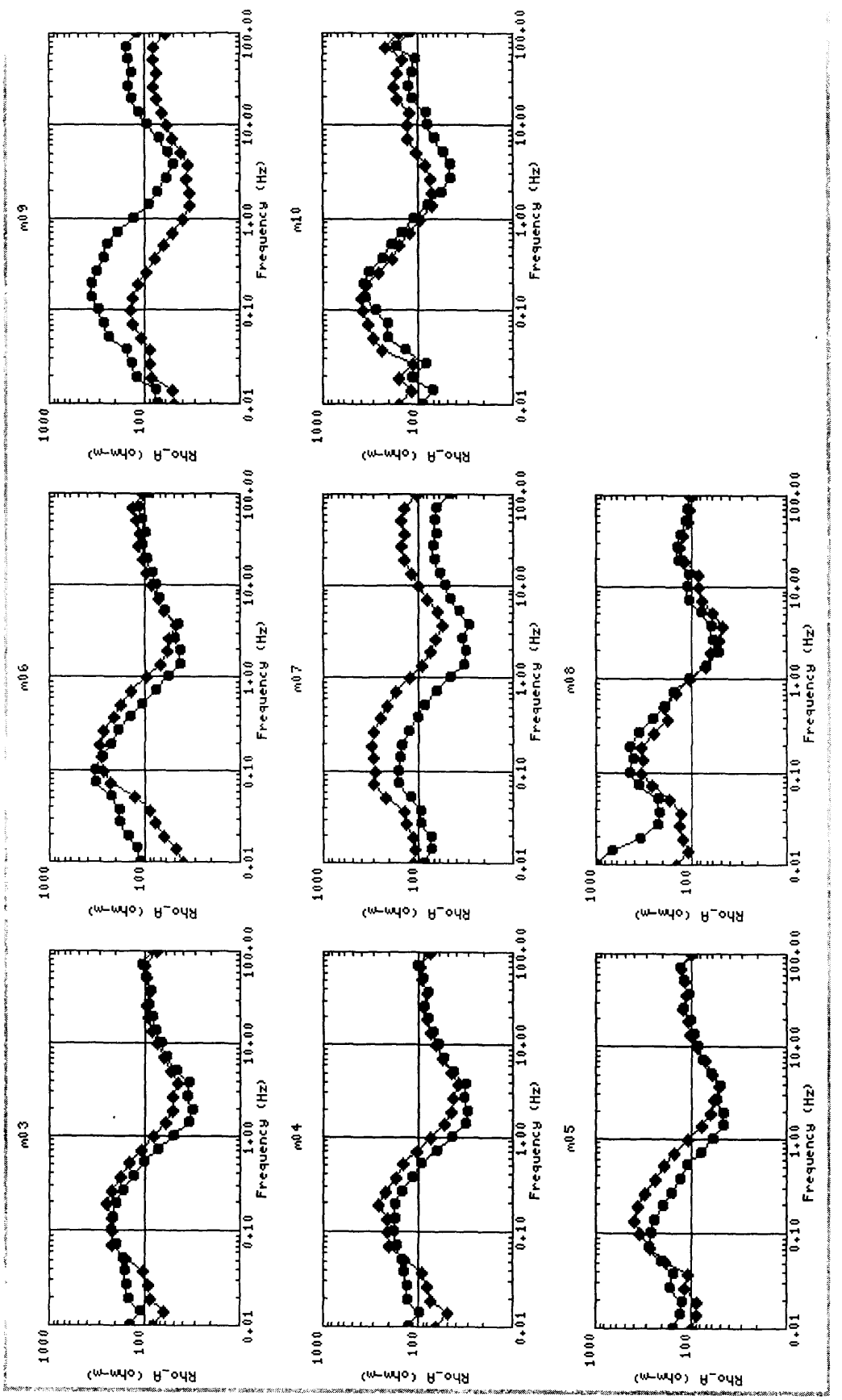

Figure B4.1: Line m - Apparent Resistivity, site m03-m10

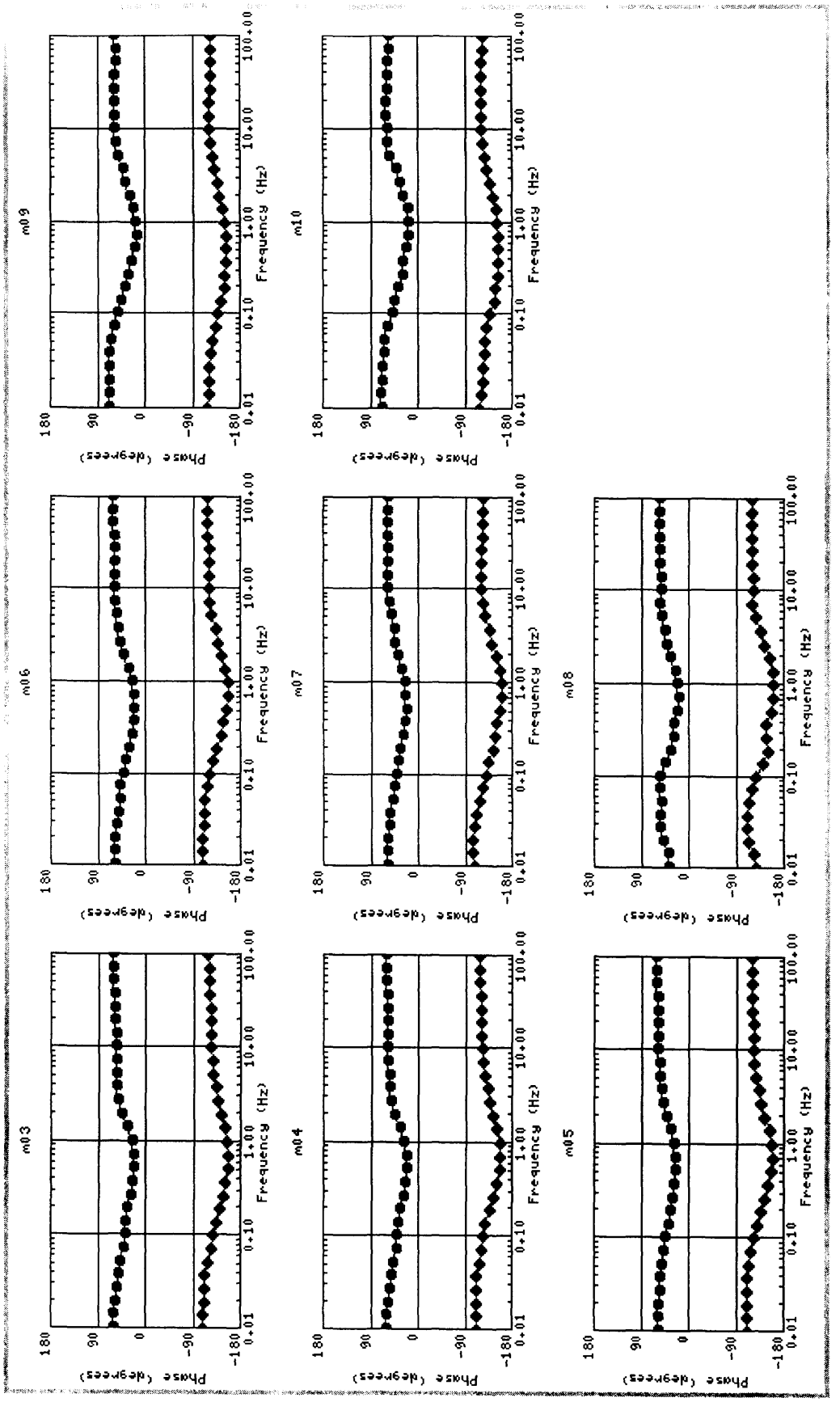

Figure B4.2: Line m - Impedance Phase, site m03-m10

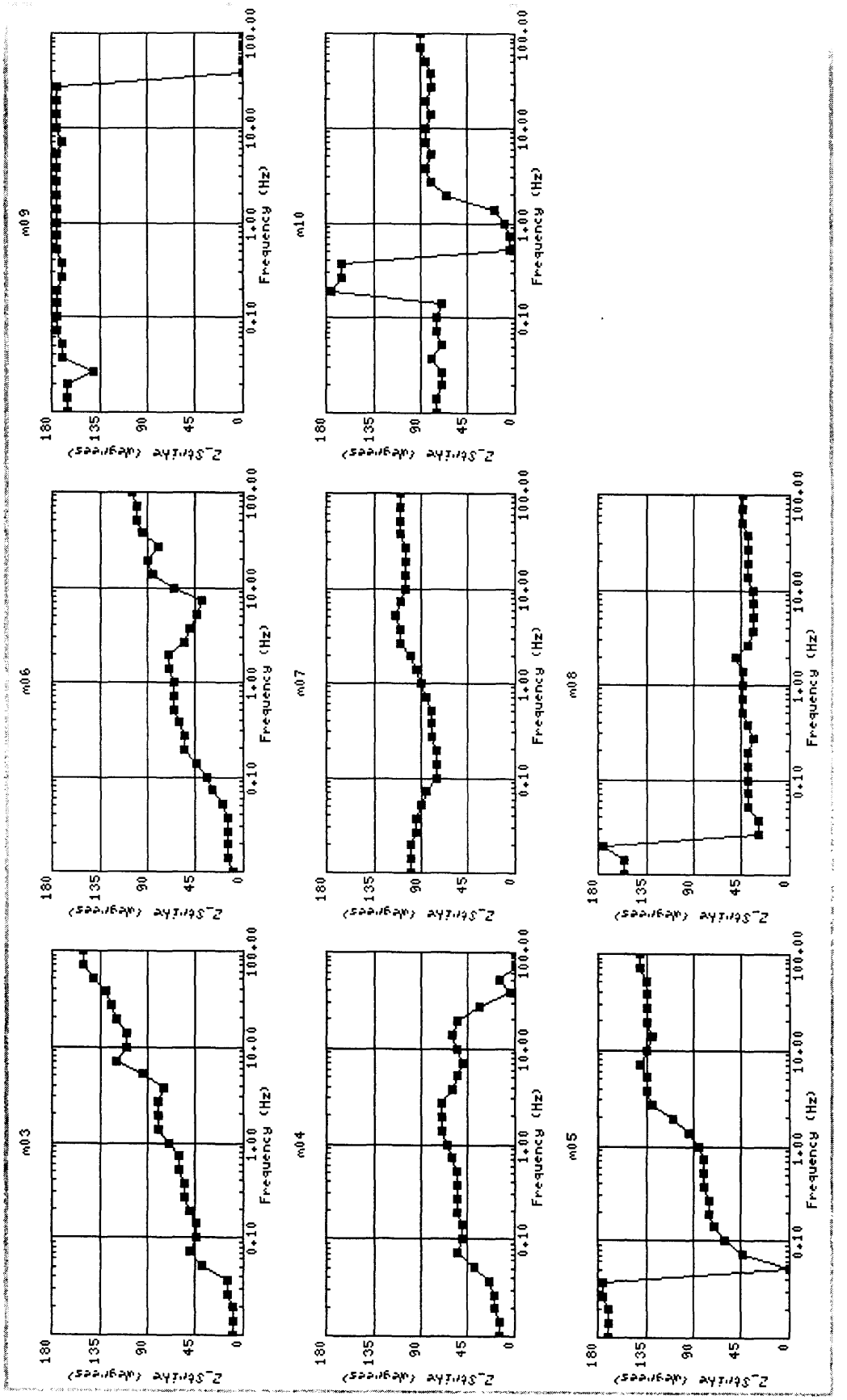

Figure B4.3: Line m - Impedance Strike, site m03-m10

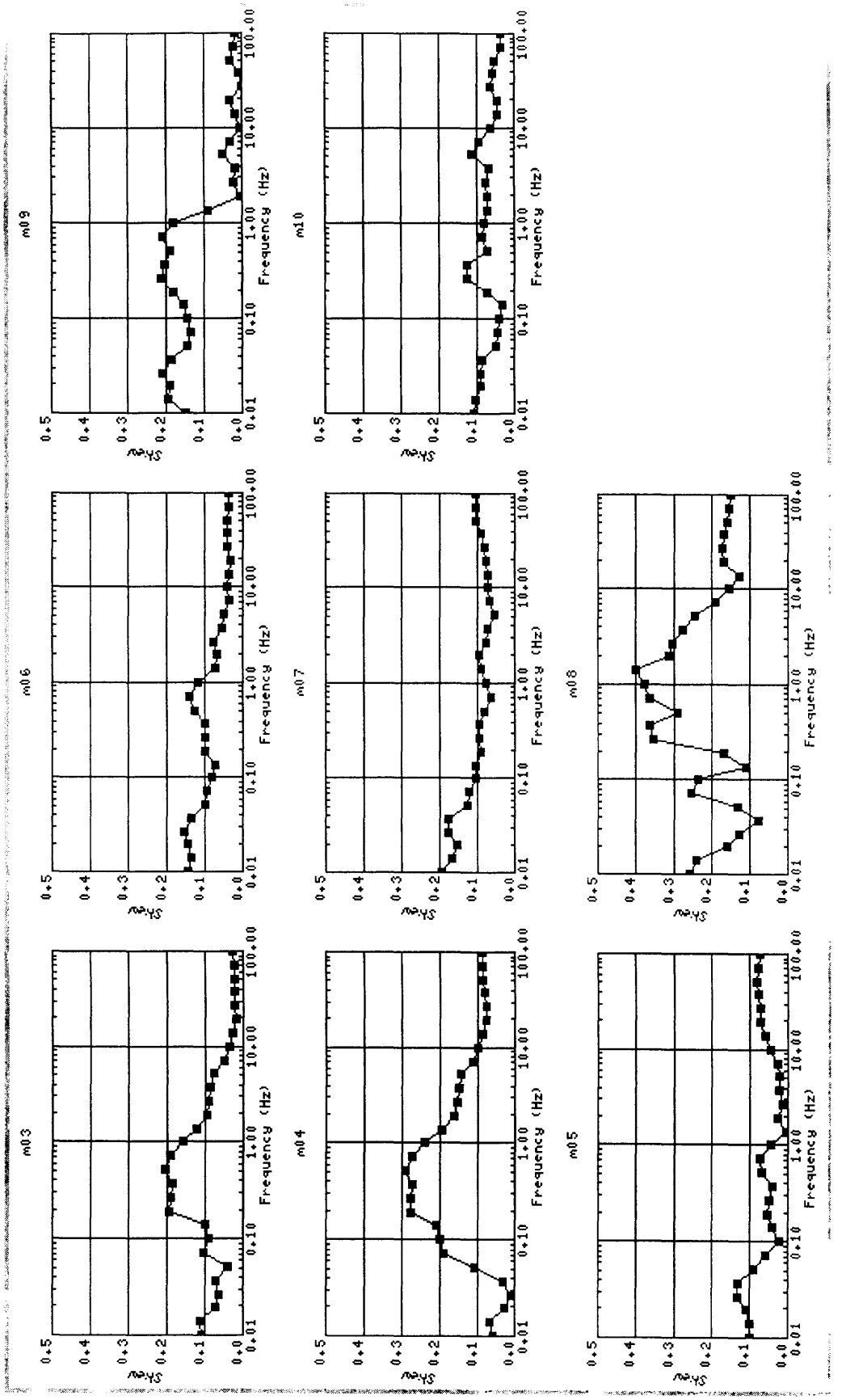

Figure B4.4: Line m - Impedance Skew, site m03-m10

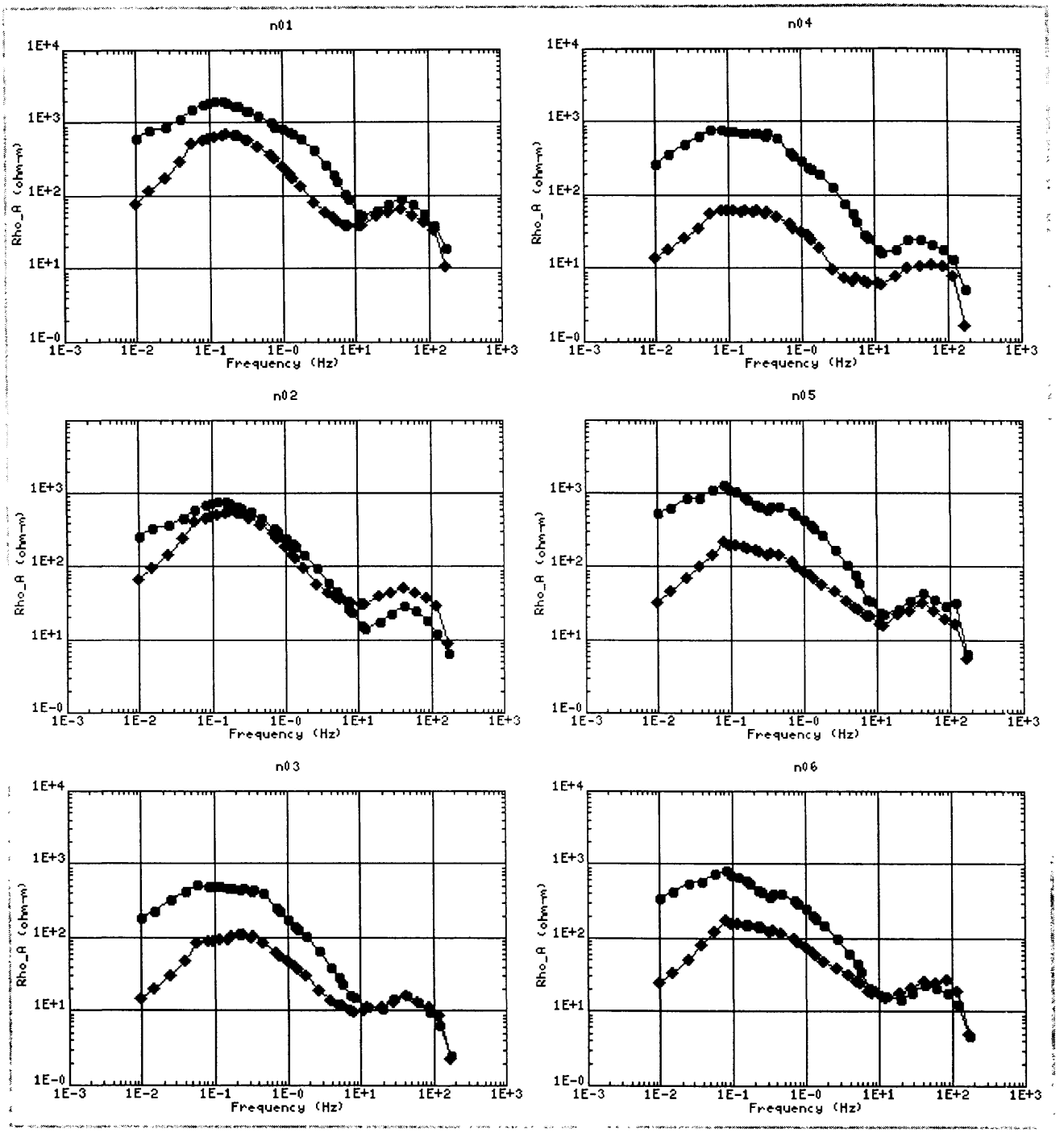

Figure B5.1: Line n - Apparent Resistivity, site n01-n14

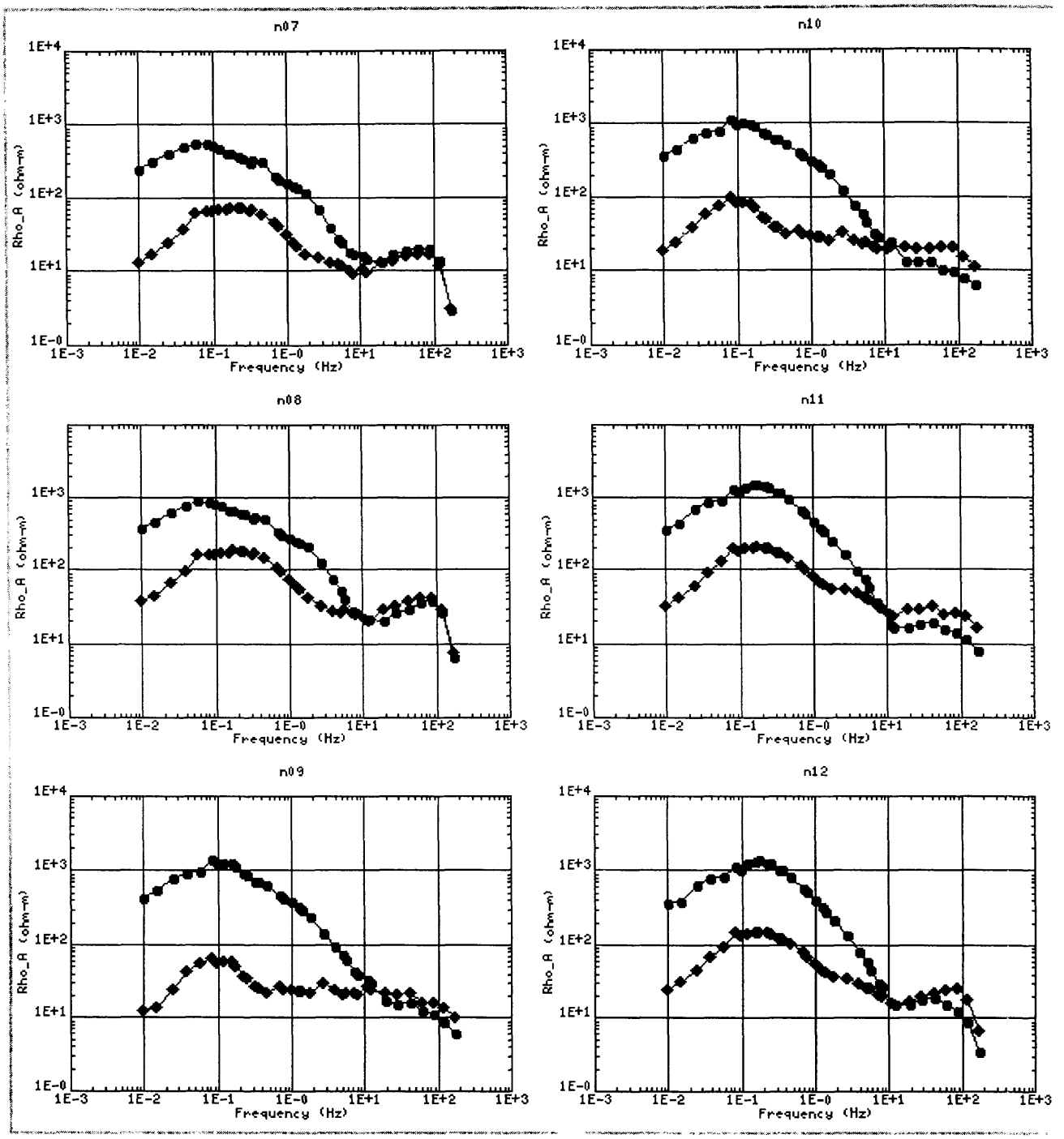

Figure B5.1: Line n - Apparent Resistivity, site n01-n14

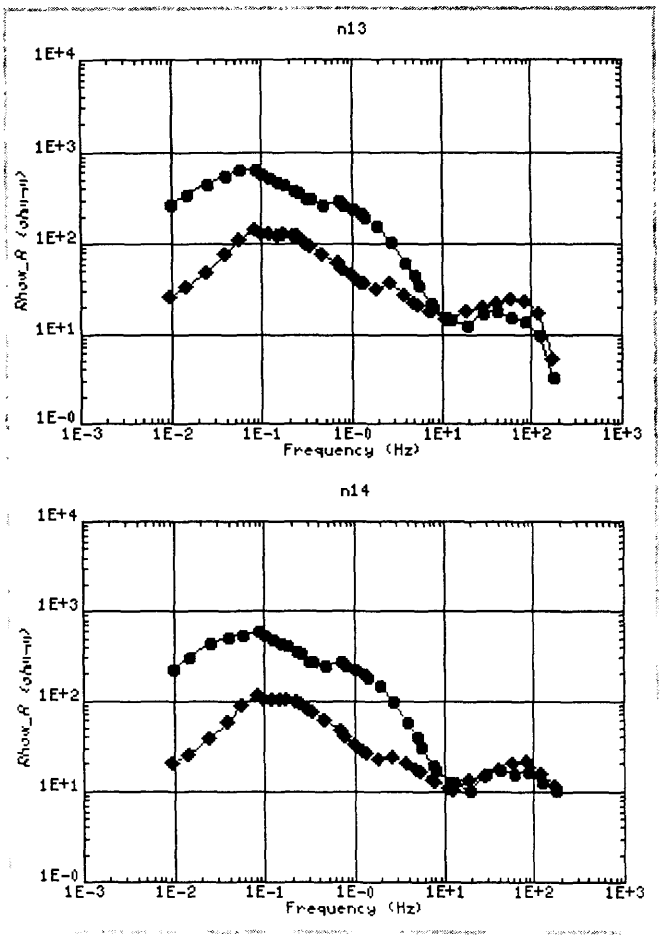

Figure B5.1: Line n - Apparent Resistivity, site n01-n14

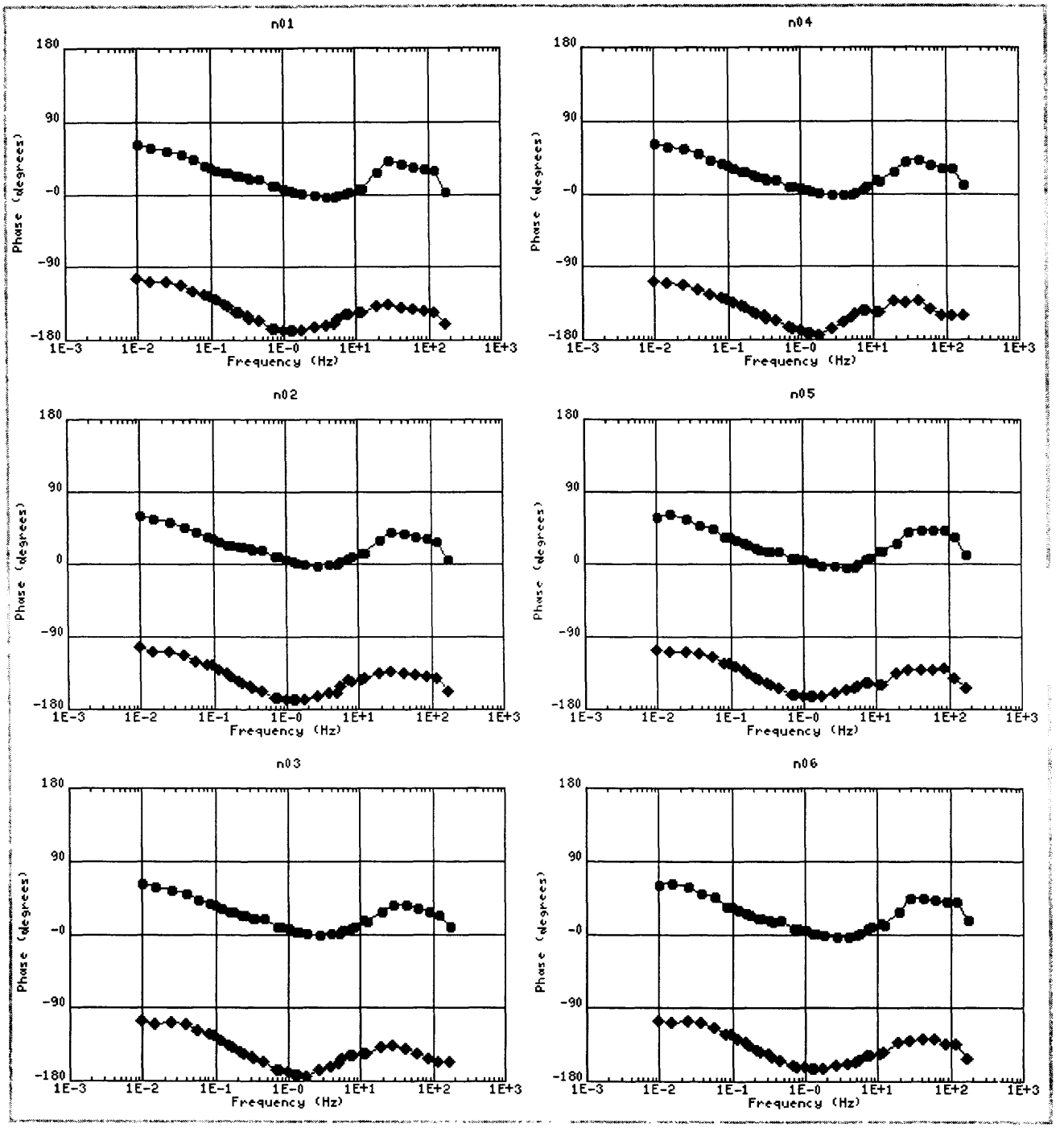

Figure B5.2: Line n - Impedance Phase, site n01-n14

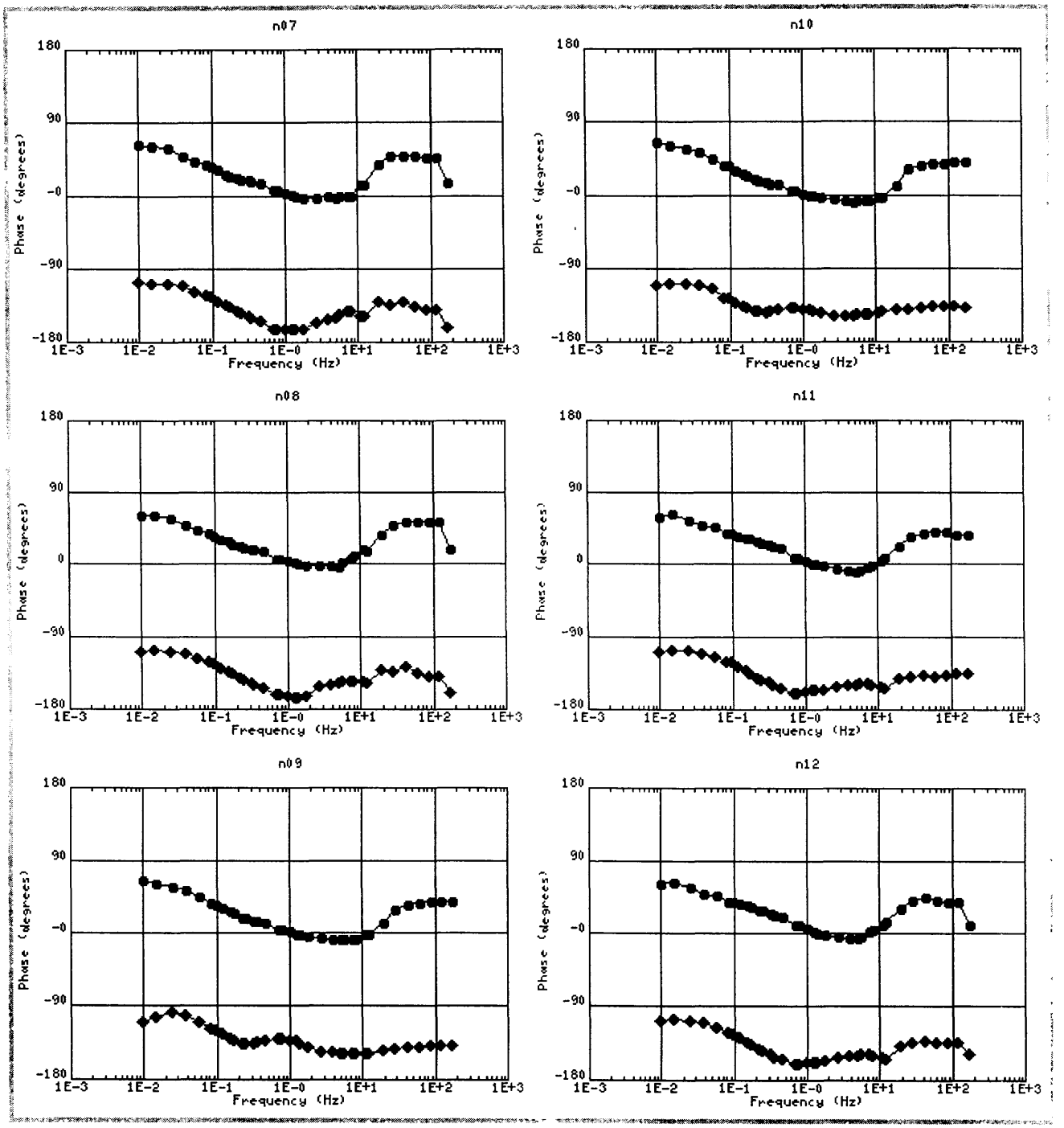

Figure B5.2: Line n - Impedance Phase, site n01-n14

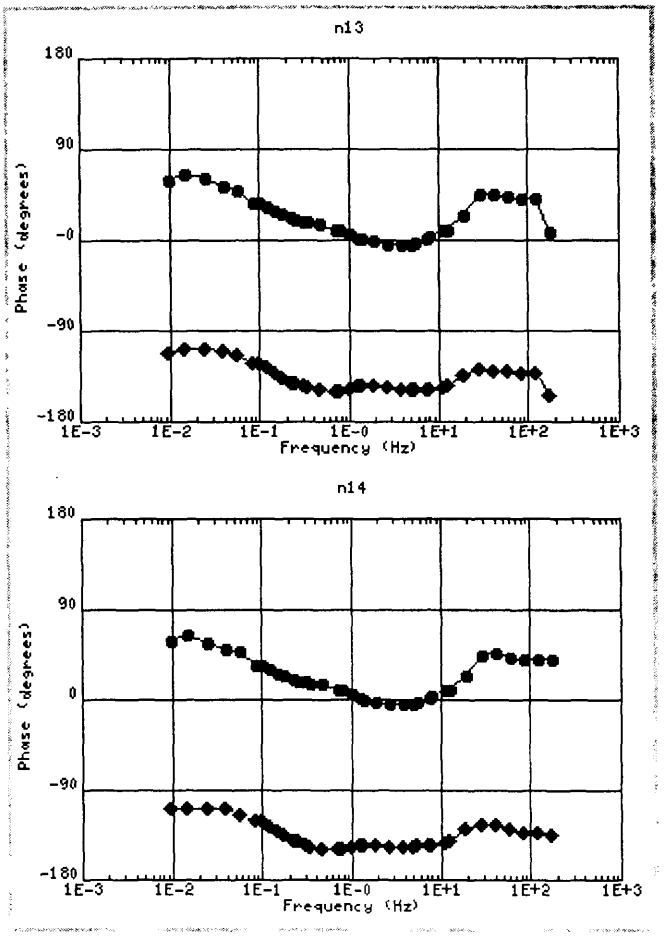

Figure B5.2: Line n - Impedance Phase, site n01-n14

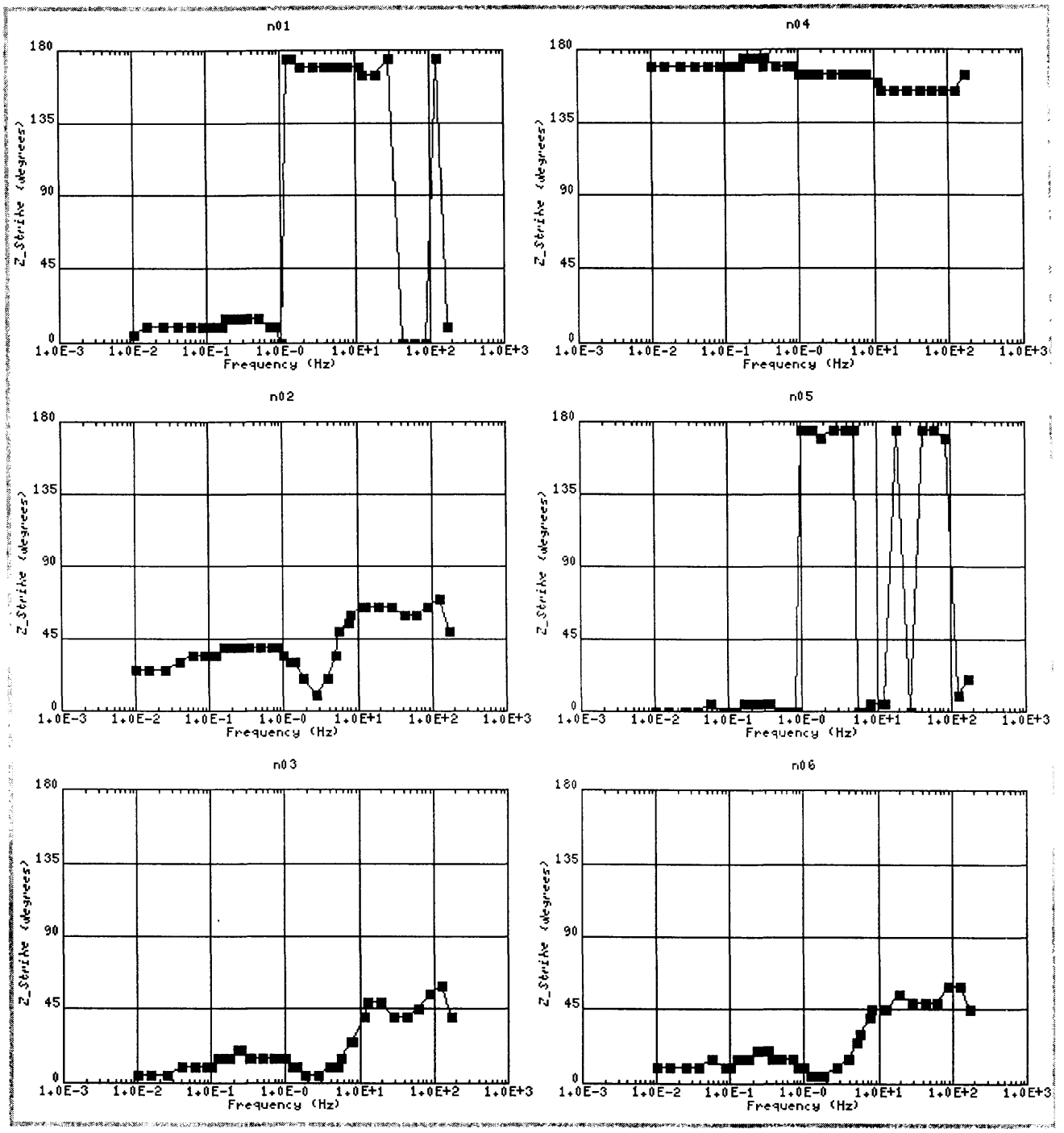

Figure B5.3: Line n - Impedance Strike, site n01-n14

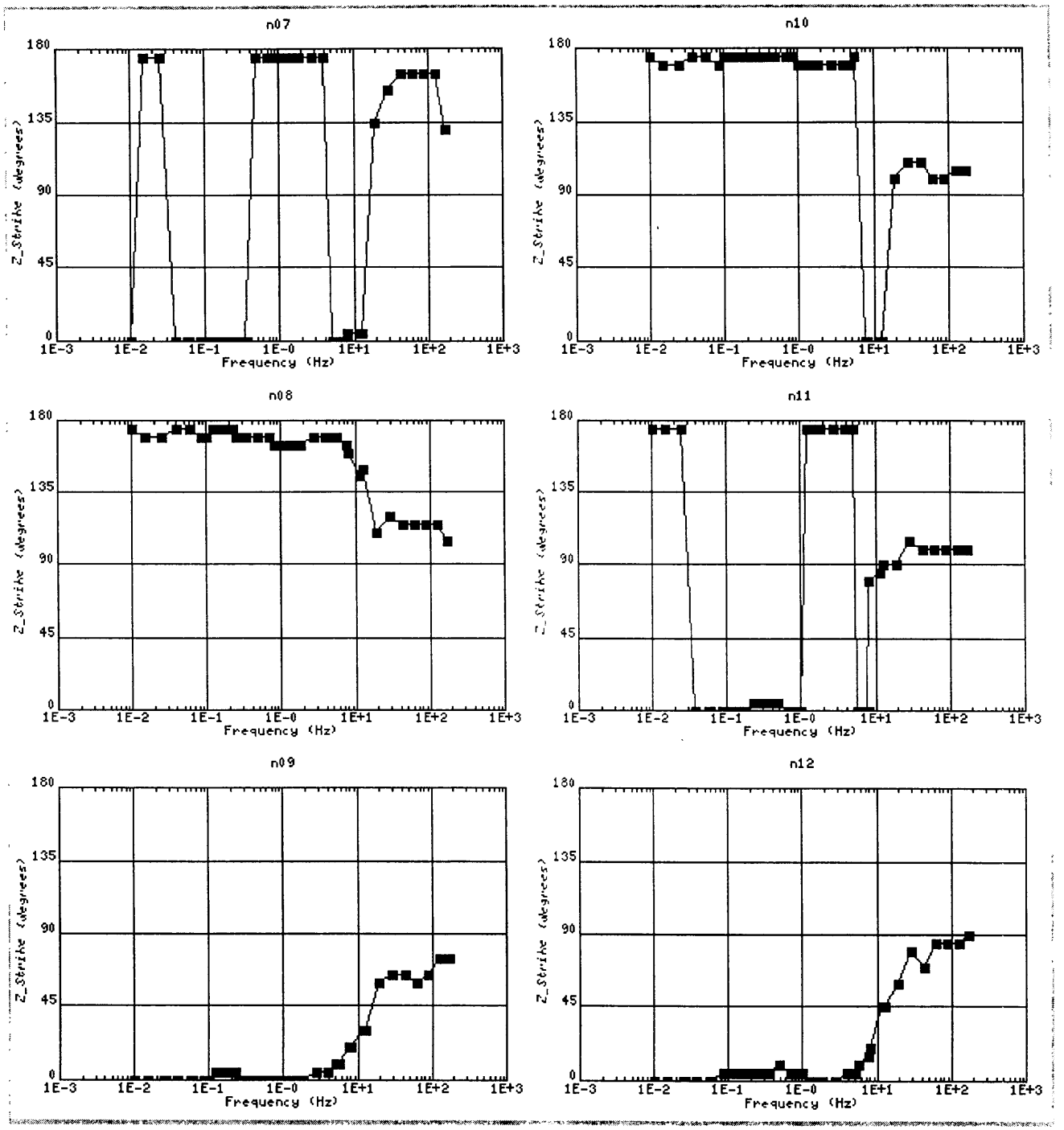

Figure B5.3: Line n - Impedance Strike, site n01-n14

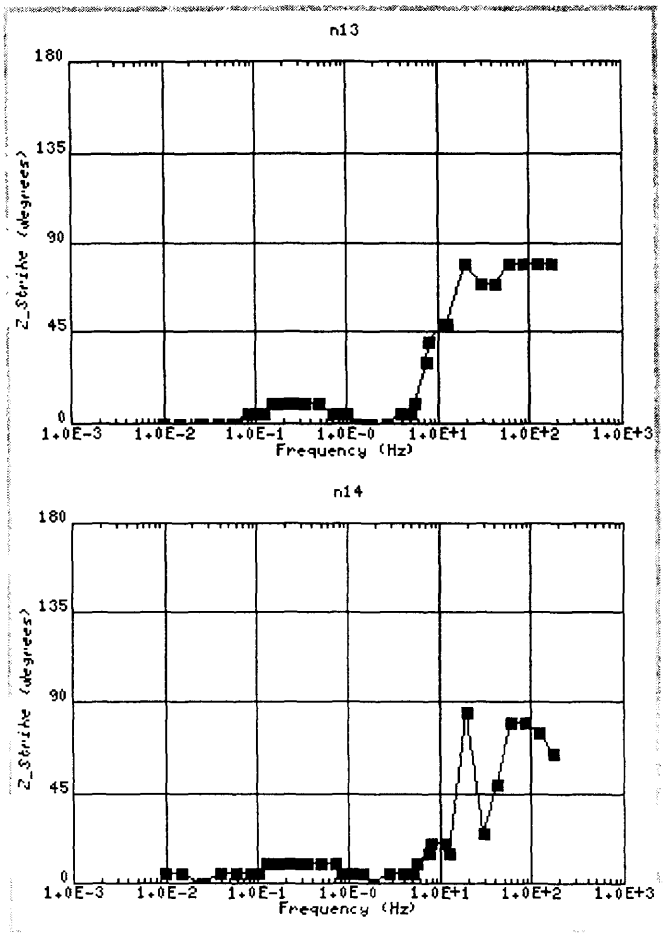

Figure B5.3: Line n - Impedance Strike, site n01-n14

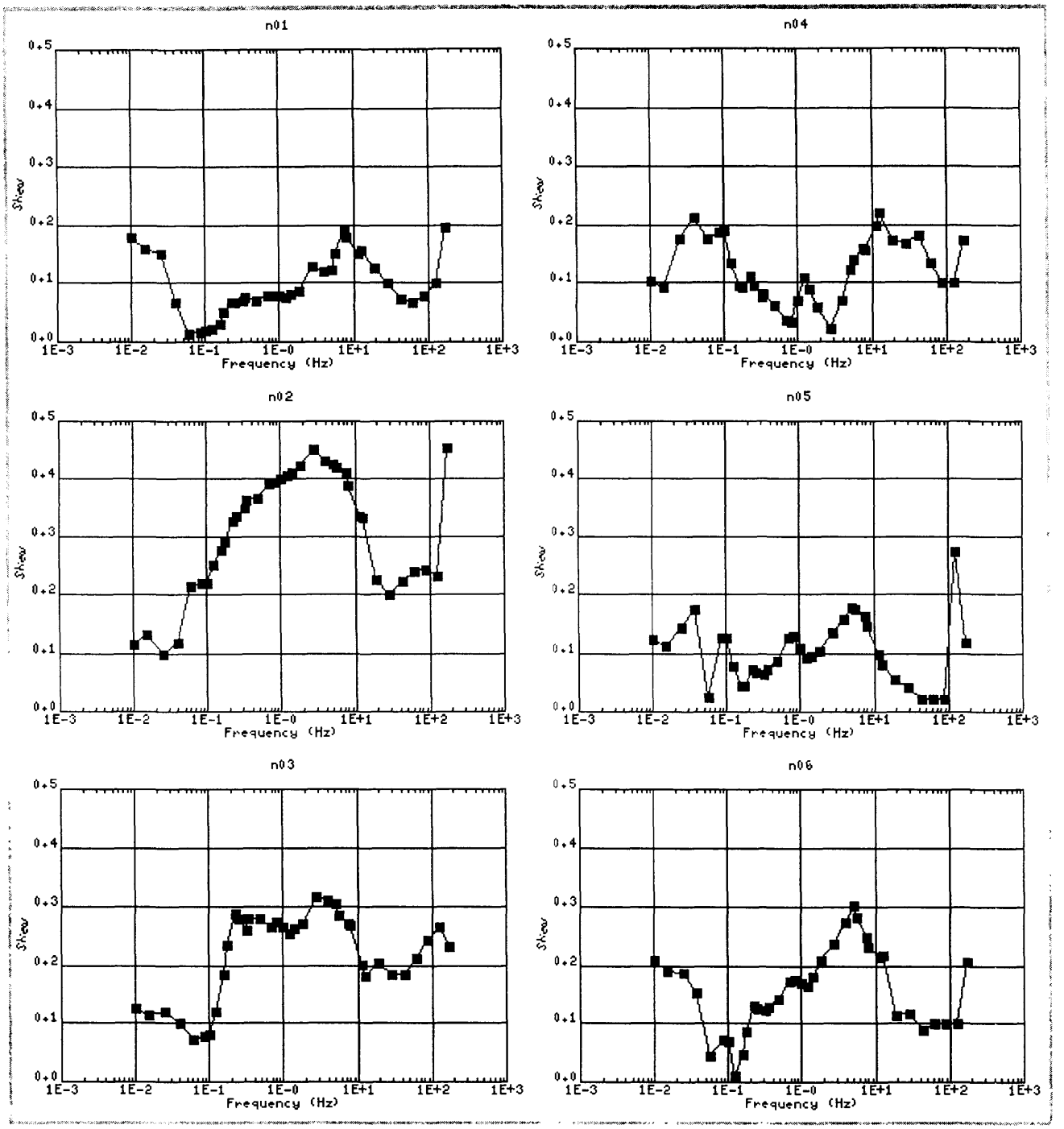

Figure B5.4: Line n - Impedance Skew, site n01-n14

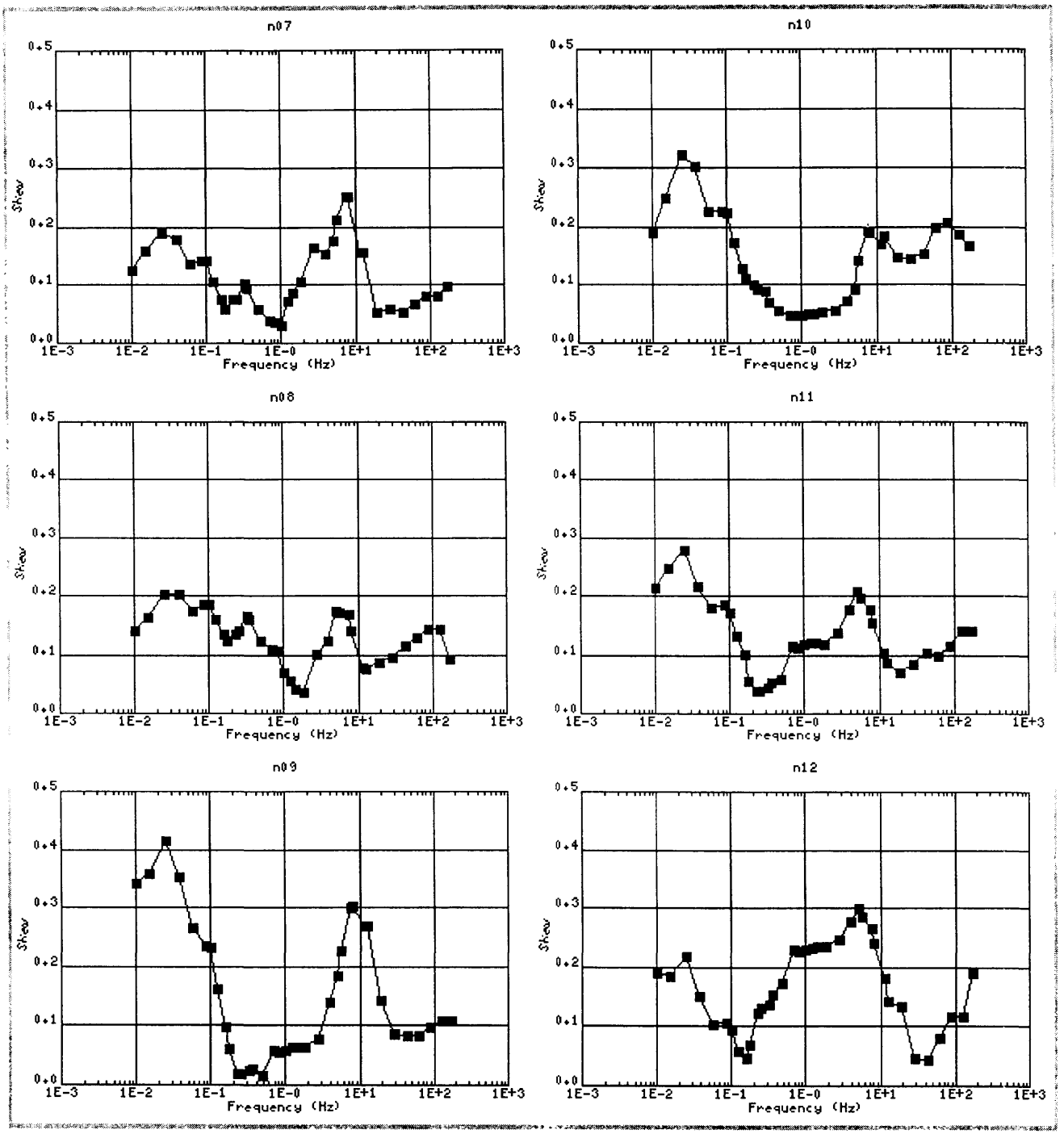

Figure B5.4: Line n - Impedance Skew, site n01-n14

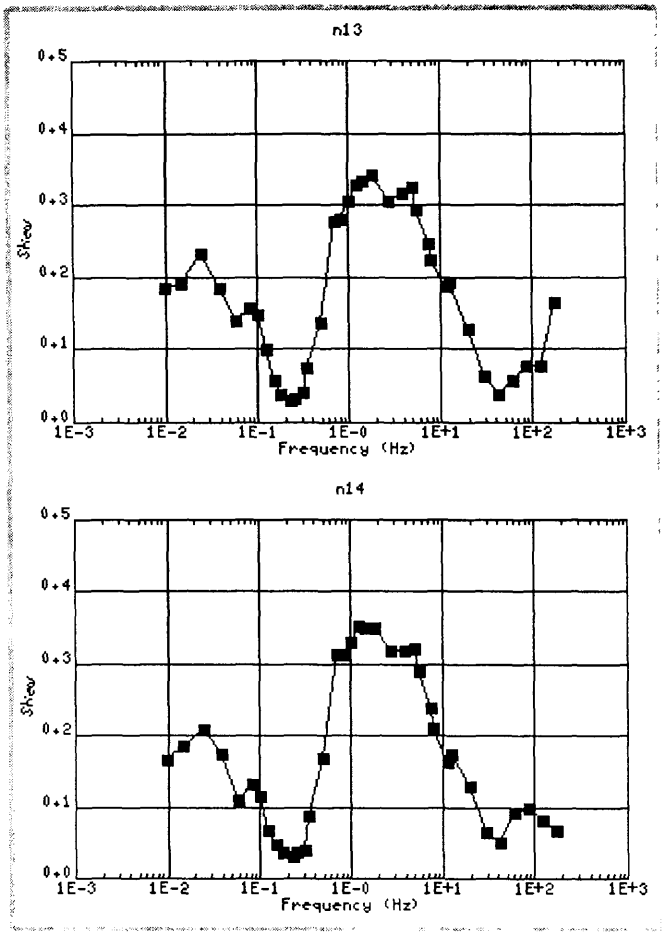

Figure B5.4: Line n - Impedance Skew, site n01-n14

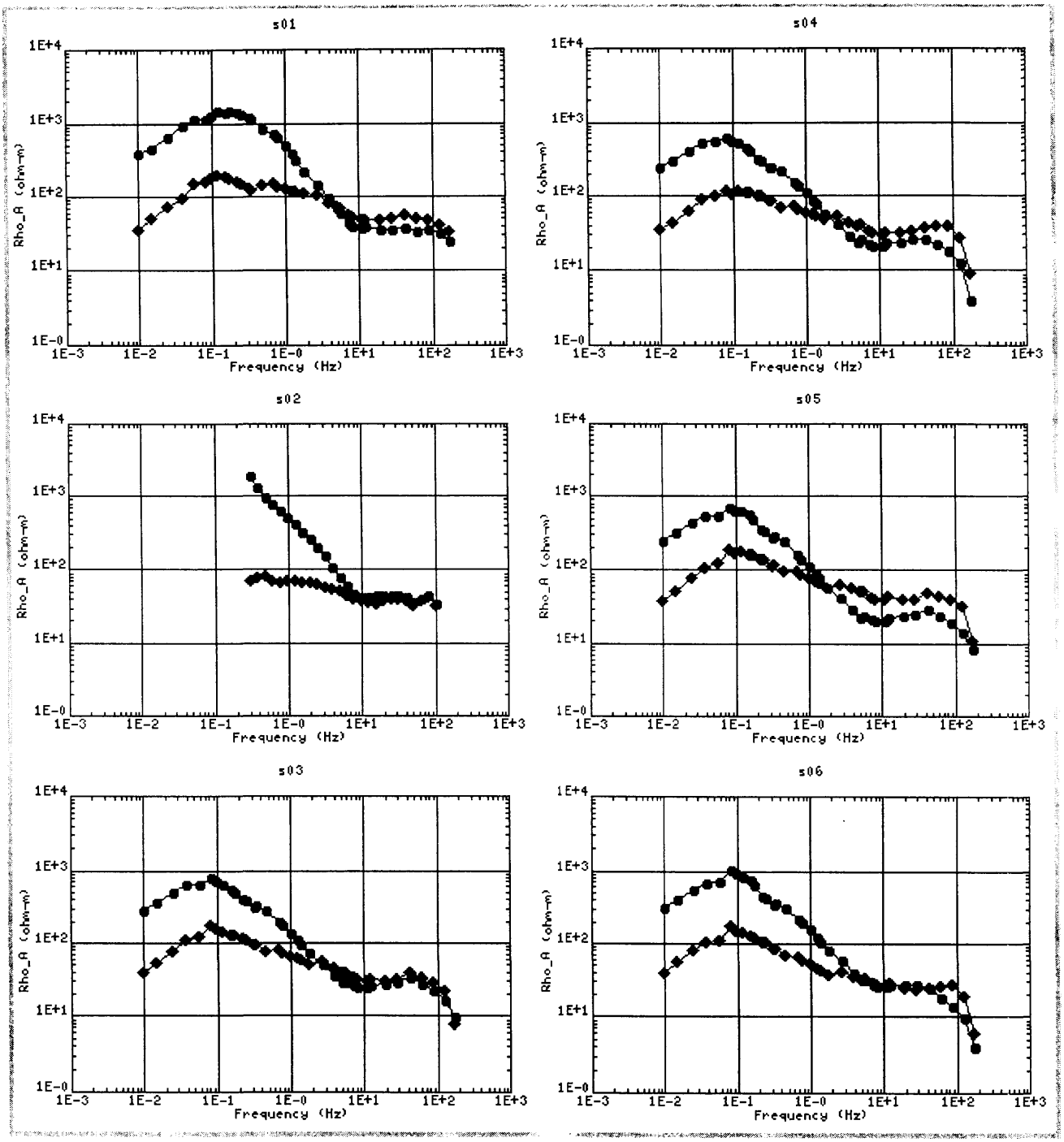

Figure B6.1: Line s - Apparent Resistivity, site s01-s26

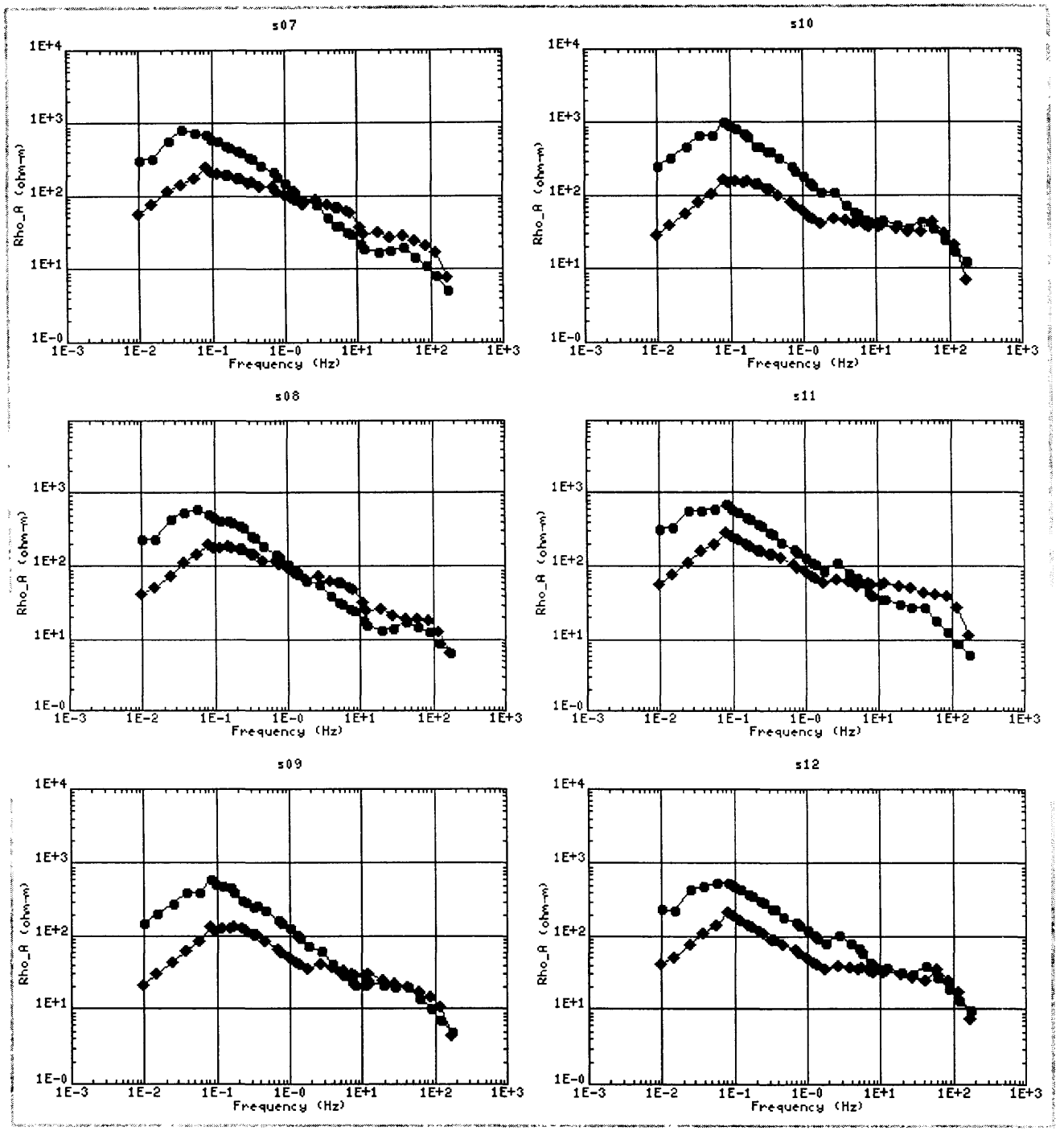

Figure B6.1: Line s - Apparent Resistivity, site s01-s26

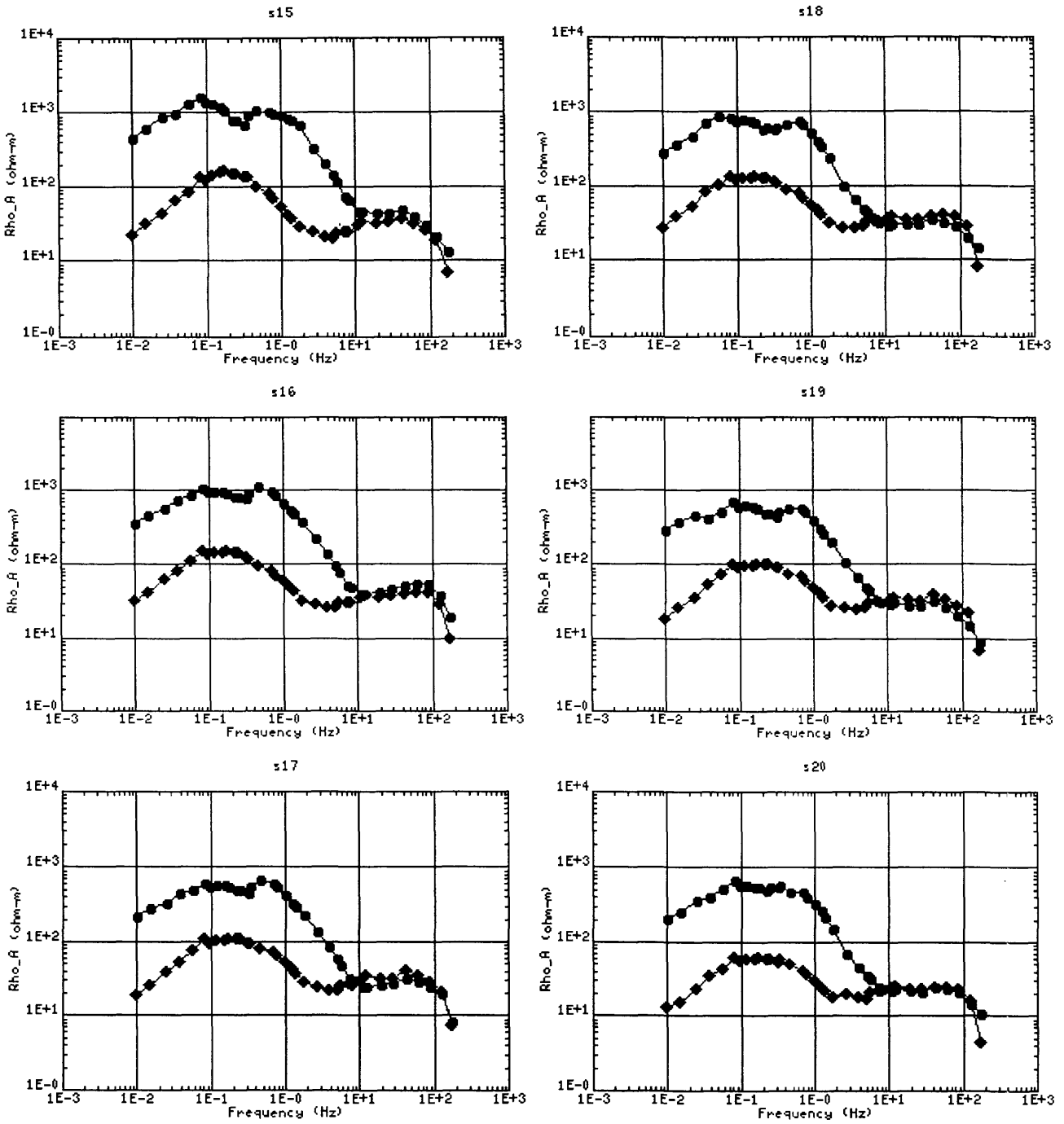

Figure B6.1: Line s - Apparent Resistivity, site s01-s26

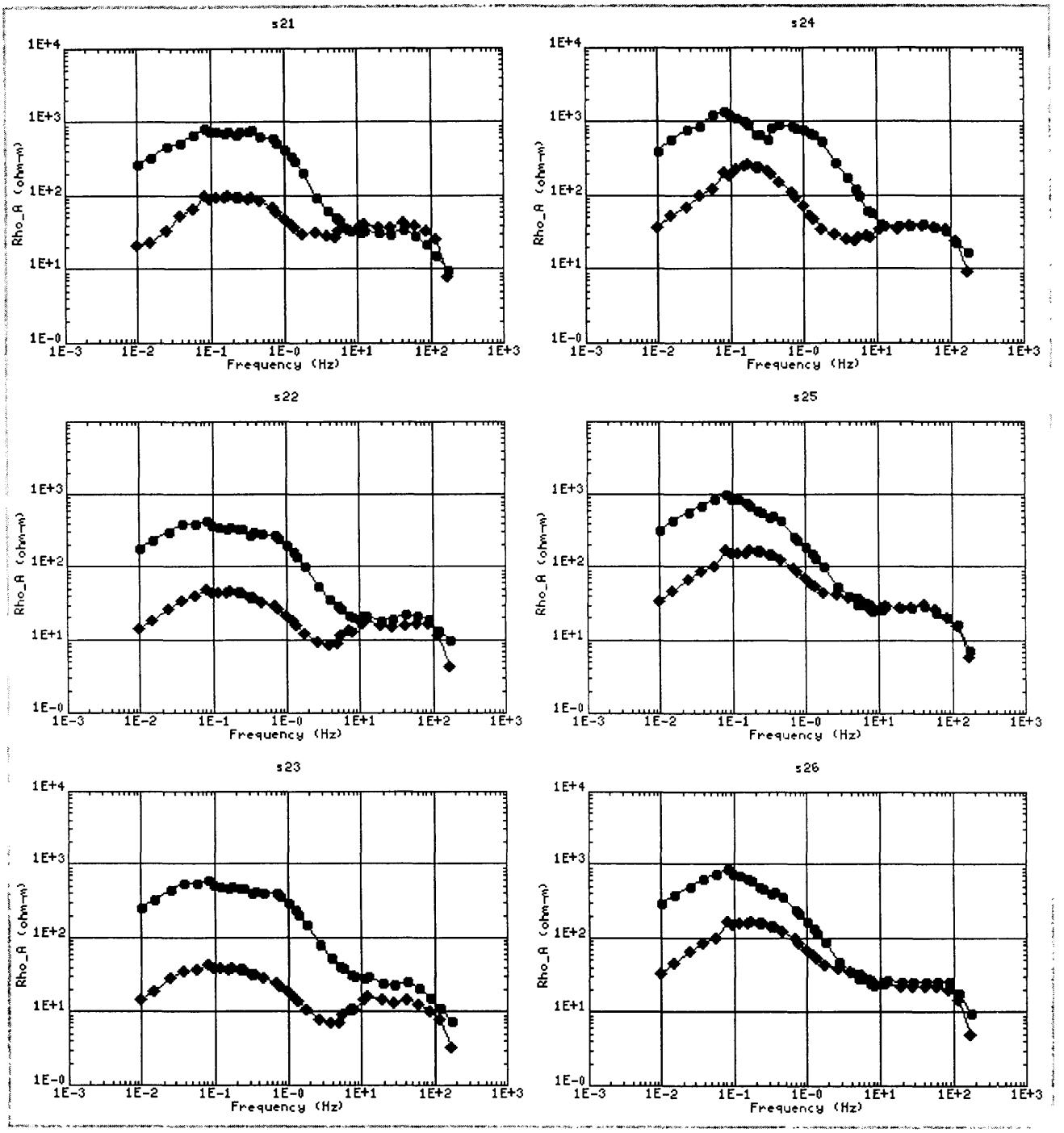

Figure B6.1: Line s - Apparent Resistivity, site s01-s26

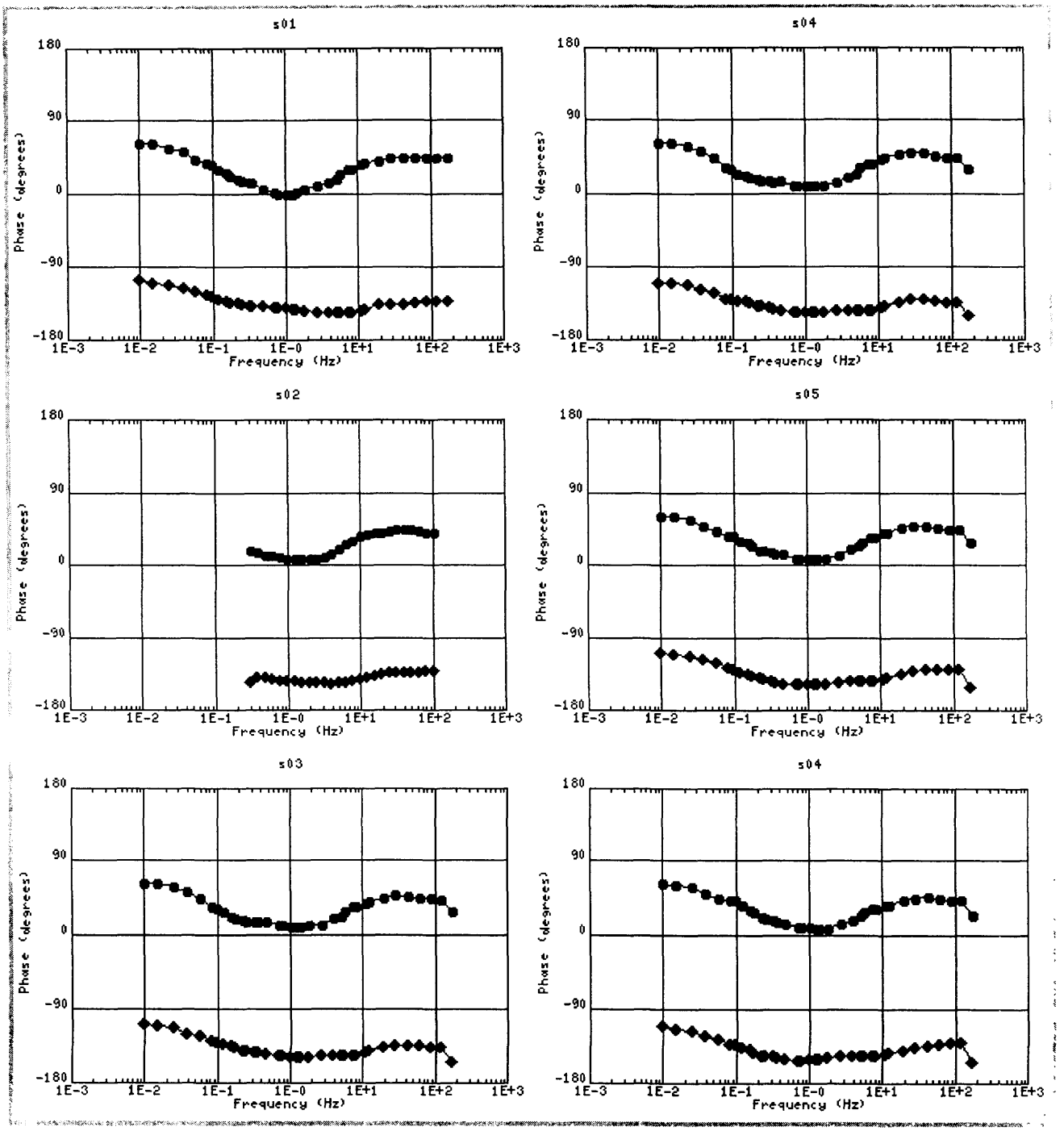

Figure B6.2: Line s - Impedance Phase, site s01-s26

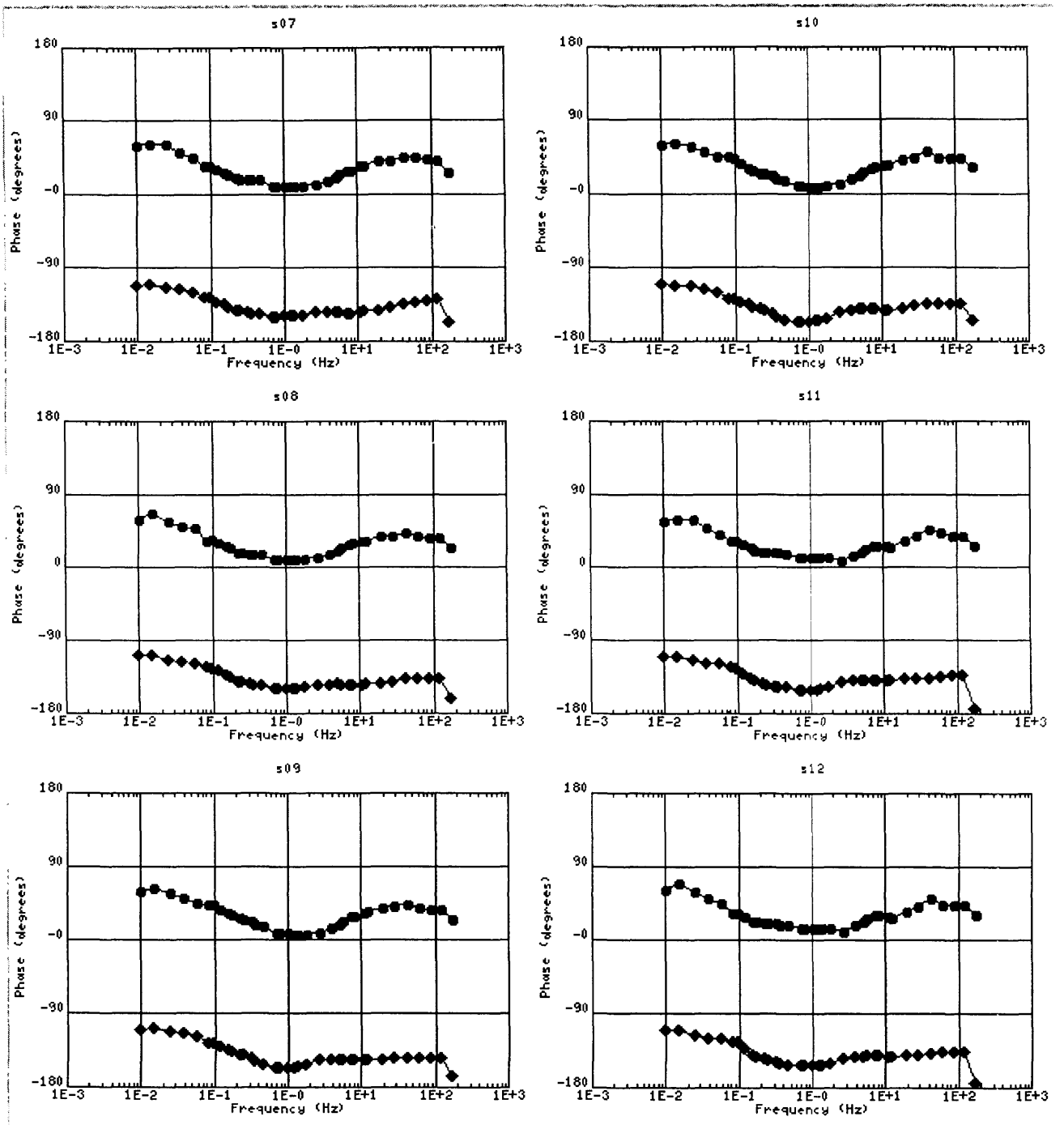

Figure B6.2: Line s - Impedance Phase, site s01-s26

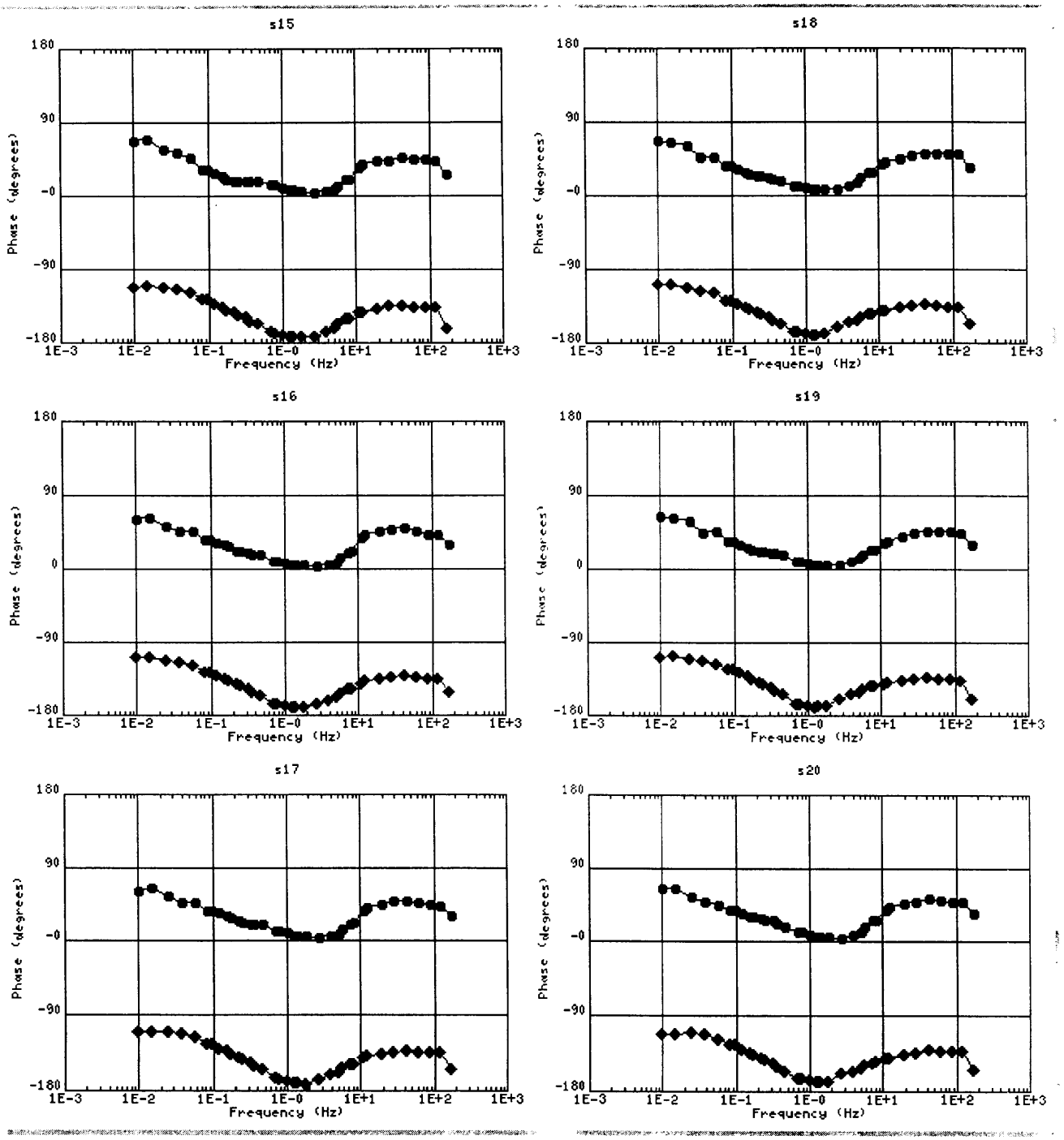

Figure B6.2: Line s - Impedance Phase, site s01-s26

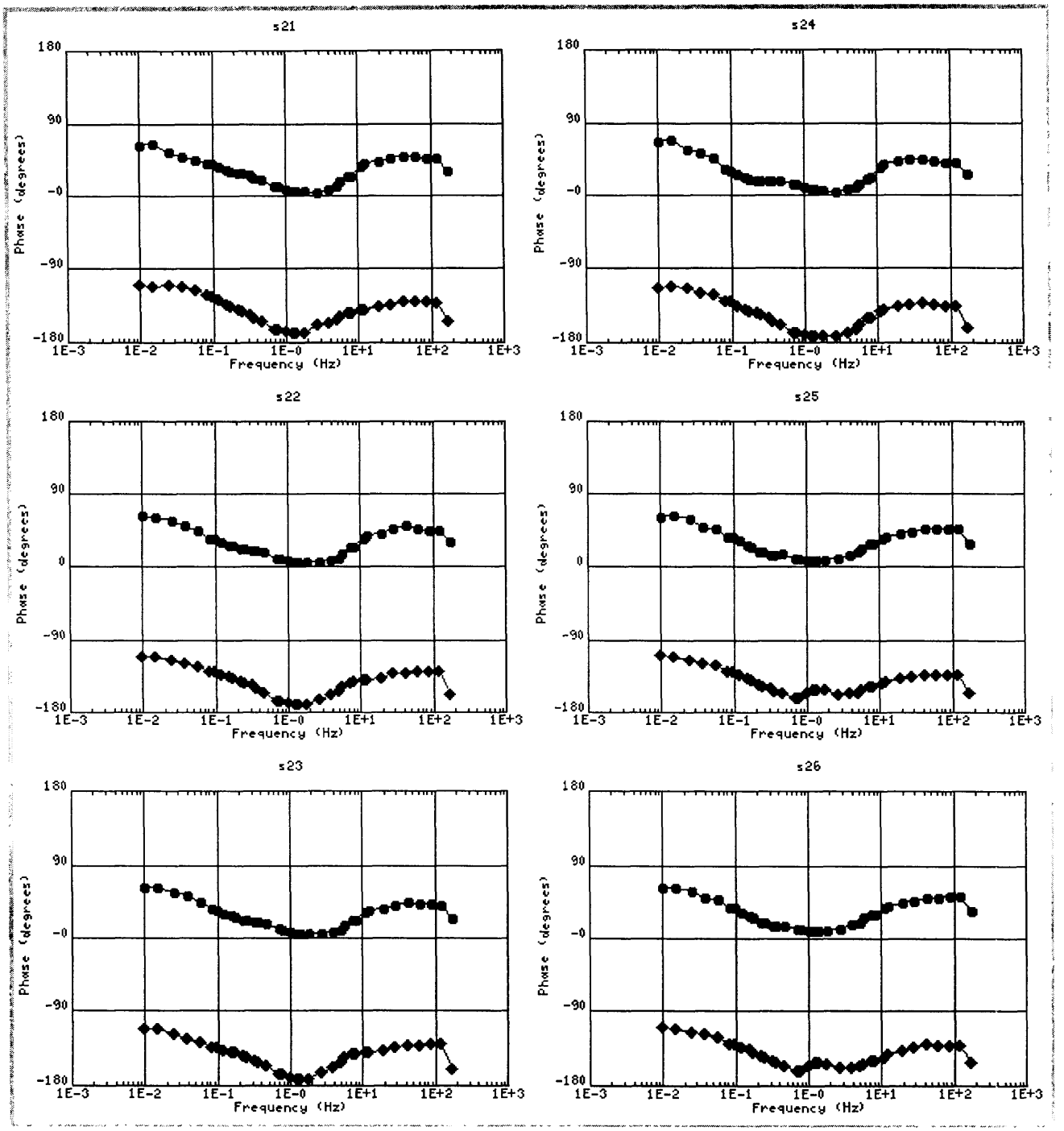

Figure B6.2: Line s - Impedance Phase, site s01-s26

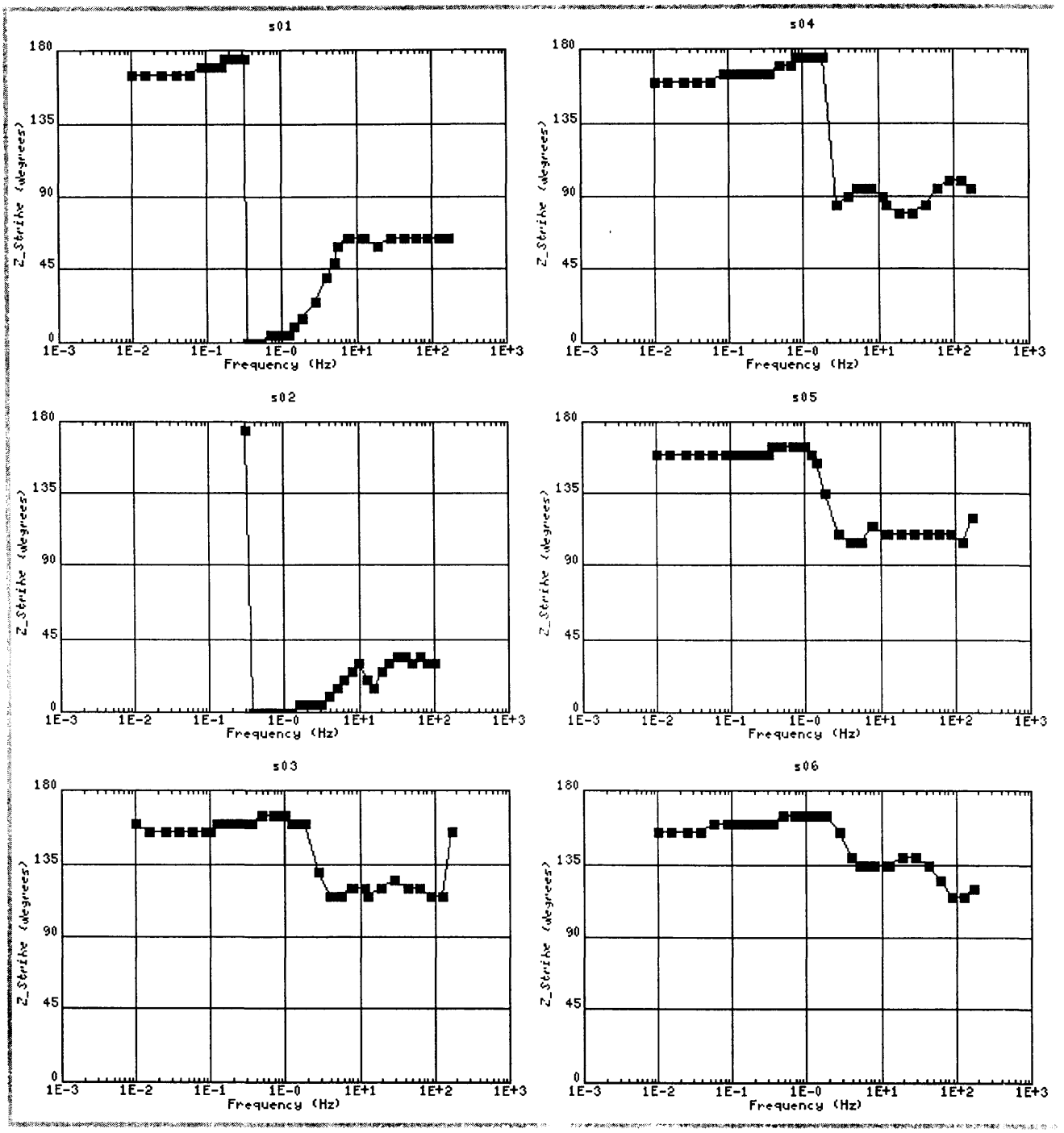

Figure B6.3: Line s - Impedance Strike, site s01-s26

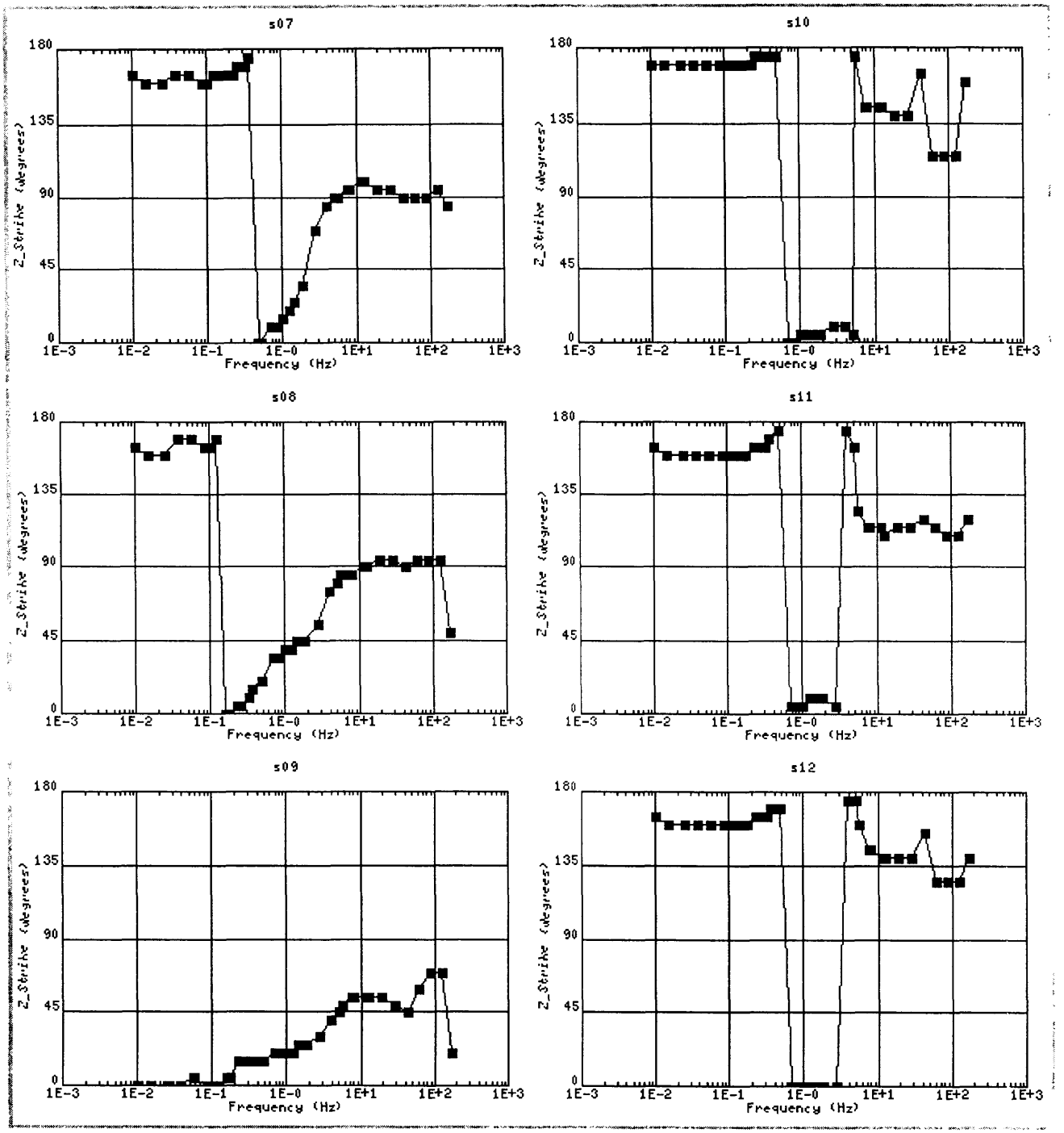

Figure B6.3: Line s - Impedance Strike, site s01-s26

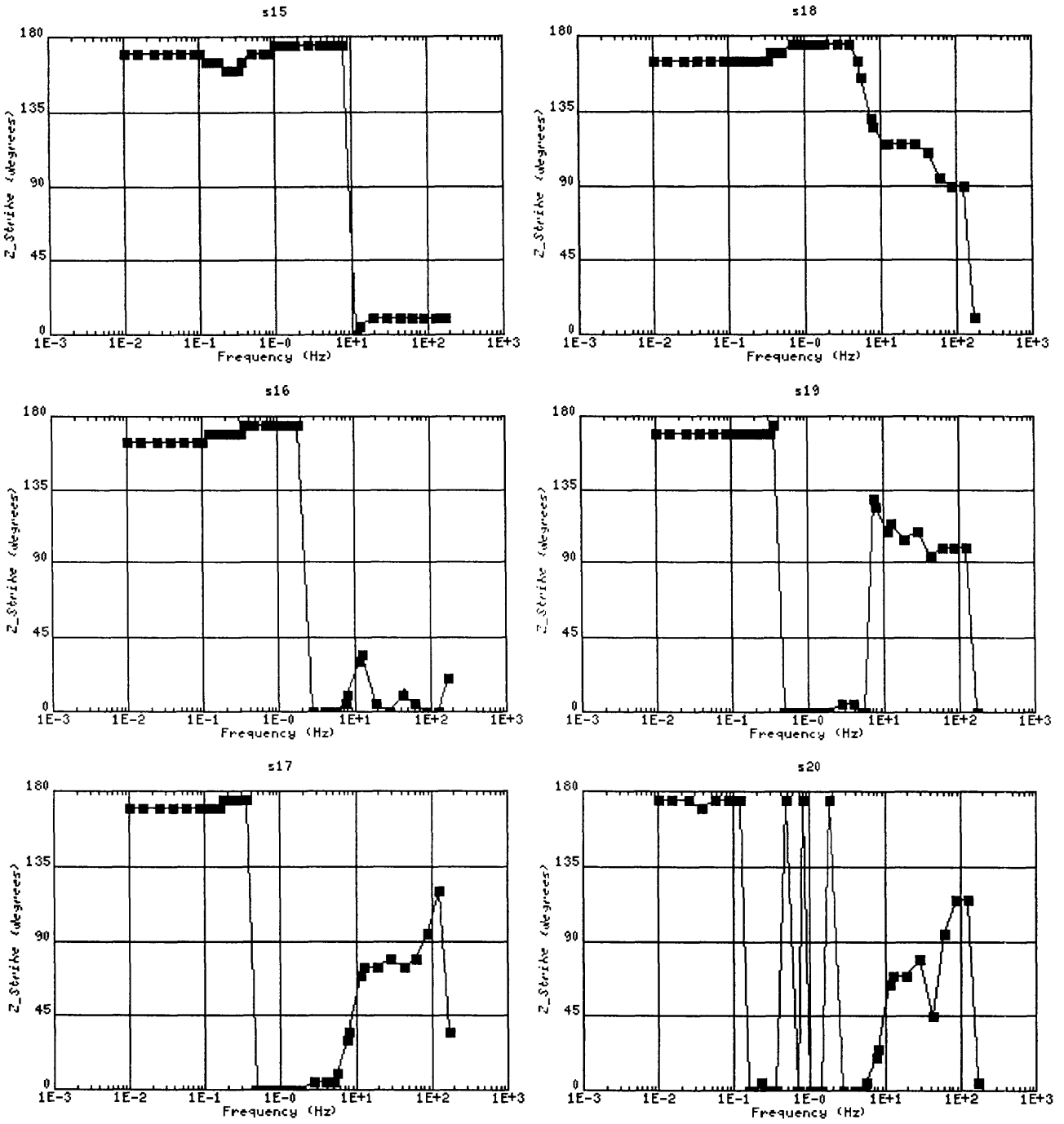

Figure B6.3: Line s - Impedance Strike, site s01-s26

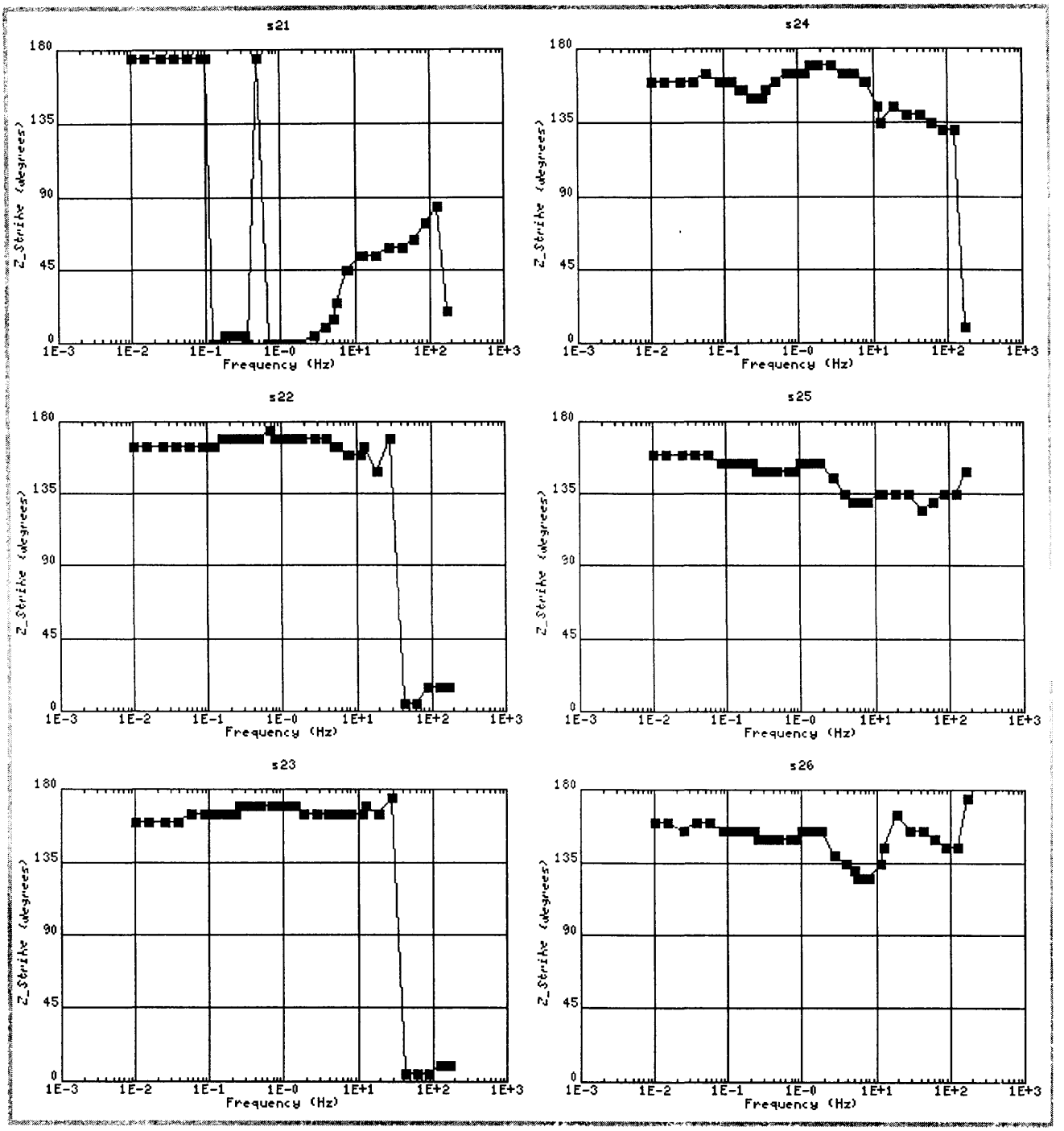

Figure B6.3: Line s - Impedance Strike, site s01-s26

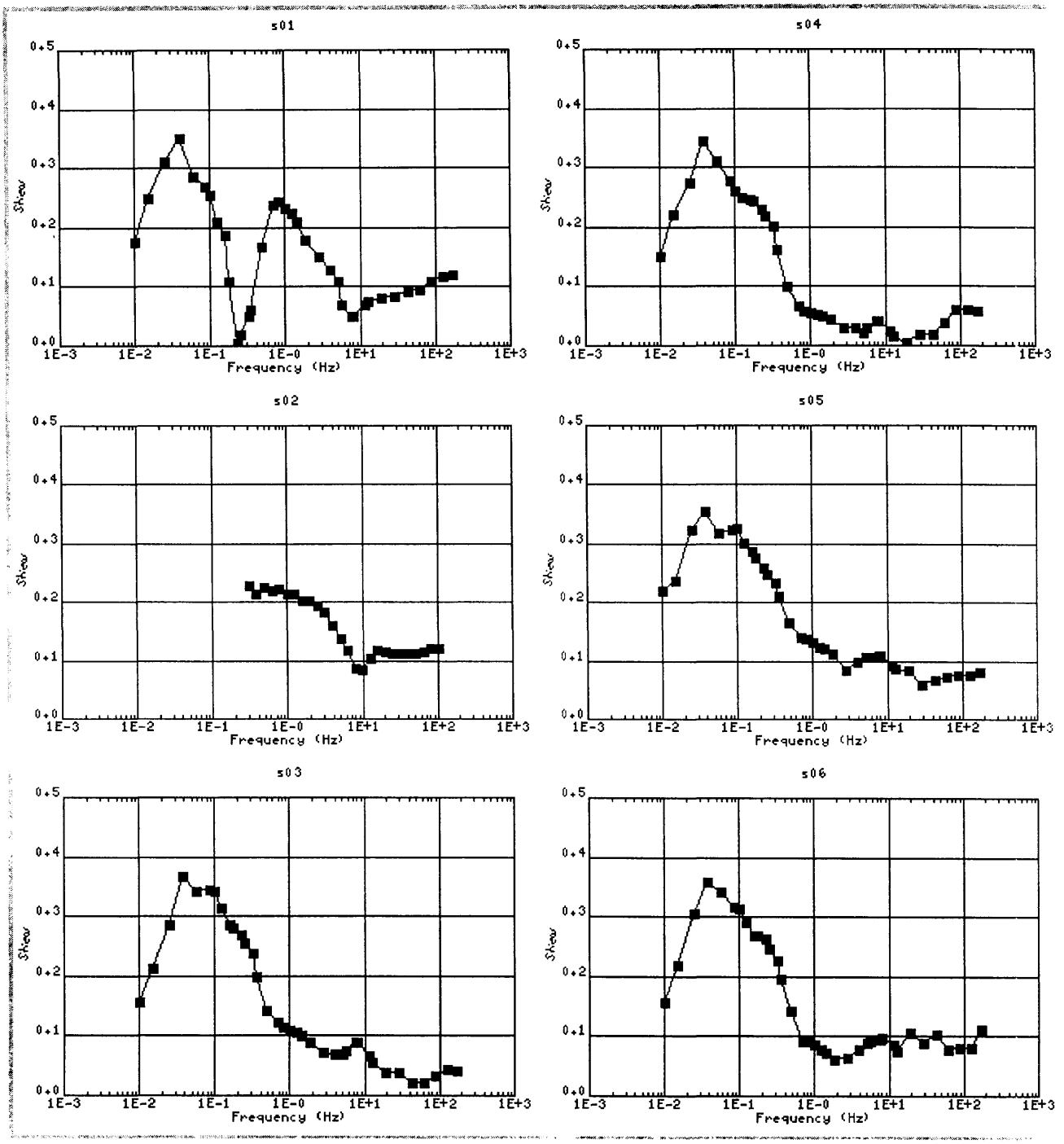

Figure B6.4: Line s - Impedance Skew, site s01-s26

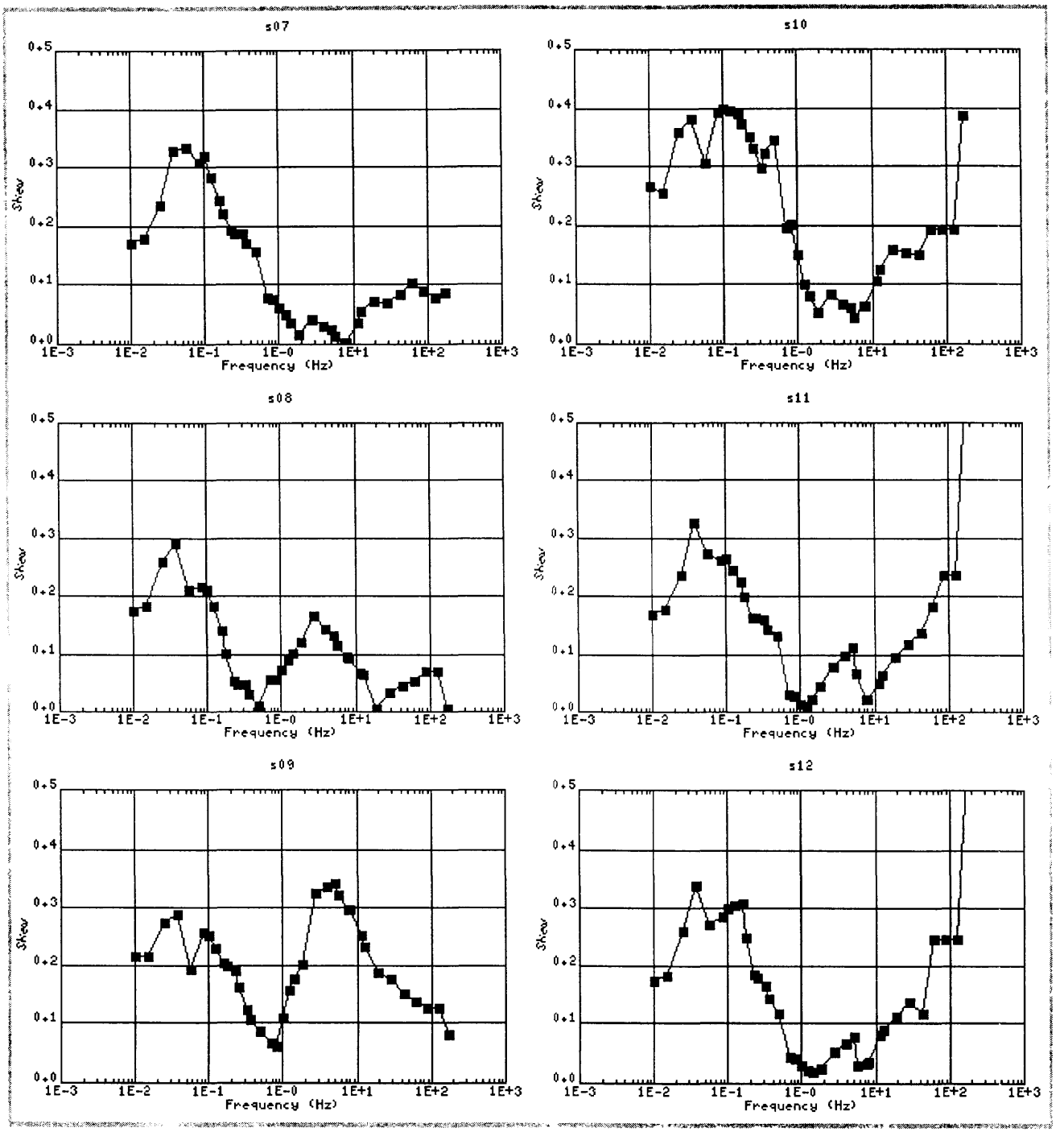

Figure B6.4: Line s - Impedance Skew, site s01-s26

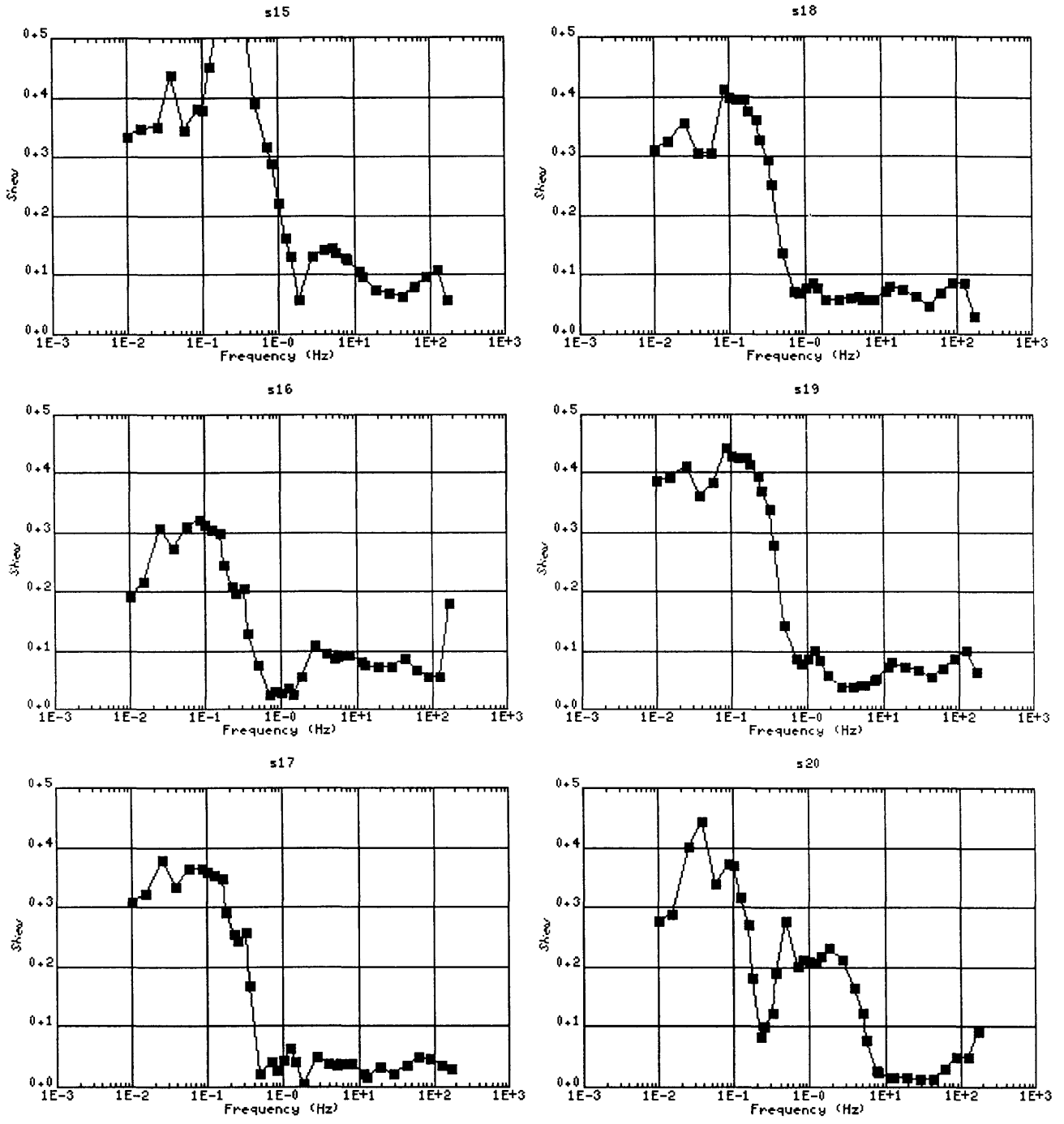

Figure B6.4: Line s - Impedance Skew, site s01-s26

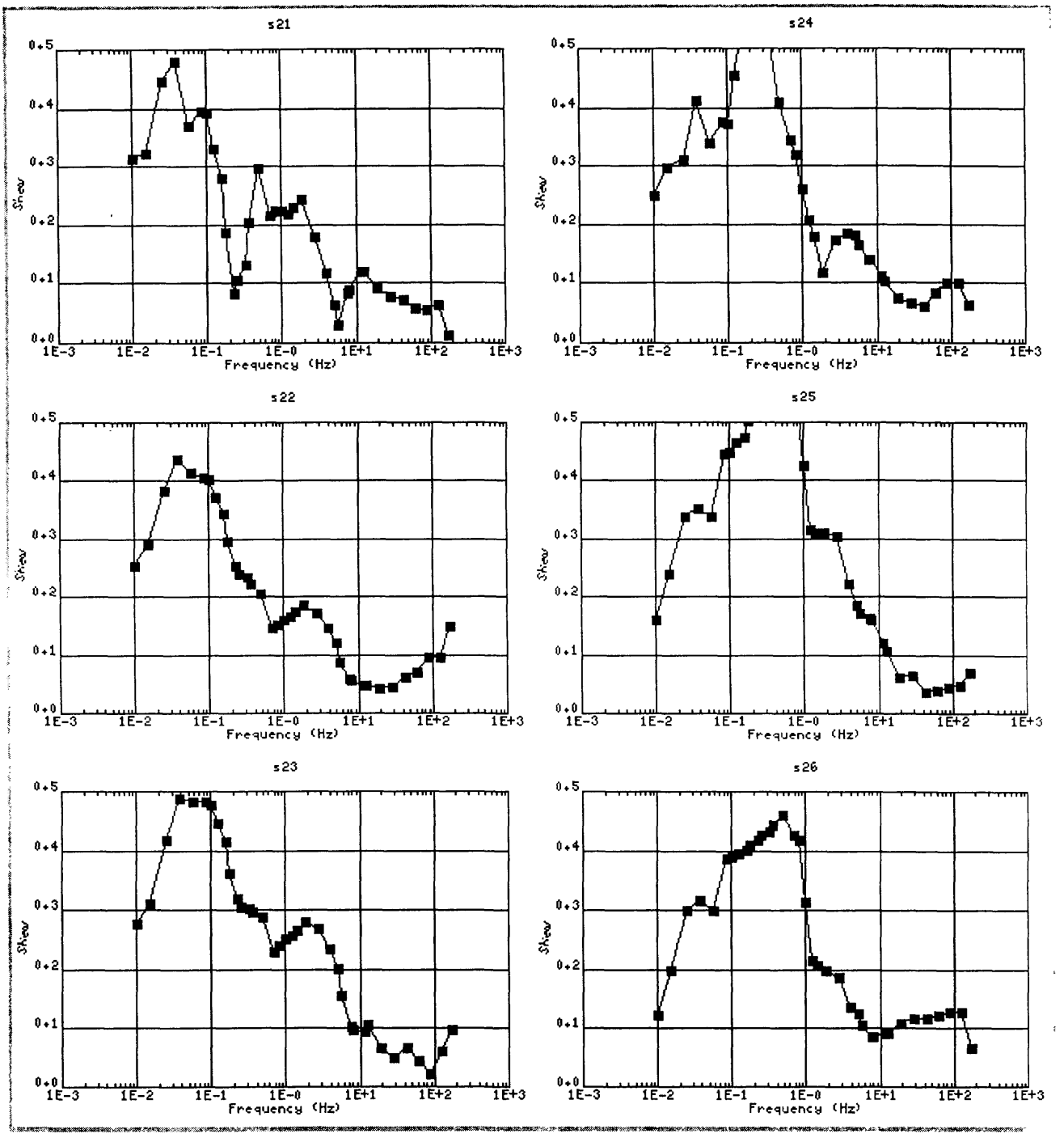

Figure B6.4: Line s - Impedance Skew, site s01-s26